Thesis

Evaluation of Inter-annual Variability and Trends of Cloud Liquid Water Path in Climate Models Using A Multi-decadal Record of Passive Microwave Observations

Submitted by

Andrew Manaster

Department of Atmospheric Science

In partial fulfillment of the requirements

For the Degree of Master of Science

Colorado State University

Fort Collins, Colorado

Spring 2016

Master's Committee:

Advisor: Christian Kummerow
Co-Advisor: Christopher W. O'Dell

David Randall
Steven Reising

Abstract

Evaluation of Inter-annual Variability and Trends of Cloud Liquid Water Path in Climate Models Using A Multi-decadal Record of Passive Microwave Observations

Long term satellite records of cloud changes have only been available for the past several decades and have just recently been used to diagnose cloud-climate feedbacks. However, due to issues with satellite drift, calibration, and other artifacts, the validity of these cloud changes has been called into question. It is therefore pertinent that we look for other observational datasets that can help to diagnose changes in variables relevant to cloud-radiation feedbacks. One such dataset is the Multisensor Advanced Climatology of Liquid Water Path (MAC-LWP), which blends cloud liquid water path (LWP) observations from 12 different passive microwave sensors over the past 27 years. In this study, observed LWP trends from the MAC-LWP dataset are compared to LWP trends from 16 models in the Coupled Model Intercomparison Project 5 (CMIP5) in order to assess how well the models capture these trends and thus related radiative forcing variables (e.g., cloud radiative forcing).

Mean state values of observed LWP are compared to those of previous observed climatologies and are found to have relatively good quantitative and qualitative agreements. Mean state observed LWP variables are compared both qualitatively and quantitatively to our suite of CMIP5 models. These models tend to capture mean state and mean seasonal cycle LWP features, but the magnitudes exhibit large variations from model to model. Several metrics were used to compare observed mean state LWP and mean seasonal cycle amplitude and the mean state LWP and mean seasonal cycle amplitude in each model. However, the models'

performance in regards to these metrics is found to not be indicative of their abilities to accurately reproduce trends on a regional or global scale.

Global trends in the observations and the model means are compared. It is found that observational trends are roughly 2-3 times larger in magnitude in most regions globally when compared to the model mean although this is thought to be at least partly caused by cancellation effects due to differing inter-annual variability and physics between models. Several regions (e.g., the Southern Ocean) have consistent signs in trends between the observations and the model mean while others do not due to spatial inconsistencies in certain trend features in the model mean relative to the observations.

Trends are examined in individual regions. In four of the six regions analyzed, the observational trends are statistically different from zero, while, in most regions, very few models have trends that are statistically significant. In certain regions, the majority of modeled trends are statistically consistent with the observed trends although this is typically due to large estimated errors in the observations and/or models, most likely caused by large inter-annual variability. The Southern Ocean and globally averaged trends show the strongest similarities to the observed trends. Almost all Southern Ocean trends are robustly positive and statistically significant with the majority of models being statistically consistent with the observations. Similarly, the observed and global trends are all positive with the majority being statistically significant and statistically consistent. We discuss why a large positive Southern Ocean trend is unlikely to be due to a trend in cloud phase.

CMIP5 model mean and observational LWP trends are compared regionally to Atmospheric Model Intercomparison Project (AMIP) and ERA-interim reanalysis trends. It is found that AMIP model mean and ERA LWPs are better than the CMIP5 model mean at capturing the inter-annual variability in the observed time series in most of the regions examined. The AMIP model mean better replicates the observed trends when the inter-annual variability is better captured. The ERA reanalysis tends to better reproduce the observed inter-annual variability when compared to the AMIP model mean in almost every region, but, surprisingly, it is either worse or roughly the same in regards to matching observed trends.

Our results suggest that observed trends are due to a combination of inter-annual and decadal-scale internal variability, in addition to external forced trends due to anthropogenic influences on the climate system. With a record spanning three decades, many modeled trends are statistically consistent with the observed trends, but a true climatically forced signal is not yet apparent in the models that agrees with the observations. The primary exception to this is in the Southern Ocean, where virtually all models and observations indicate an increasing amount of cloud liquid water path.

Acknowledgements

Thanks to Chris O'Dell and Gregory Elsaesser for providing insight and knowledge on this subject matter; to Chris O'Dell and Robert Nelson for proofreading and providing helpful critiques and comments; to Tommy Taylor, Robert Nelson, Emily Bell, and everyone else in the O'Dell group; to Dave Randall, Christian Kummerow, and Steven Reising for serving on my committee; to Chris O'Dell for advising me; to the Colorado State University Department of Atmospheric Science; to Rob, Joanne, Amanada, Abby, and Adam Manaster for their continual love and support; to all of my friends and bandmates who put up with me being routinely absent to finish this thesis. This work was funded through the NASA Making Earth System Data Records For Use In Research Environments (MEaSUREs), via subcontract with the NASA Jet Propulsion Laboratory (JPL)

This thesis is typset in LaTeX using a document class designed by Leif Anderson.

Table of Contents

List of Tables

List of Figures

CHAPTER 1

Introduction

Clouds play an important role in the climate system. They are intimately linked to the global hydrologic cycle and its associated processes such as condensation and precipitation. They also greatly impact the global radiation budget by altering the net amount of radiative flux at the top of the atmosphere (TOA) in both the reflected solar shortwave (SW) radiation and the outgoing longwave (LW) radiation. Clouds are widespread across the globe, covering approximately 70% of the earth's surface at any given time (Rossow and Schiffer, 1999). Due to their large impacts on the climate system from their frequency both spatially and temporally, it is imperative that they be studied in great detail in order to accurately assess their impact on the earth climate system both in the future and at present.

1.1. Cloud Radiative Forcing

One of the most important aspects of climate science is the study of how clouds and changes in clouds affect the global radiation budget. The basic variable used in these kinds of studies is known as cloud radiative forcing (CRF). CRF is a measure of the difference in radiative fluxes seen at the TOA between an atmosphere containing clouds and a completely clear atmosphere (i.e., no clouds). It is the net effect clouds have on changing the TOA radiative fluxes and is given by the following equation:

$$CRF = R_{all-sky} - R_{clear-sky} \tag{1}$$

where R is equal to the incoming minus outgoing radiative flux at the TOA in Wm^{-2}. $R_{clear-sky}$ represents the incoming minus outgoing radiation in a clear atmosphere while

$R_{all-sky}$ is equal to the incoming minus outgoing radiation in a cloudy atmosphere. A net negative CRF indicates that cloud effects lead to more radiation leaving the TOA than coming in (a cooling effect) when compared to a clear-sky case whereas a net positive CRF indicates that the presence of clouds leads to less radiation leaving the TOA than coming in (a warming effect).

CRF can be split into both the shortwave CRF (SWCRF) and the longwave CRF (LWCRF) contributions in order to determine how much of an effect each has on the net TOA radiative flux. Figure 1.1 from the Intergovernmental Panel on Climate Change Assessment Report 5 (IPCC AR5) (Boucher et al., 2013) displays the SWCRF, LWCRF, and net CRF from 2001-2011 as measured from the Clouds and Earth's Radiant Energy System (CERES) Energy Balanced and Filled (EBAF) Ed2.6r dataset (Loeb et al., 2009). Figure 1.1(a) shows a strong negative SWCRF, indicating that clouds act to increase the outgoing TOA shortwave radiation. Conversely, 1.1(b) shows a positive LWCRF in the same time period that is roughly 50%-75% the magnitude of the the negative SWCRF. This indicates that clouds cause a net decrease in outgoing longwave radiation (OLR) at the TOA, which is by itself a warming influence. When these effects are added together, the net CRF is obtained. This is negative (a cooling effect) due to the large magnitude of the SWCRF, which is partially offset by the smaller magnitude, positive LWCRF, indicating that, on average, clouds act to cool the planet.

Figure 1.1 is indicative of the present state of shortwave, longwave, and net CRF, which provides insight as to how clouds affect the net radiation budget in our current climate. However, it is also important to know how CRF will change in a future climate. This is the basis for cloud feedback studies. Cloud feedbacks are how the TOA cloud radiative forcing changes with changing surface temperature. A positive cloud feedback indicates that clouds

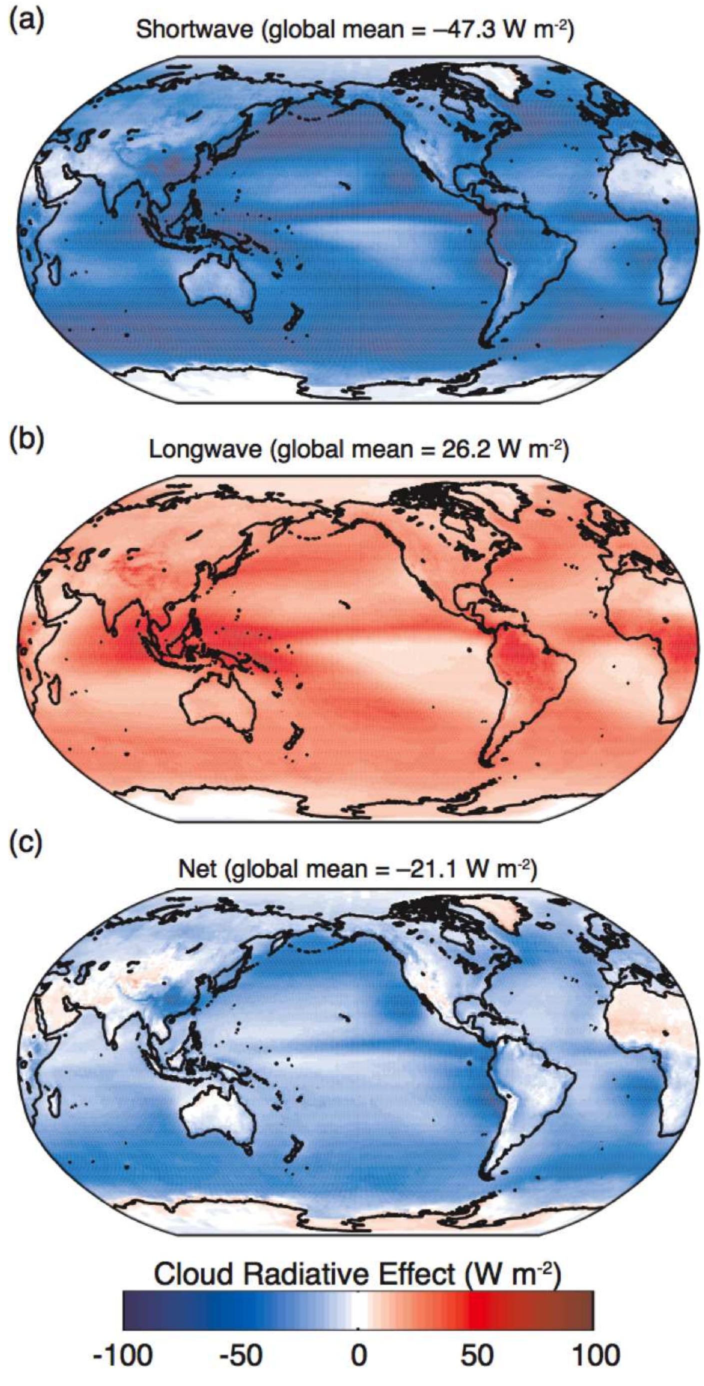

Figure 1.1. Taken from the IPCC AR5 figure 7.7 (Boucher et al., 2013), this figure shows the annual-mean global distribution of (a) SWCRF, (b) LWCRF, and (c) net CRF from 2001-2011. Measurements were taken from the Clouds and Earth's Radiant Energy System (CERES) Energy Balanced and Filled (EBAF) Ed2.6r dataset (Loeb et al., 2009).

will change in such a way that will amplify any future climate response while a negative cloud feedback indicates that changes in clouds will lead to a dampening in future climate response. The following section looks at studies of modeled cloud feedbacks and how our ability to predict future changes in cloud properties has evolved.

1.2. Modeled Cloud Feedbacks

Changes in cloud properties have been examined for years, using models, in an attempt to determine the sign of the cloud feedback both at present and in the future and the contribution of different cloud properties to the sign of the feedback. Schneider (1972), who used models to study potential feedback mechanisms of clouds, determined that an increase in cloud height would lead to a net warming of the surface assuming that cloud amount and cloud albedo were held fixed, thus making it a potential positive feedback. This is due to the fact that an increase in cloud height will decrease the amount of outgoing longwave radiation "seen" at the TOA. Schneider (1972) also determined that an increase in the amount of lower clouds will lead to a reduction in surface temperature at low and mid-latitudes if cloud height and albedo are held fixed, making it a potential negative feedback. This is because increases in lower clouds will increase the amount of shortwave radiation reflected back into space.

Somerville and Remer (1984) used a radiative-convective equilibrium model in order to study changes in cloud optical thickness with changes in CO_2 (they note that this is an extension of work already done by Paltridge (1980) and Charlock (1982)). They found that as the amount of greenhouse gas forcing from CO_2 increased, the optical depths of clouds in the model increased as well, offsetting roughly half of the surface temperature warming due to a doubling of CO_2. This confirmed their hypothesis that, in a warmer climate, the warmer air will be able to hold more water vapor which would lead to more water available to condense into cloud droplets. This would lead to optically thicker clouds which would reflect more shortwave radiation to space and partially offset warming due to an increase in greenhouse gases. Betts (1987) further expanded upon this work, showing that this optical depth feedback is roughly twice as large at high latitudes than it is in the tropics.

Roeckner et al. (1987), however, found that (after a rebuttal from Schlesinger (1988)), the cloud optical depth feedback was a net positive in a doubling of CO_2 simulation where cloud liquid water path (LWP) was prognostically calculated and optical depth was allowed to vary based on an LWP-optical depth relationship derived in Stephens (1978). This was due to the fact that reduction in the amount of outgoing longwave radiation due to increases in high cloud optical depth (a positive feedback) was greater than the increased amount of shortwave radiation reflected back into space due to an increase in the optical depth of low and mid-level clouds (a negative feedback).

Studies by Cess et al. (1990) and subsequently Cess et al. (1996) investigated the spread in cloud feedbacks from a suite of 19 general circulation models and found that roughly half of the models exhibited negative cloud feedbacks while the other half were positive. However, Soden et al. (2004) found that the method used to calculate these feedbacks in these studies did not take cloud masking effects on other, non-cloud feedbacks (temperature, water vapor, surface albedo, etc...) into account. This led to and underestimation of cloud feedback magnitudes on the order of approximately 0.3 $W/m^2/K^{-1}$, which is non-negligible when compared to current modeled net cloud feedbacks (see figure 1.3). Soden et al. (2004) conclude that if cloud masking had been taken into account, most models in Cess et al. (1996) that exhibited a negative feedback would have likely exhibited a positive feedback instead. Even with this correction, the spread in cloud feedbacks among the 19 GCMs examined was still rather large.

Dufresne and Bony (2008) examined the spread of various feedbacks in a suite of 12 CMIP3 models in order to estimate both the model mean equilibrium climate sensitivity (ECS, i.e., how much the planet will warm due to an instantaneous doubling of CO_2 from pre-industrial levels) and the model mean transient climate response (TCR), which represents the global mean temperature change at the end of a climate simulation in which the CO_2 increases at a rate of 1%/yr until it reaches double its preindustrial level. TCR is generally smaller than ECS due to the fact that TCR includes the effects of ocean heat uptake (Flato et al., 2013). Figure 1.2 displays figures 1-4 from Dufresne and Bony (2008). 1.2 (a) and (c) display the model mean ECS and TCR respectively and the associated contributions of each of the different feedback mechanisms (left panels) and the intermodel differences for each feedback normalized by the intermodel standard deviation (right panels). 1.2 (b) and (d) show the ECS and TCR respectively for each model analyzed in the study and the contributions of each feedback to the total ECS or TCR. It can be seen in the right panels of figures 1.2 (a) and (c) that cloud feedbacks contribute to roughly 70% and 90% of the intermodel standard deviation respectively, easily making them the biggest source of uncertainty in the model mean ECS and TCR. This can also be seen in 1.2 (b) and (d) where the cloud feedbacks (brown bars) show the largest differences in magnitude of all feedbacks among the 12 models examined in this study.

In more recent work, Zelinka et al. (2012a,b) use the radiative kernel method (described in Soden et al. (2008) and Shell et al. (2008)) at each individual grid box in the International Satellite Cloud Climatology Project (ISCCP) simulator cloud histogram, which gives cloud fraction as a function of cloud top pressure and cloud optical depth, for a suite of global models in order to separate out the individual contributions of different cloud types and properties to the total cloud feedback. Figure 1.3 (taken from Zelinka et al., 2012a and

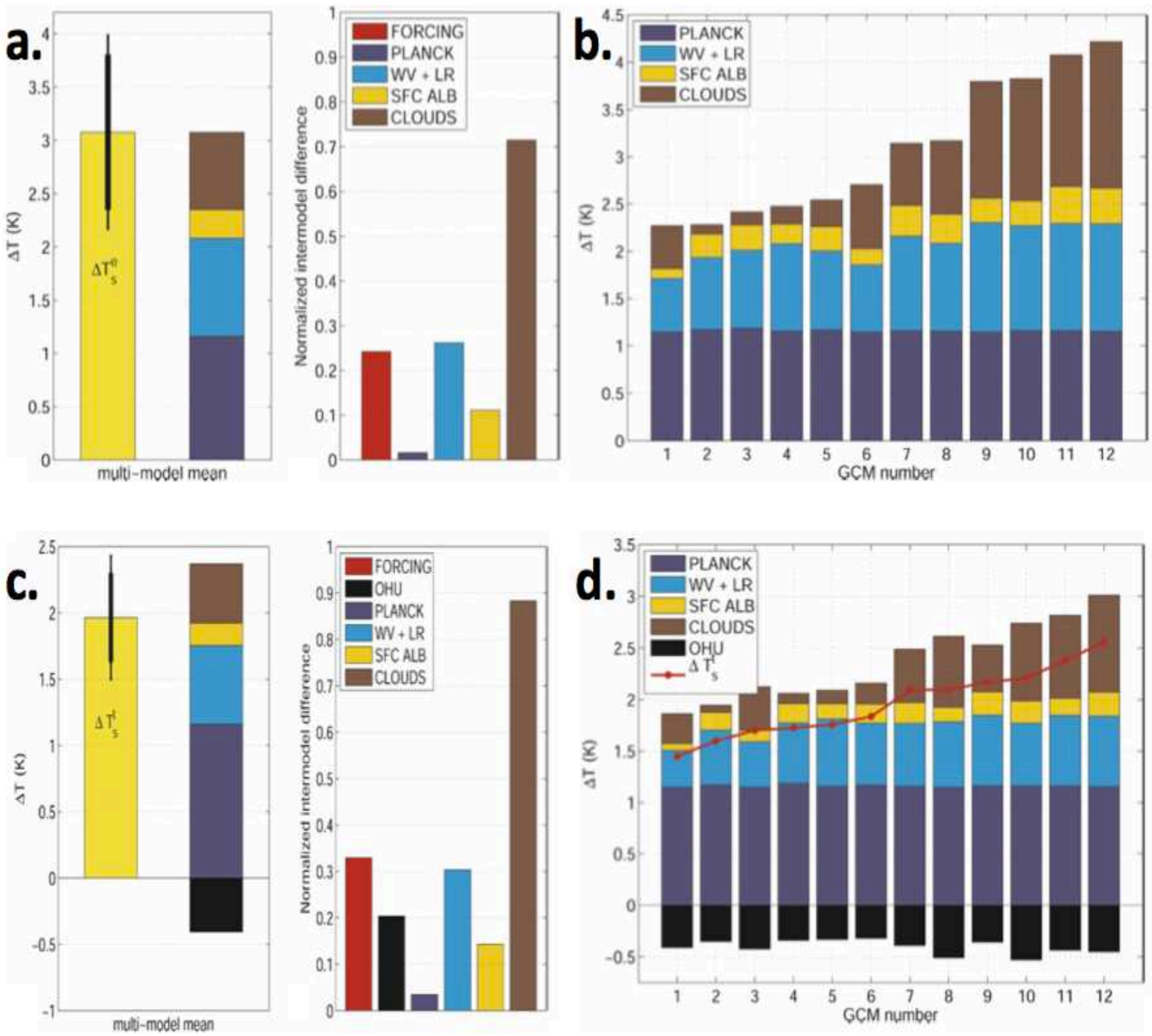

FIGURE 1.2. Figures adapted from figures 1-4 in Dufresne and Bony (2008) show (a) the model mean ECS, associated error bar (thick line is ±1 standard deviation while the thin line is the 5%-95% confidence limits), and the relative contribution of each feedback (left panel) and the intermodel difference of each feedback normalized by the intermodel standard deviation (right panel), (b) the individual model ECS's and the relative contributions of the different feedbacks to the total ECS, (c) same as (a) except for TCR (i.e., now includes the ocean heat uptake indicated by the black bar), and (d) same as (b) except it includes the ocean heat uptake (black bar). Red line in (d) indicates the TCR

Zelinka et al. (2012b)) shows the partitioning of cloud feedbacks into various components and the relative contribution of each to the total cloud feedback in the shortwave, longwave,

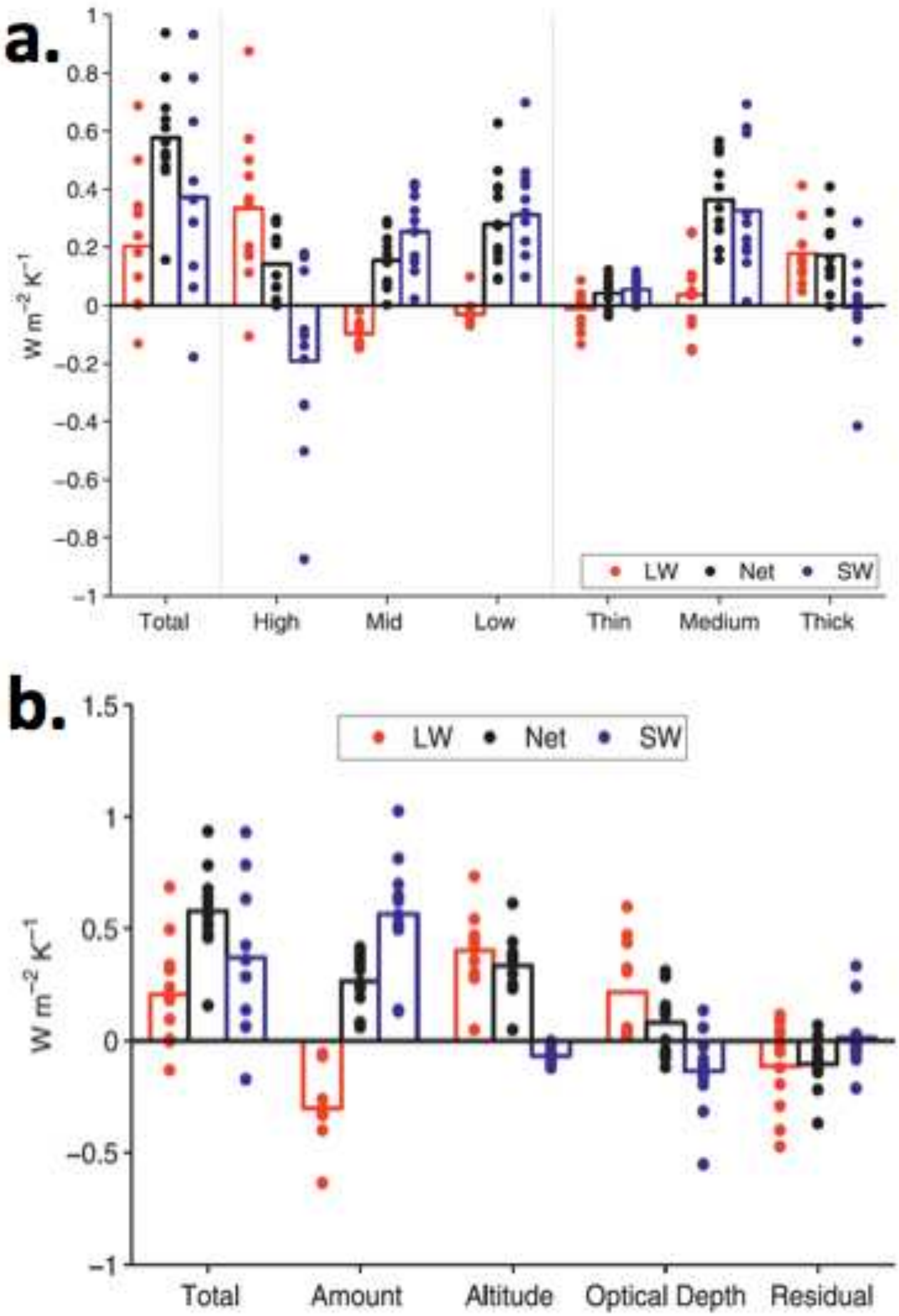

FIGURE 1.3. Figures taken from Zelinka et al. (2012a,b) show the relative contribution of various cloud properties to the total cloud feedbacks for each individual model examined (dots) and the model mean (bars) in the shortwave (blue), longwave (red), and net (black)

and the net feedback. It can be seen that the total longwave and shortwave cloud feedbacks are positive for almost every model and the total net feedback is positive for every model although the relative contributions of each vary between negative and positive depending on the cloud type, cloud property, and type of radiation. Although these models all display a total net positive cloud feedback, they exhibit a relatively large spread in these feedbacks ranging from approximately 0.2 $W/m^2/K^{-1}$ to approximately 1 $W/m^2/K^{-1}$. To date, this spread in cloud feedback size amongst models is one of the largest sources of uncertainty in predicting the future equilibrium climate sensitivity (Cess et al., 1990, 1996, Bony and Dufresne, 2005, Stephens, 2005, Soden and Held, 2006, Randall et al., 2007, Dufresne and Bony, 2008, Boucher et al., 2013).

Similar to figure 1.2, figure 1.4 taken from Chapter 9 in the IPCC AR5 Flato et al. (2013) shows the model spread for all major feedbacks from CMIP3 and Coupled Model Intercomparison Project 5 (CMIP5) models. It can be seen that the spread in most feedbacks has stayed relatively consistent from the time of the IPCC Assessment Report 4 (2007) to the time of the IPCC AR5 (2013). Again, as shown by many previous studies, (e.g., Soden and Held, 2006, Dufresne and Bony, 2008), the largest spread appears to be in cloud feedbacks, with CMIP5 models seemingly exhibiting a larger range of feedbacks than CMIP3, although this appears to mostly be due to two outlying models: the largely positive IPSL-CM5A-LR and the slightly negative CCSM4. When all of the feedbacks are combined, CMIP5 models appear to exhibit a marginally larger spread than the CMIP3 models. The range of equilibrium climate sensitivities for CMIP5 and CMIP3 reflect this when compared. CMIP3 models show a range of 2.1°C-4.4°C for the ECS while CMIP5 models show a range of 2.1°C-4.7°C (Flato et al., 2013), an almost indistinguishable difference.

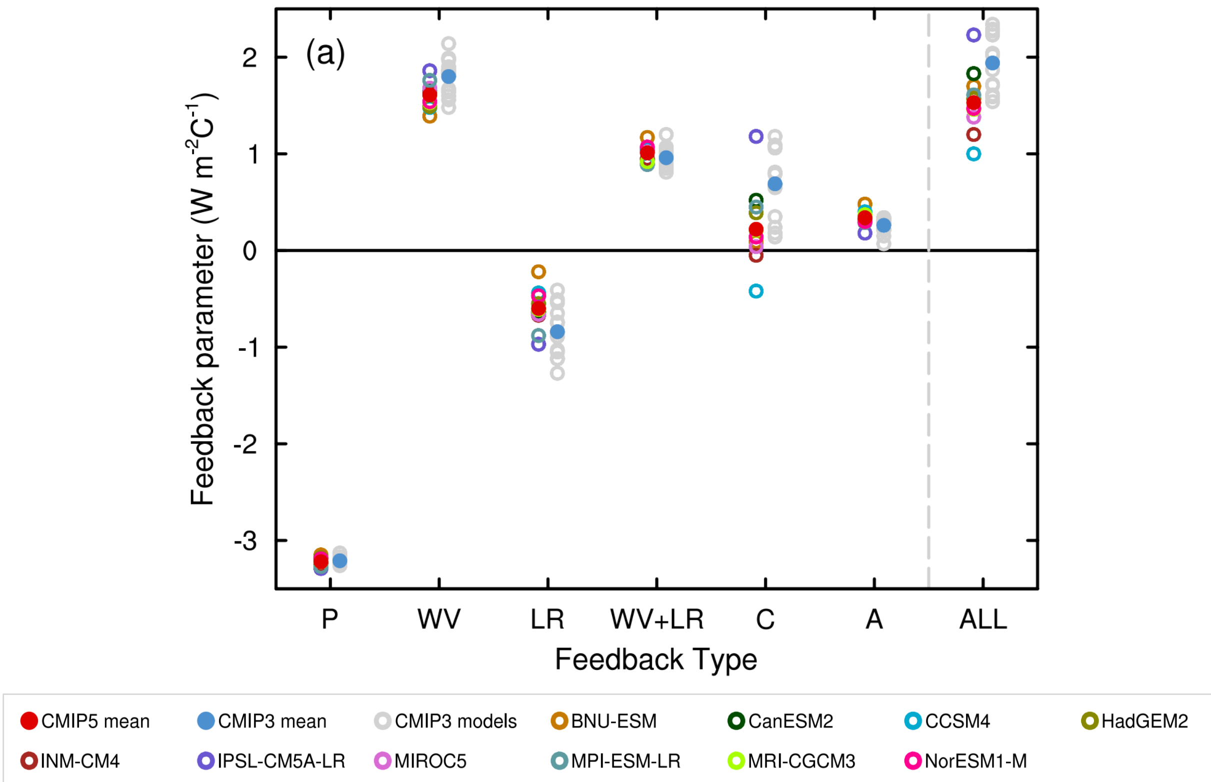

FIGURE 1.4. Taken from Chapter 9 figure 9.43 of the IPCC AR5 (Flato et al., 2013), shows the spread in Planck, water vapor, lapse rate, water vapor+lapse rate, cloud, and albedo feedbacks from CMIP3 (gray circles) and CMIP5 (colored circles) models

It has been shown that the large spread in equilibrium climate sensitivity in state of the art climate models is due in large part to the intermodel spread in cloud feedbacks (e.g., Soden and Held, 2006, Dufresne and Bony, 2008). These cloud feedbacks are very closely associated with changes in cloud radiative forcing which itself depends on changes in cloud variables. Therefore, in order to reduce this spread in cloud feedbacks, it is imperative that we use observational data to examine changes in CRF and the underlying variables that cause these changes.

1.3. Observing Changes in Cloud Properties

Ideally, in order to accurately assess changes in CRF (and thus cloud feedbacks) that are seen in models, we would want to examine observed changes in CRF. The CERES-EBAF dataset (Loeb et al., 2009) provides observational CRF data from March, 2000 to the present day and is one of the most comprehensive observational CRF datasets that is available to us. Several studies (Dessler, 2010, Dessler and Loeb, 2013, Zhou et al., 2013) have used this dataset to calculate observed, short-term, global cloud feedbacks in recent years. However, the CERES CRF data only spans the past 15 years or so which makes it unideal for diagnosing modeled long-term (i.e., on the scale of centuries) cloud feedbacks due to the time dependence of such feedbacks (Dessler, 2010).

Since there are no other robust, long-term CRF datasets, we must turn to relating long term changes in cloud variables to long term changes in CRF. Although we do not have any datasets of cloud variables that extend for hundreds of years (which would be ideal for diagnosing long-term cloud feedbacks), we have datasets that extend for much longer than the aforementioned CERES-EBAF CRF product. These datasets can help to give a better idea of which models (if any) may be more likely to give an accurate prediction of long-term cloud feedbacks since they are beginning to approach the appropriate timescales. One such dataset is ISCCP, which extends from July, 1983 to the present day and includes observations of cloud fraction, cloud optical depth, and cloud top pressure from various geostationary and polar orbiting satellites (Rossow and Schiffer, 1999). One of the most striking features to come out of ISCCP is an apparent downward trend in global cloudiness (figure 1.5) from the late 1980's to the late 1990's. Many studies that have used these observed changes ISCCP cloud amount to do science related to changes in the planetary radiation budget (e.g., Pallé et al., 2004, Cess and Udelhofen, 2003). However, several studies noted the possibility that

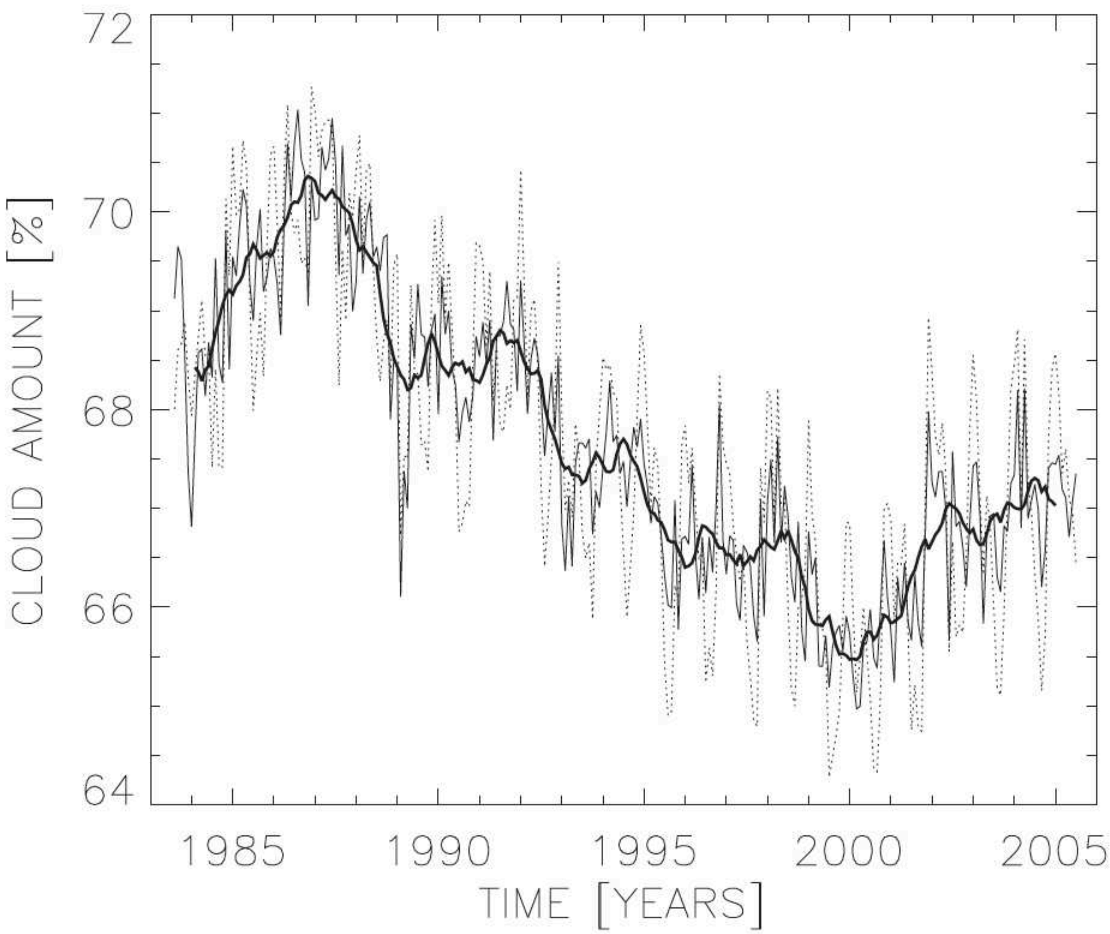

Figure 1.5. Globally averaged ISCCP cloud amount from 1983-2006 (figure 1, Evan et al., 2007)

these cloud amount trends were spurious due to artifacts related to the viewing geometry of geostationary satellites (Norris, 2000, Campbell, 2004, Evan et al., 2007). Evan et al. (2007), found that the regions contributing most to the observed cloud fraction trend in the ISCCP data tended to occur at the edges of geostationary satellite fields of view. Cloud fraction tends to be overestimated in these regions due to a phenomenon known as 'limb-darkening' (Joyce et al., 2001). Evan et al. (2007) discovered that if these areas were removed from the cloud fraction trend calculation, the trend became indistinguishable from zero. They also found that these areas were highly correlated with changes in global, satellite viewing angle geometry due to geostationary satellites being added, removed, or repositioned. They concluded that the ISCCP cloud fraction trends were likely spurious artifacts caused by changes to the satellites used in the dataset. This caused the validity of ISCCP cloud fraction trends to be called into question. Despite this, many efforts have been made in recent studies to remove artifacts from ISCCP cloud fraction data in order to use it to help provide observational evidence for cloud feedbacks (Clement et al., 2009, Bellomo et al., 2014, Norris and Evan, 2015).

Due to observational datasets being much too short and long-term, satellite-based cloud fraction datasets being fraught with errors, we must turn to datasets of other cloud variables in order to help us observe long-term changes in CRF. One such variable is cloud liquid water path (LWP), which is a measure of the amount of vertically integrated cloud water in a column of the atmosphere from the surface to the TOA. LWP is important because it contains information on both cloud optical depth (i.e., a measure of how thick a cloud is) and cloud fraction (i.e., the areal coverage of a cloud). Rather simply, if clouds get thicker (thinner) LWP will increase (decrease). Similarly, if the amount of clouds in a given region increases (decreases) LWP will also increase (decrease), however, it should be noted that neither optical depth nor cloud fraction have an exact 1:1 relationship with LWP.

1.4. Cloud Liquid Water Path Observed in the Microwave

Remote sensing of cloud liquid water path from satellite observations is a relatively new science with most higher quality data only being available for the past 30 years from both passive microwave sensors (e.g., SSM/I, TMI, AMSR-E)(e.g., Greenwald et al., 1993) and visible-near infrared sensors (MODIS, sensors in the ISCCP dataset)(Nakajima and King, 1990). Both microwave and visible-near infrared retrieval techniques (which will be called optical techniques for the remainder of this paper) of LWP have their merits and drawbacks.

Since ground based validation techniques suffer from their own biases and are generally lacking in spatial coverage (Turner et al., 2007), validation of both retrieval methods has generally been done by comparing one technique to the other. This has generally resulted in good correlation between the two techniques (e.g., Greenwald et al., 1993, Lin and Rossow, 1994, Greenwald et al., 1997, Horvath, 2004, Borg and Bennartz, 2007, Horváth and Davies, 2007, Seethala and Horváth, 2010) in most cloud regimes, however, there are discrepancies when looking at certain other cloud regimes. For instance, Horváth and Davies (2007), generally found good agreement between microwave AMSR-E and optical MODIS LWP retrievals in warm, non-precipitating clouds (within 5-10% of one another) having a correlation of approximately 0.85, but found that in cold, precipitating clouds, the correlation reduced to 0.5 or less. Seethala and Horváth (2010), looked at warm, non- precipitating clouds only and found that AMSR-E and MODIS LWPs had a correlation of roughly 0.74 when compared globally. The two were very consistent over large marine stratocumulus decks, having correlations of up to 0.95 and had correlations of 0.83 in overcast cloud scenes. The correlations dropped off significantly in broken cloud scenes (i.e., scenes where the cloud fraction was less than 50% for a given domain) to approximately 0.45.

The lower correlations between the two retrieval methods arise from both errors in passive microwave and optical techniques, the former of which is discussed in greater detail in Chapter 4. Despite the errors in both, the passive microwave technique has several distinct advantages over the optical retrieval technique, which makes it better suited for examining LWP trends. First, the optical technique determines LWP based on solar reflectance and therefore is only applicable during the daytime and can be subject to aliasing of the diurnal cycle into trends, most commonly via drifts in the equator crossing time. In contrast, the passive microwave technique measures LWP based on observed brightness temperatures and therefore can measure LWP any time of day and is not subject to the same sampling bias as the optical technique. The fact that the optical technique computes LWP based on solar reflectance measurements also leads to a large solar zenith angle dependence of the LWP measurement (see Seethala and Horváth (2010) figure 8). In contrast, passive microwave retrievals are insensitive to the solar zenith angle, again, due to the fact that they measure brightness temperature as opposed to solar reflectance. Finally, passive microwave retrievals are also relatively insensitive to the presence of ice whereas optical retrievals can be easily subject to scattering effects due to ice. Ice and large water droplets ($>150\mu$m) can scatter microwave radiation, especially at higher frequency channels (i.e., 89 GHz), leading to a brightness temperature depression and thus a retrieved LWP that is biased low. Systematic errors due to ice/large droplet scattering in the microwave are discussed in Chapter 4. However, ice's effect here is not as great as in the optical retrieval technique. These advantages of the microwave technique are at the core of the decision to use a passive microwave dataset of LWP as opposed to an optically retrieved dataset.

Many microwave algorithms have been developed in the past 30 years in order to retrieve LWP (e.g., Petty, 1990, Greenwald et al., 1993, Liu and Curry, 1993, Lin and Rossow, 1994, Greenwald et al., 1995, Weng et al., 1997). However the passive microwave retrieval algorithm developed by Wentz (1997) and Wentz and Spencer (1998) (and further updated in Wentz and Meissner (2007) and Hilburn and Wentz (2008)) is one of the most widely used passive microwave LWP retrieval algorithms available at present. The dataset used in this study is an updated version of the University of Wisconsin (UWisc) cloud liquid water path climatology developed by O'Dell et al. (2008), known as the Multisensor Advanced Climatology of Liquid Water Path (MAC-LWP) (Elsaesser et al., 2015). It uses data from 12 passive microwave sensors, all of which use the passive microwave Wentz retrieval, that

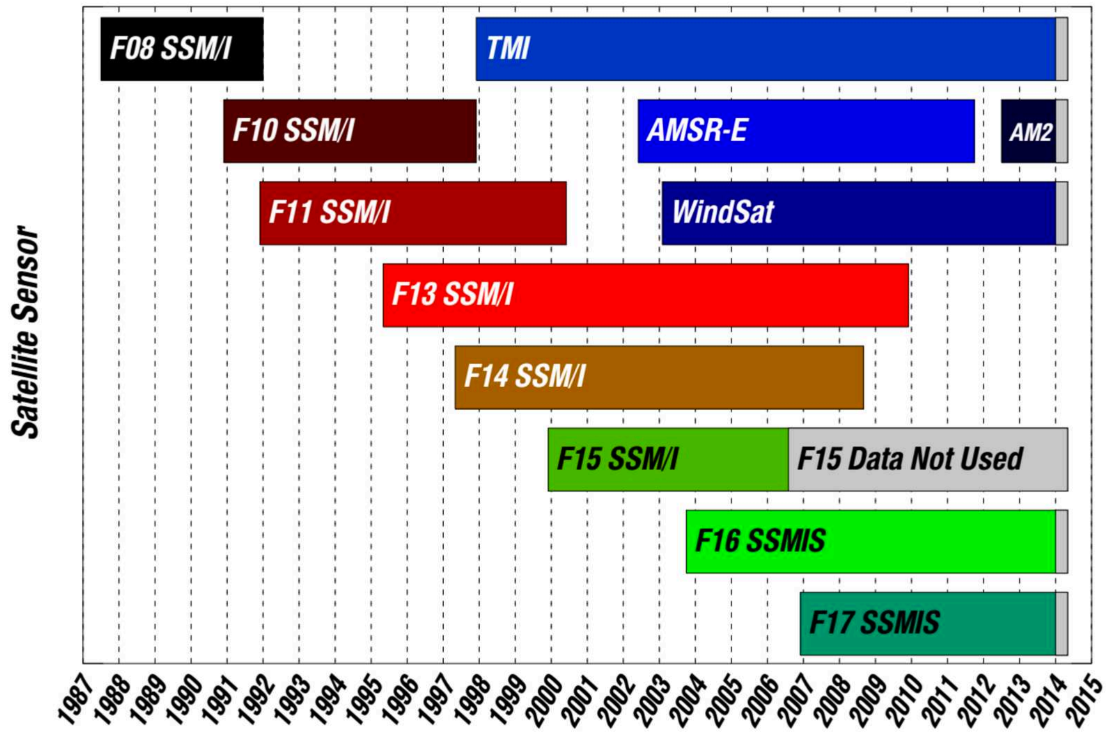

FIGURE 1.6. Taken from Elsaesser et al. (2015), figure shows the passive microwave sensors included in the MAC-LWP dataset

are intercalibrated by Remote Sensing Systems (RSS) in Santa Rosa, California. Figure 1.6 shows the passive microwave sensors blended into the MAC-LWP dataset, which extends 27 years from January 1988-December 2014 and provides a monthly mean value of LWP for each 1°x1° grid box over the ocean for every month. Each monthly value is corrected for diurnal cycle, a method not used in earlier LWP studies (e.g., Petty, 1990, Greenwald et al., 1993, Liu and Curry, 1993, Lin and Rossow, 1994, Weng et al., 1997), by fitting for the mean monthly diurnal cycle and monthly mean simultaneously (O'Dell et al., 2008).

This 27 year period of data is long enough to start seeing significant trends in the observed LWP, something which O'Dell et al. (2008) chose not to examine. Figure 1.7 shows the percentage of the globally averaged total LWP trend that the error associated with said trend represents for time series spanning various lengths of time (i.e., 3 years to 27 years at year increments). The total LWP trends were calculated using the MAC-LWP dataset using

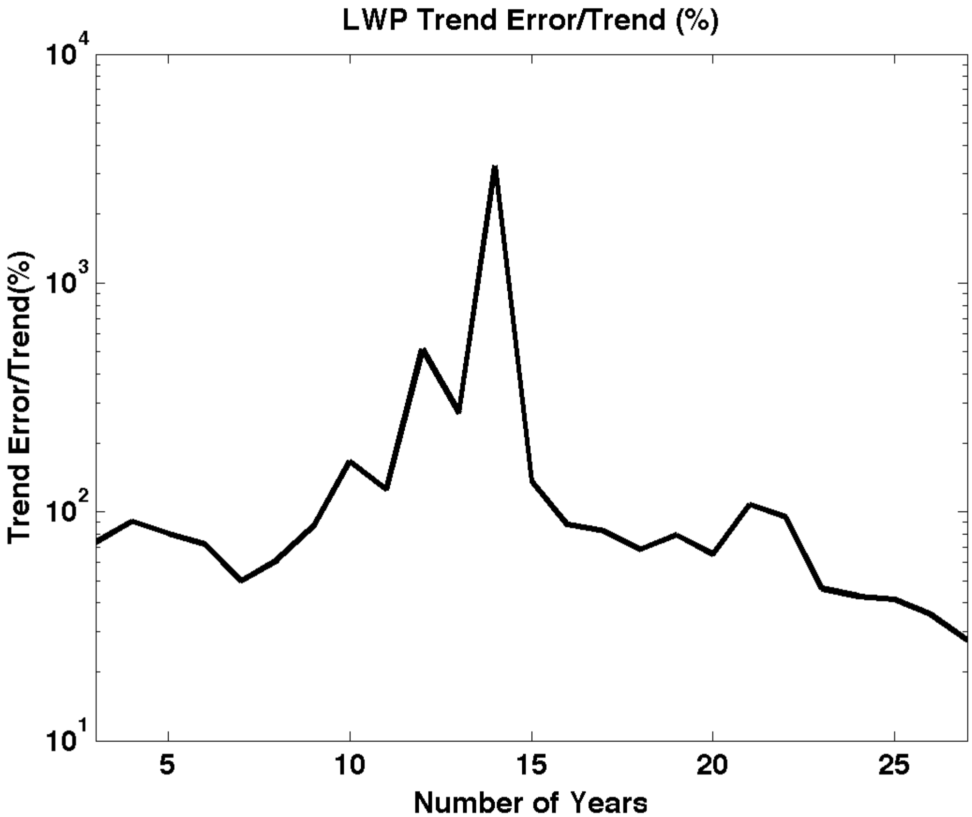

FIGURE 1.7. Calculated globally averaged LWP trend errors divided by their respective trends and expressed as a percentage for times series spanning N years where N = [3,4,5...27]

methods described in Chapter 3 while errors were calculated using the method outlined in Santer et al. (2000) which is discussed in Chapter 4. It can be seen from figure 1.7 that the percent error in trends has itself a general downward trend as the length of the LWP trend increases with an error of approximately 75% for the observed 3 year trend decreasing to an error that is only about 25% of the total observed 27 year trend. However, it can be seen that, despite the general downward trend, there is a peak midway through the time series. This corresponds to LWP trends that end in the years surrounding one of the strongest El Niño-Southern Oscillation's on records. This is a result of the method used to calculate trend errors which takes inter-annual variability into account (see Chapter 4 for more details on this method). The more of an effect inter-annual variability (e.g., the El

Niño-Souther Oscillation) has on a trend, the higher the trend's error will be as evidenced by the aforementioned peaks seen in 1.7.

It should be noted that this figure is only representation of global trends and their corresponding errors. Regional trends will generally have higher corresponding errors. In fact, most regions analyzed in this study had errors that were larger than 40% of their total trend by 27 years since they are not subject to the same cancellations of inter-annual variability and long-term climate forcing effects that the global trends are. Because of this, regional trends may require longer datasets in order for their trend error to be the same percentage of their corresponding trends that the global trend error is at the end of year 27 of the current MAC-LWP dataset. The main exception to this is the Southern Ocean, which has an error of approximately 12% of its total trend by 27 years. This Southern Ocean trend is discussed in greater detail in Chapter 3.

The MAC-LWP dataset is not without its shortcomings, however. Because all of the sensors in the dataset retrieve in the microwave, they cannot retrieve data over land, since the brightness temperatures of clouds and land surfaces are very similar. This makes accurate measurements of cloud LWP over land difficult. Microwave sensors also have difficulty separating cloud water from rain water, especially using only frequencies below 50 GHz, such as in the RSS algorithm. Although only about 6% of scenes are thought to be raining (Wentz and Spencer, 1998), this adds an extra source of error to our dataset, which is discussed in Chapter 4 along with other potential sources of systematic errors.

1.5. LWP-CRF Comparison

As mentioned previously, we wish to use this observational dataset to be able to observe long term changes in cloud radiative forcing in order to see how well they compare to modeled cloud radiative forcing. Figure 1.8 shows the correlation coefficients from January 2001-December 2014 between the observed LWP time series taken from the MAC-LWP dataset (O'Dell et al., 2008, Elsaesser et al., 2015), and the observed SWCRF and LWCRF time series taken from he CERES EBAF-TOA dataset. 1.8(a) shows strong negative correlations nearly everywhere between the observed LWP time series and observed SWCRF time series; i.e., as LWP increases (decreases) the SWCRF decreases (increases) leading to a net cooling (heating) effect. This makes physical sense, since it is expected that more (less) shortwave radiation will be reflected back to space within the presence of optically thicker (thinner) or more (fewer) clouds. 1.8(b) also shows a fairly large correlation between observed LWP and LWCRF. Unlike the correlation between LWP and SWCRF however, this correlation is positive and slightly weaker, especially in regions of low stratocumulus clouds off the Western coasts of North America, South America, and Africa where, due to the low cloud height, changes in their optical thickness do not have a large impact on OLR.. This positive correlation indicates that as LWP increases (decreases), LWCRF will also increase (decrease) leading to a net heating (cooling) effect. Again, this makes physical sense as the amount of longwave radiation absorbed by the atmosphere is expected to increase (decrease) as clouds become optically thicker (thinner) or the cloud amount increases (decreases).

The relatively strong correlations between LWP and CRF are also seen in state of the art climate models detailed in the IPCC AR5 (Flato et al., 2013). Figure 1.9 shows the correlations between the modeled LWP time series and the modeled SWCRF and LWCRF time series in NCAR's Community Earth Systems Model - Biogeochemical Cycles (CESM1-BGC), one of the models in CMIP5, from January 2001-December 2014 (information on how LWP and CRF time series were created using CMIP5 data can be found in section 2.2). It should be noted that other models examined in this study (Table **??**) exhibit similar

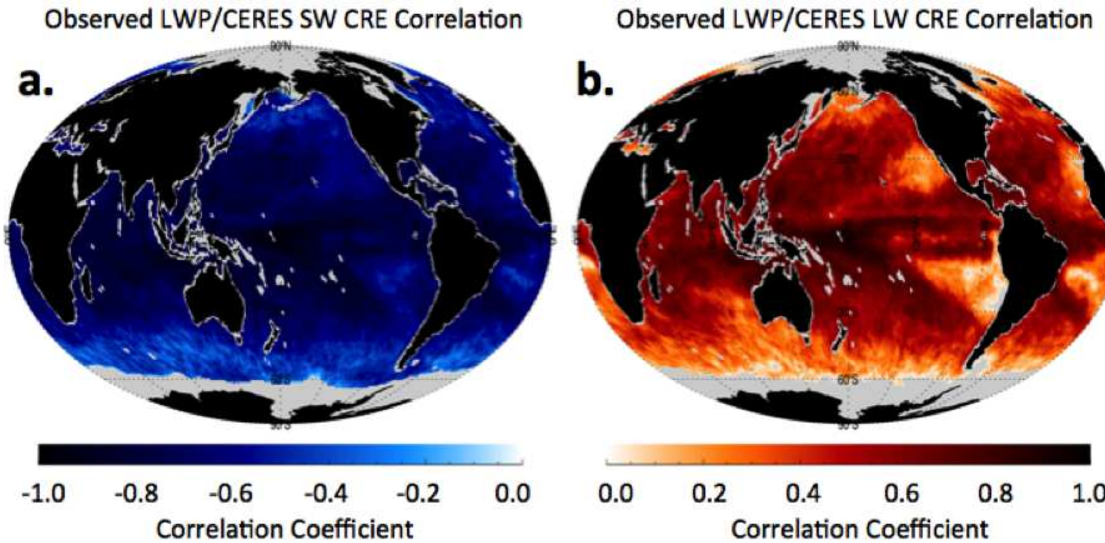

FIGURE 1.8. Correlation coefficients between the observed LWP time series and the observed (a) SWCRF and (b) LWCRF time series from January 2001-December 2014. LWP observations are from the MAC-LWP dataset (O'Dell et al., 2008). CRF observations are from the CERES EBAF Ed2.8 dataset. Black areas indicate landmasses while gray shading indicates missing data. Note that (a) ranges from -1.0 to 0 while (b) ranges from 0 to 1.0

correlations and behavior to CESM1-BGC. When compared to figure 1.8, figure 1.9 shows very similar relationships between the modeled LWP and CRFs and the observed LWP and CRFs even capturing some of the features seen in the observations, e.g., the relative minima in correlation coefficient between LWP and LWCRF in the marine stratocumulus regions.

In this work, the MAC-LWP dataset is used to calculate trends in LWP both globally and regionally. These trends are subsequently compared to global and regional trends of LWP in a suite of CMIP5 models. The hope is that by comparing these trends, it will illuminate whether or not changes in cloud liquid water path are correctly modeled and how this affects cloud radiative forcing, which subsequently affects cloud feedbacks and equilibrium climate sensitivity. The rest of this thesis is organized as follows: Chapter 2 further discusses the MAC-LWP dataset and the suite of CMIP5 models used and compares several mean state LWP variables between the two. Chapter 3 discusses and compares the observational and

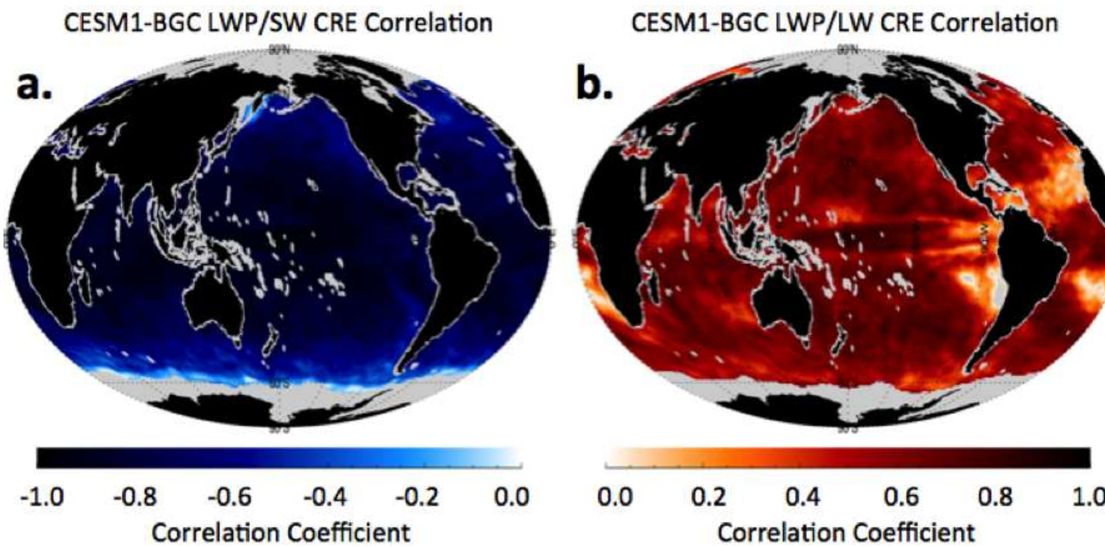

Figure 1.9. Correlation coefficients between the modeled LWP time series and the modeled (a) SWCRF and (b) LWCRF time series from January 2001-December 2014. Data are taken from the NCAR Community Earth Systems Model - Biogeochemical Cycles (CESM1-BGC) from the CMIP5 database. See Table **??** for more information. Black areas indicate landmasses while gray shading indicates missing data. Note that (a) ranges from -1.0 to 0 while (b) ranges from 0 to 1.0

modeled trends. Chapter 4 discusses potential systematic error sources in both mean state LWP and LWP trends. Chapter 5 provides a summary of the work, conclusions, and potential future directions for this work.

CHAPTER 2

Datasets and Methods

This chapter outlines the main datasets used in this work. These include the MAC-LWP record and a suite of CMIP5 models. Mean state LWP and the mean seasonal cycle range of LWP in the MAC-LWP record are examined to lend validity to the choice of using this dataset to assess the realism of modeled LWP. The suite of CMIP5 models and variables used in this experiment is outlined in detail. Qualitative and quantitative comparisons of mean state LWP metrics in the MAC-LWP dataset and the CMIP5 models are made in an attempt to determine which models (if any) are more likely to capture observed trends in LWP.

2.1. MAC-LWP Dataset

As mentioned in section 1.4, the MAC-LWP dataset (Elsaesser et al., 2015) is an updated version of University of Wisconsin (UWisc) cloud liquid water path (LWP) climatology O'Dell et al. (2008). It contains 27 years of LWP data (1988-2014) observed from 12 different passive microwave sensors. The dataset provides a monthly mean value of LWP for each 1°x1° grid box over the ocean for every month. It should be noted that the LWP given for each grid box represents the average LWP over the entire grid box i.e., sections of clear-sky where LWP is theoretically zero are included in the grid box averaged LWP (the LWP output at each grid box in the suite of CMIP5 models is averaged in the same way). The MAC-LWP data used inter-calibrated, level-2 ocean retrievals from Remote Sensing Systems' (RSS) version 7 algorithm (Wentz, 1997, Wentz and Spencer, 1998, Wentz and Meissner, 2000, Hilburn and Wentz, 2008, Wentz, 2013). MAC-LWP monthly mean LWP values were corrected for diurnal cycle by fitting for the mean monthly diurnal cycle and monthly mean simultaneously. Figure 2.1 shows the LWP time series from two different sensors in the MAC-LWP dataset for 3 different grid boxes before and after this diurnal cycle correction. When this correction is applied, the sensors show little to no difference from one another. Thus this correction helps to eliminate any spurious LWP trends that may arise from averaging non-diurnally corrected LWP time series over multiple sensors. For more information on these diurnal cycle corrections please see O'Dell et al. (2008) and Elsaesser et al. (2015). Systematic errors present in the dataset can be as large as 30% O'Dell et al. (2008) and include, but are not limited to: cross-talk errors, cloud-rain partitioning, effects from ice, cloud top temperature errors, and clear-sky biases. These errors and their potential effects on LWP trends are discussed in greater detail in Chapter 4.

2.1.1. Mean State LWP. In order to asses the validity of the MAC-LWP as a diagnostic tool for climate models, two key factors must be examined: the validity of the observed LWP and the validity to compare this LWP to models. Figure 2.2 shows the observed mean state LWP from MAC-LWP. The data is first deseasonalized, then the monthly means from every month in the dataset are averaged at each 1°x1° grid box. If more than 10% of monthly data is missing for a given grid box, the mean is not calculated and is set to missing. These missing values, indicated by gray shading, tend to occur in regions of sea ice and close to land masses. This is due to the difficultly of retrievals by passive microwave sensors in these areas.

Qualitatively, figure 2.2 appears to be consistent with our knowledge of clouds and cloudiness in various regions in the world. There is a maximum of LWP in the equatorial Intertropical Convergence Zone (ITCZ) region, due to high amounts of deep convective clouds along the equator. Other relative maxima exist in the cloudy storm track regions in the North Atlantic, North Pacific, and Southern Oceans. Several minima can be seen in figure 2.2,

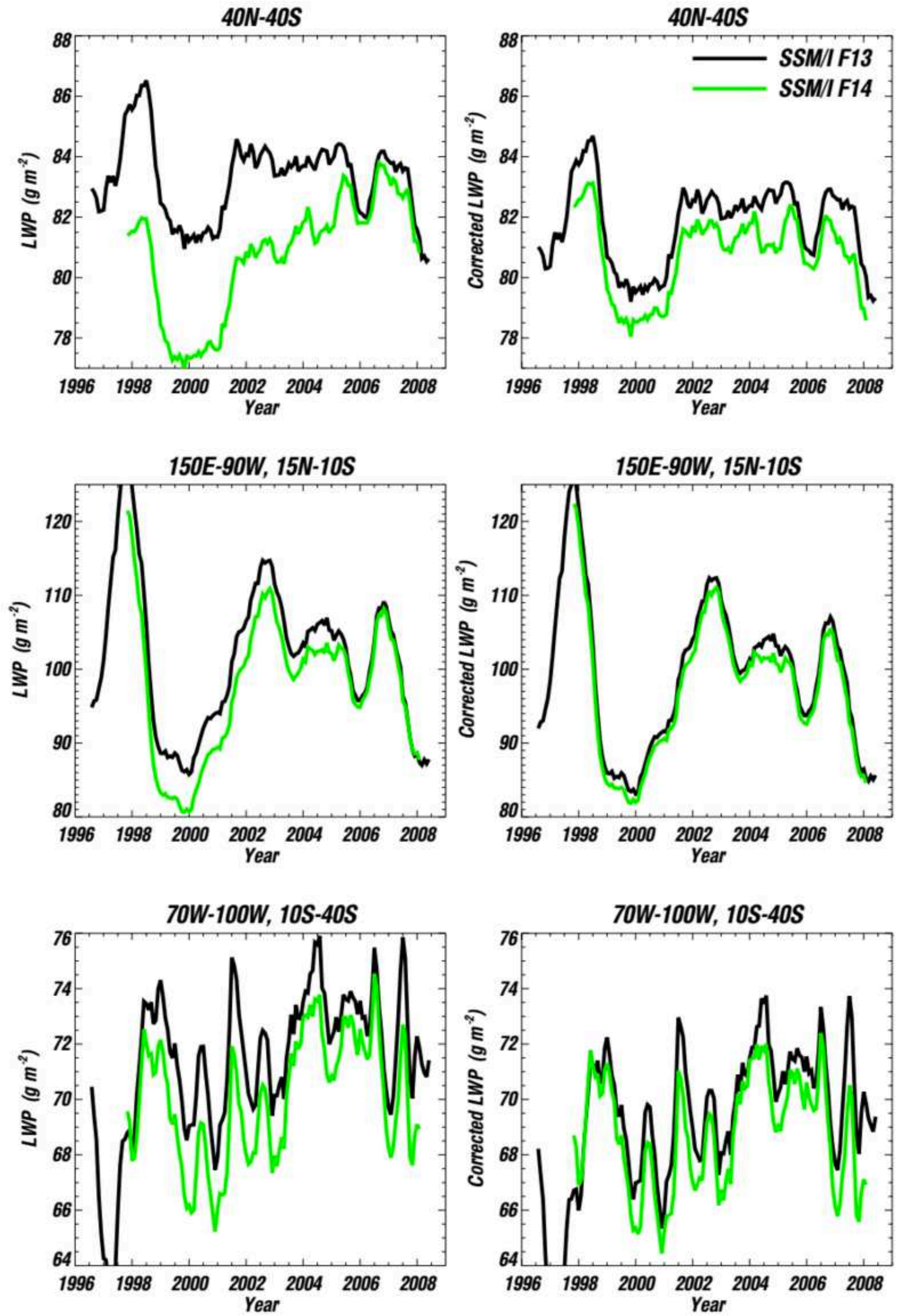

FIGURE 2.1. Adapted from Figure 9 of Elsaesser et al. (2015). Shows LWP time series for 3 different grid boxes from two different sensors used in the MAC-LWP dataset (SSM/I F13 and SSM/I 14). The left panel displays the time series before the diurnal cycle correction while the right panel displays the two time series after the diurnal cycle correction

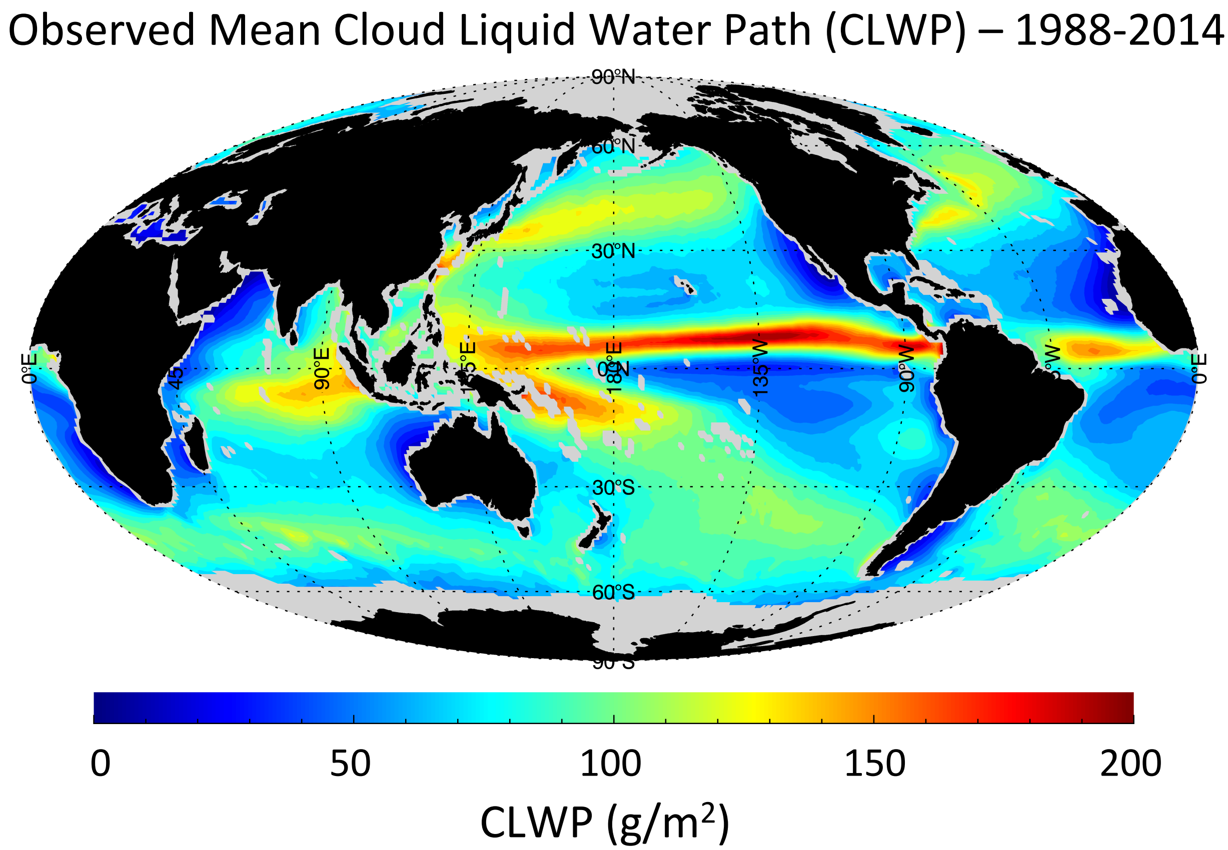

Figure 2.2. Observed mean state LWP for the period 1988-2014. Black shading indicates land while gray shading indicates areas of missing data

most occurring in regions of subsidence such as the latitudes immediately North and South of the ITCZ.

The information presented in figure 2.2 also appears to be quantitatively consistent with our knowledge of global variations in LWP. The calculated globally averaged LWP from the MAC-LWP dataset is approximately 81 g/m^2, which is consistent with previous estimates of this quantity given in Horvath (2004).

2.1.2. Mean Seasonal Cycle of LWP. Another variable we can discuss in the MAC-LWP dataset is the mean seasonal cycle amplitude of LWP at each grid-box. To determine these values, the average LWP for January, February, etc... was computed at each individual

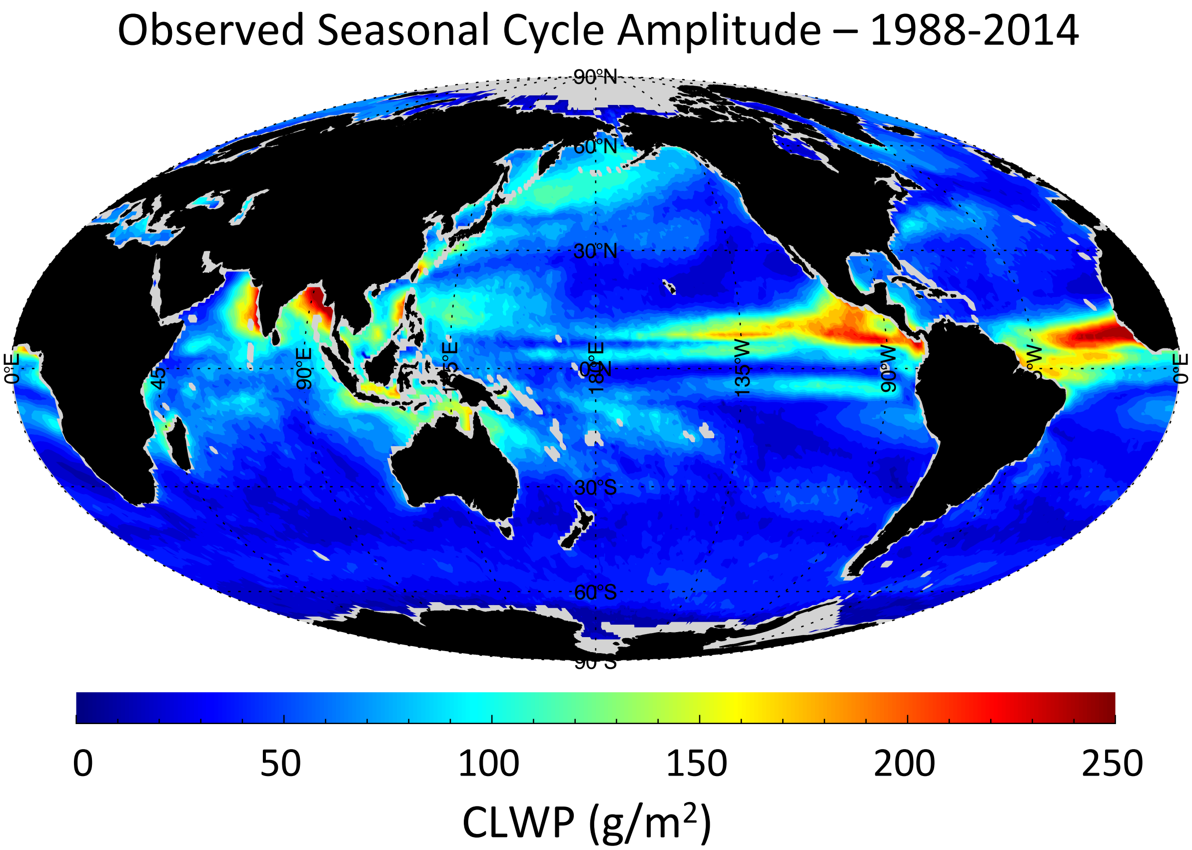

FIGURE 2.3. Observed amplitude of the mean seasonal cycle for each pixel for the period 1988-2014. Black shading indicates land while gray shading indicates areas of missing data

grid-box to give the mean seasonal cycle. The maximum and minimum values of the resulting mean seasonal cycle were differenced. Note that amplitude is defined here as the peak-to-peak difference in the mean seasonal cycle. The results of the calculation can be seen in figure 2.3.

Much like the observed mean state LWP, these data are qualitatively consistent with our knowledge of the seasonal cycles of LWP. The largest amplitudes in the mean seasonal cycle occur in regions that are subject to extreme seasonal variations in cloudiness and storms. For instance, some of the highest values on the globe can be found in the Bay of Bengal and the Arabian Sea just West of India. These regions are subject to seasonal monsoons and which cause large variations in their cloudiness between the wet and dry seasons. Similarly, areas where tropical cyclones tend to form, such as off the West coasts of Africa and South America, also have large ranges in the mean seasonal cycle since these tropical cyclones only form at certain times of year. Small ranges in the mean seasonal cycle tend to occur in regions such as the West coast stratocumulus regions off most continents where cloud amount and thickness remain relatively constant throughout the year.

2.2. CMIP5 Data

For this work, the observed trends LWP from the MAC-LWP dataset were compared against LWP trends in 16 different models from CMIP5 (Taylor et al., 2012). These models are listed in figure 2.4 which is partially adapted from tables 1 and 2 in Jiang et al. (2012) and Lauer and Hamilton (2013), respectively. The data were obtained from the Program for Climate Model Diagnosis and Intercomparison (PCMDI) archive (https://pcmdi9.llnl.gov/projects/cmip5/. First accessed August, 2014). 12 models with CMIP3 counterparts, as outlined by Jiang et al. (2012), were initially chosen so a comparison between between LWP trends in CMIP3 and CMIP5 could be done. However, it was later decided that an analysis of CMIP3 data was not pertinent to the current work and 4 other models (CCSM-4, CMCC-CM, CESM1 BGC, GFDL esm2g) were added to the suite of models used in the current experiment.

For this analysis, only data from the r1i1p1 ensemble run for every model were used. This removed potential errors from averaging several different ensemble runs together since different models had different numbers of ensemble runs, and would have artificially reduced noise associated with inter-annual variability. A brief analysis to determine the magnitude of the spread in LWP trends in ensemble runs was done. It was found that the spread in

Model	Center	Country	Resolution	AMIP(Y/N)	References
BCC csm1.1	Beijing Climate Center	China	2.8°x2.8°, L26	Y	Wu et al. (2010), Wu et al. (2012)
CCMA canesm2	Canadian Center for Climate Modeling and Analysis	Canada	2.8°x2.8°, L35	N	Arora et al. (2011)
CCSM-4	National Center for Atmospheric Research	United States	1.25°x0.9°, L26	Y	Gent et al. (2011)
CESM1 BGC	National Center for Atmospheric Research	United States	1.25°x0.9°, L26	N	Lindsay et al. (2014)
CESM CAM5	National Center for Atmospheric Research	United States	1.25°x0.9°, L26	N	Conley et al. (2012)
CMCC-CM	Centro Euro-Mediterraneo per I Cambiamenti Climatici	Italy	0.75°x0.75°, L31	Y	Scoccimarro et al. (2011)
CNRM cm5	Centre National de Recherches Meteorologiques	France	1.4°x1.4°, L31	Y	Voldoire et al. (2013)
CSIRO mk3.6	CSIRO Marine and Atmospheric Research, Queensland Climate Change Center of Excellence	Australia	1.9°x1.9°, L18	N	Rotstayn et al. (2010)
GFDL cm3	NOAA Geophysical Fluid Dynamics Laboratory	United States	2.5°x2°, L48	Y	Donner et al. (2011)
GFDL esm2g	NOAA Geophysical Fluid Dynamics Laboratory	United States	2.5°x2°, L24	N	Dunne et al. (2012)
GISS e2-h	NASA Goddard Institute for Space Studies	United States	2.5°x2°, L40	Y	Schmidt et al. (2014)
GISS e2-r	NASA Goddard Institute for Space Studies	United States	2.5°x2°, L40	N	Schmidt et al. (2014)
INM cm4	Institute for Numerical Mathematics	Russia	2°x1.5°, L21	Y	Volodin et al. (2010)
IPSL cm5a-MR	Institute Pierre-Simon Laplace	France	2.5°x1.25°, L39	Y	Dufresne et al. (2013)
MIROC miroc5	AORI, NIES, and JAMSTEC	Japan	1.4°x1.4°, L40	Y	Watanabe et al. (2010)
NCC noresm	Norwegian Climate Centre	Norway	2.5°x1.9°, L26	Y	Kirkevåg et al. (2013)

FIGURE 2.4. List of the 16 CMIP5 models used in this study along with pertinent information

trends between various ensemble members was much smaller than the intermodel differences, therefore reaffirming the use of only one ensemble. For each model the 'historical' and 'rcp4.5' experiments were combined to create a time series that spanned the exact same length as the MAC-LWP dataset (27 years from 1988-2014).

In order to better facilitate a one-to-one comparison, all the model data were regridded to the same 1°x1° grid spacing as the observations using a simple bi-linear interpolation. Every model contained LWP information at every grid box, so each model was masked the same as the observations i.e., data that were missing in a given month in the observed dataset were also set to missing in the model output.

Since LWP does not have a specific output variable in the CMIP5 suite of models, it needed to be calculated by subtracting the ice water path variable, 'clivi', from the total water path variable, 'clwvi'. For some models, however, 'clwvi' was liquid water path (Jiang et al., 2012). This could be seen when subtracting 'clivi' from 'clwvi' resulted in large negative values of LWP. These models included CCSM-4, CMCC-CM, CESM CAM5, and IPSL cm5a-MR. A list of other models where this error is present can be found on the PCMDI CMIP5 errata webpage (http://cmip-pcmdi.llnl.gov/cmip5/errata/cmip5errata.html). The CMCC was contacted about this problem since their model did not show up as one containing this error on the errata webpage. They are currently in the process of fixing it. It also should be noted that in recent studies (Jiang et al., 2012, Lauer and Hamilton, 2013), the CSIROmk3.6 model was found to contain this error as well, however, in the current work, it appeared to be fixed.

2.3. Comparisons of Mean State LWP Observations to CMIP5 Models

Although comparisons of trends are the focus of the current study, it is important to examine how the observations of mean state LWP compare to the mean state produced by CMIP5 models. This follows similar work done by Lauer and Hamilton (2013). By evaluating these mean states, it can be better understood how the models handle LWP and potentially provide insight as to which models can be expected to better capture trends in LWP both regionally and globally. Presumably, models that better reproduce mean state LWP variables will have better underlying moist physics and will thus better replicate observed LWP trends.

2.3.1. Qualitative Model Metrics. Two different mean states were examined in the models and compared to observations. The first of these was the mean state LWP. This was calculated for the models in the exact same way as the observed mean state LWP as described in section 2.1.1. Figure 2.5 shows the mean state LWP for 4 arbitrarily chosen models from the 16 used in this study. In comparing these models to the observed mean state LWP in figure 2.2 it can be seen that these models tend to capture some features seen in the observations e.g., the relative higher amounts of LWP in the ITCZ. However, the magnitudes of certain features can vary dramatically between the models and observations and even from model to model. For instance, in 2.5(a) shows generally higher values of model LWP across most of the globe when compared to observations, including unrealistically high ($>$200 g/m^2) LWPs in the high latitudes. Conversely, 2.5(c) shows unrealistically low LWPs everywhere while still capturing some features such as the storm track and South Pacific Convergence Zone (SPCZ) regions.

The other quantity that was examined was the mean seasonal cycle amplitude for LWP. This was, again, calculated the exact same way as it was for the observed mean seasonal cycle amplitude in section 2.1.2. Figure 2.6 shows the mean seasonal cycle amplitude for the same 4 models as figures 2.5. Similar to the mean state LWP, the mean seasonal cycle amplitude in the models captures some features seen in the observations e.g., the relative maxima in the North Pacific storm track, but vary in magnitude. Some models appear to capture certain mean seasonal cycle amplitudes seen in the observations, while others do not. For instance figure 2.6(a) depicts the large mean seasonal cycle amplitude in LWP in the monsoon region in the Bay of Bengal, while this does not appear to be present in other models such as the INM cm4 (figure 2.6(c)).

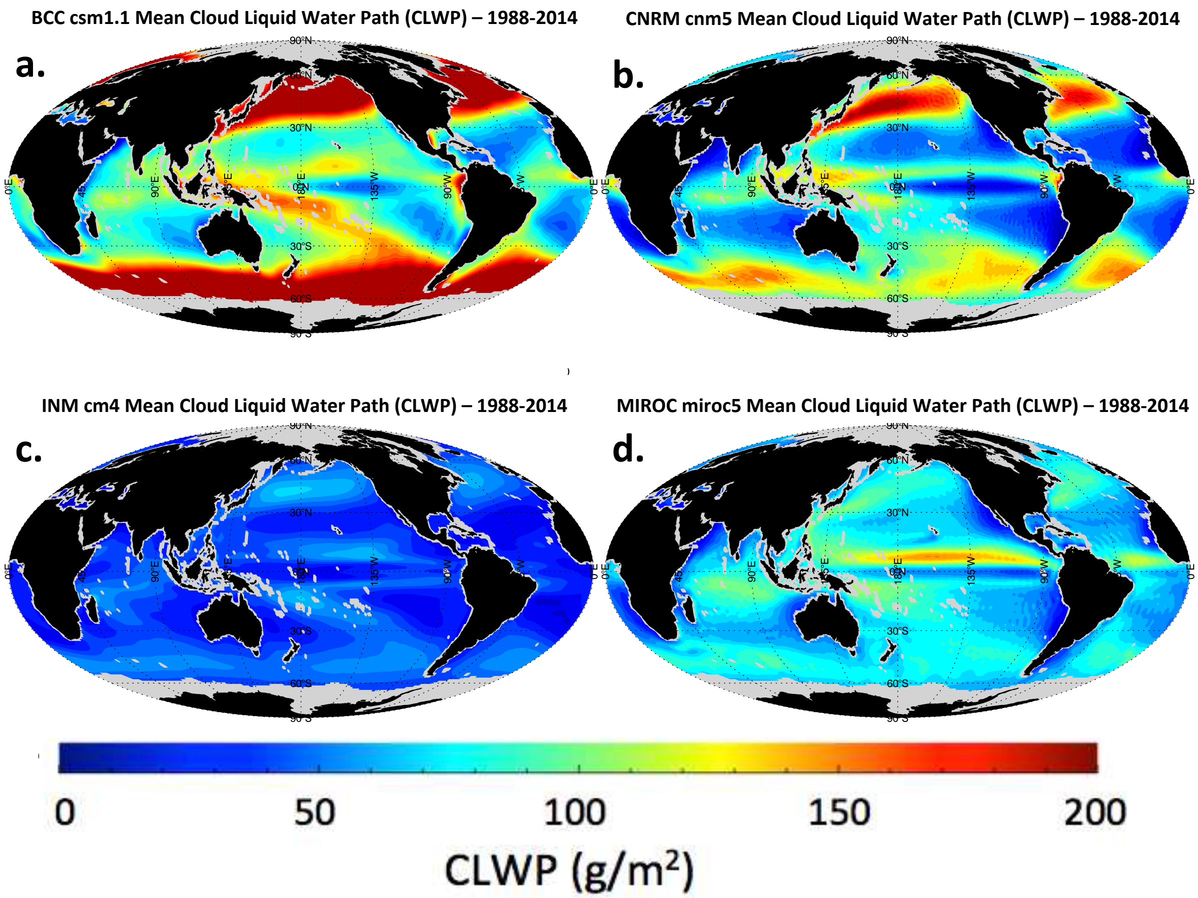

FIGURE 2.5. Mean state LWP in g/m^2 for the period 1988-2014 for several different models including (a) BCC csm1.1 (b) CNRM cm5 (c) INM cm4 (d) MIROC miroc5. For more information on these models see figure 2.4

2.3.2. QUANTITATIVE MODEL METRICS. Qualitatively it can be seen that the models share similarities and differences with the observations. This begs the question as to how well these similarities and differences can be used as predictors of model performance in capturing LWP trends. In this work, quantitative model metrics were calculated in an attempt to use them as predictors for model performance. Two different metrics were chosen: the pattern correlation coefficient and the Root Mean Square Error (RMSE) which were both calculated between the observed and modeled mean state LWP and the observed and modeled mean seasonal cycle amplitude in each model. The mean state pattern correlation coefficient shows how well various maxima and minima are captured on a mean state global map. High positive

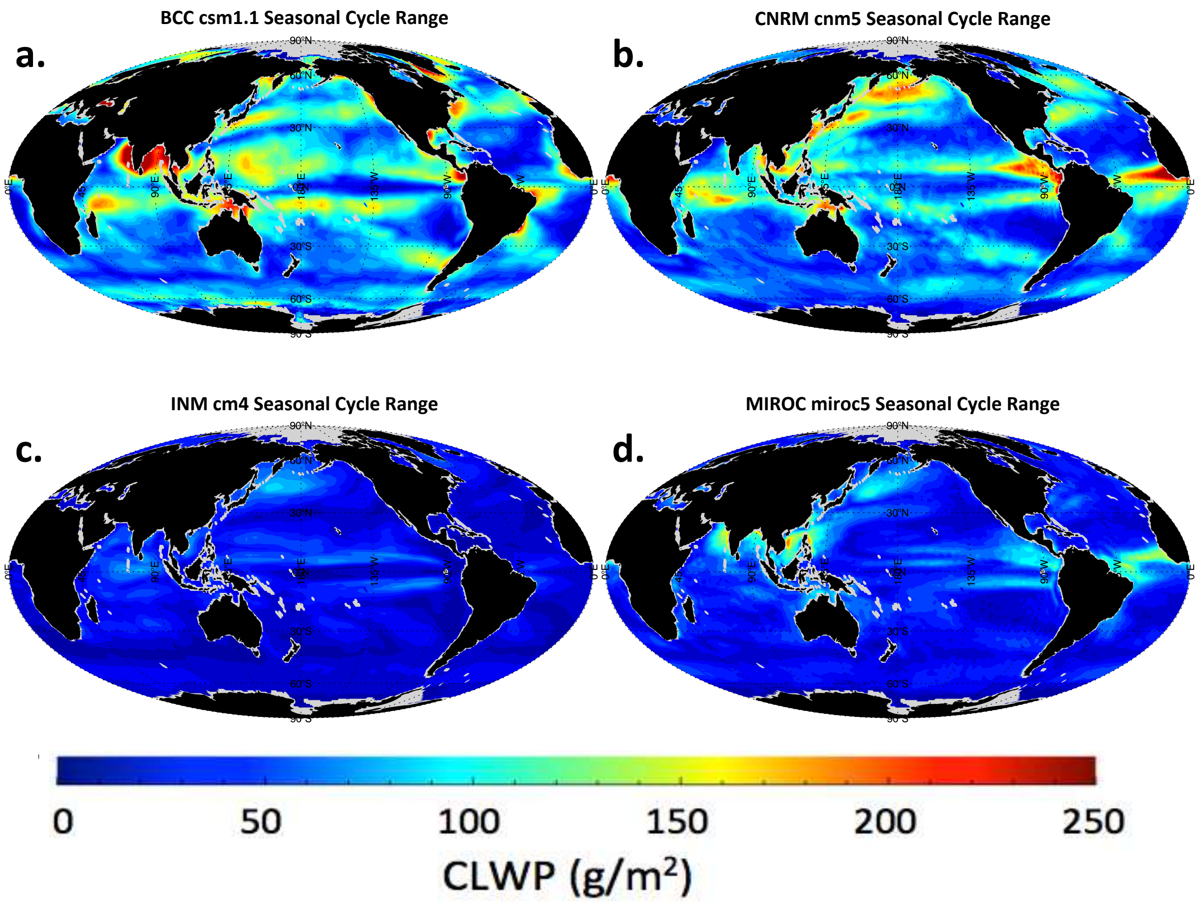

Figure 2.6. Amplitude of the mean seasonal cycle in g/m^2 in for each pixel for the period 1988-2014 for several different models including (a) BCC csm1.1 (b) CNRM cm5 (c) INM cm4 (d) MIROC miroc5. For more information on these models see figure 2.4

values of pattern correlation coefficient indicate stronger co-location of maxima and minima between the observed mean state and the modeled mean state. Large negative values of this metric indicate regions of maximum mean state values being more co-located with regions of minimum mean state values and vice versa. The second metric that was used to compare models and observations was the Root Mean Square Error (RMSE) as it is a good measure of the accuracy of the model at predicting observed behavior. Equation 2 is used to calculate the global mean area weighted RMSE between the observations and the models

$$RMSE = \sqrt{\frac{\sum_{i=1}^{N}(x_i - y_i)^2 w_i}{\sum_{i=1}^{N} w_i}} \tag{2}$$

where N is the total number of grid boxes, x is the observed mean state variable for grid box i, y is the model mean state variable for grid box i, and w is equal to the cosine of the latitude of grid box i. The closer the RMSE is to zero, the better the model is at predicting the observed mean state.

Figure 2.7 shows the Pattern Correlation Coefficient and RMSE for all 16 models used in this study for mean state LWP. Models that have a higher Pattern Correlation Coefficient tend to have a lower RMSE and vice versa. This work yielded similar results to Lauer and Hamilton (2013). Although the exact values and the ranking of the models differed slightly, the models that performed better/worse in capturing the mean state in Lauer and Hamilton (2013) tended to perform likewise in this study. The slight differences could potentially be due to differences in the time period examined (Lauer and Hamilton (2013) compared mean states from 1988-2005 instead of 1988-2014).

Similar to figure 2.7, figure 2.8 shows the Pattern Correlation Coefficient and RMSE for all 16 models used in this study only this time for mean LWP seasonal cycle amplitude. Like the mean state LWP, models that tend to have a higher Pattern Correlation Coefficient tend to have a lower RMSE and vice versa, however, this relationship is not as pronounced as in the mean state LWP with more models having a high correlation coefficient but also a high RMSE and vice versa. Models that tend to capture the mean state LWP better also tend to better capture the mean LWP seasonal cycle amplitude.

As previously mentioned, these model metrics were calculated to test the hypothesis that models which capture mean state LWP variables more accurately may be expected to capture LWP trends more accurately. However, these metrics were found to be relatively

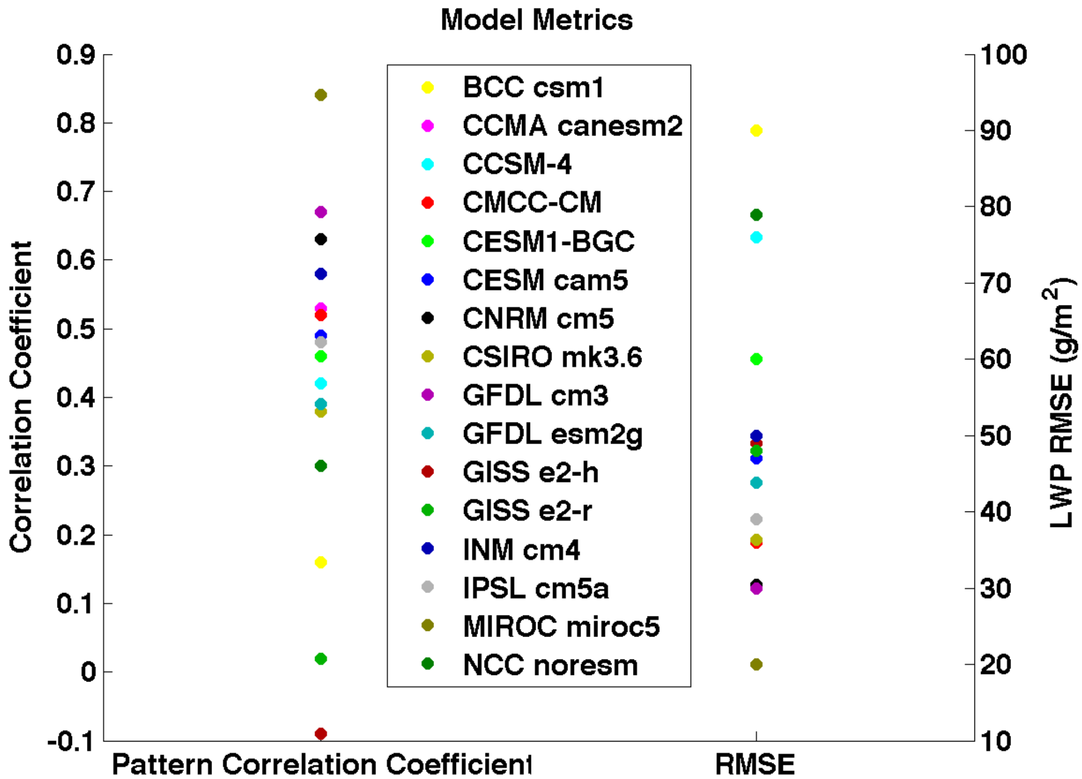

FIGURE 2.7. 2 different model metrics, Pattern Correlation Coefficient and Root Mean Square Error (RMSE), used to compare models to observations. Higher values of Pattern Correlation Coefficient and lower values of RMSE indicate better model performance when capturing mean state LWP

poor predictors of trends in LWP. In the various regions that were examined (see Chapter 3), different models better captured the observed trends in LWP with no models performing consistently better than others. This would seem to imply that LWP trends in models are driven more by large-scale climatic drivers or some other modeled process as opposed to moist physics parameterizations. Chapter 3 examines the trends in observed and modeled LWP in greater detail.

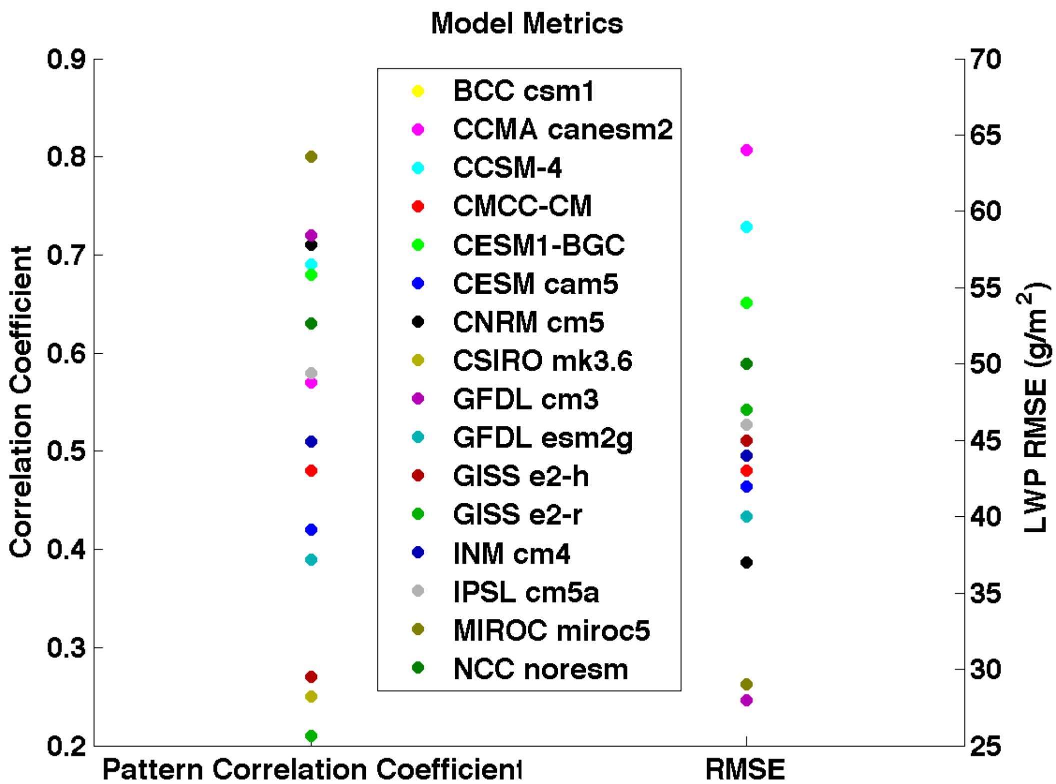

FIGURE 2.8. Same metrics (Pattern Correlation Coefficient and RMSE) as calculated for figure 2.7 except for mean LWP seasonal cycle amplitude

CHAPTER 3

Trend Analysis

This chapter analyzes trends in liquid water path and other related constituents from the datasets outlined in Chapter 2. As previously discussed, changes in LWP are closely related to changes in CRF, therefore analysis of LWP changes is important for our understanding of changes in CRF. One can imagine that, assuming robustness of the observed dataset (discussed in Chapter 4), the better CMIP5 models capture trends in LWP, the more accurately they will capture changes in CRF and subsequently cloud feedbacks. This chapter attempts to show how well the modeled and observed trends agree. Details are given on how the trends are calculated. 27 year trends for 6 regions examined in this study are analyzed using the CMIP5 models given in figure 2.4. LWP trends in the various regions are examined using the AMIP experiments of the CMIP5 models which use prescribed sea surface temperature as opposed to an ocean model. Similarly, LWP trends are examined using the ERA-interim model reanalysis data as a test to see if datasets that included more observational data would better replicate observed LWP trends. Finally trends in Total Water Path obtained from the passive microwave sensors in the MAC-LWP dataset are calculated and compared to the MAC-LWP Liquid Water Path in an attempt to help determine any errors that may present themselves in the LWP trend calculation due to the cloud-rain partitioning in the retrieval algorithm used in the sensors that make up the MAC-LWP dataset.

3.1. General Overview of Data

Trends in LWP were calculated in two different datasets, the observed MAC-LWP and modeled CMIP5 (as described in Chapter 2), and then compared in order to assess the realism of the model LWP trends. Six different regions were chosen for comparison: The Western Pacific Warm pool (14.5°S-15.5°N, 120.5°E-150.5°E), the North American Stratocumulus Deck (15.5°N-35.5°N, 144.5°W-124.5°W), the South American Stratocumulus Deck (29.5°S-9.5°S ,89.5°W-69.5°W), the Southern Ocean (59.5°S-44.5°S, 0.5°E-359.5°E), the North Atlantic Storm Track (35.5°N-50.5°N, 74.5°W-34.5°W) , and the entire globe. These regions were chosen because they encompassed a wide range of cloud regimes some of which vary significantly depending on the time of year, others which remain relatively constant in cloud amount and optical depth from season to season. These regions are shown as boxes in figure 3.1.

Before this comparison, several modifications were applied to the data. First, the models were sampled exactly like the observed values, in terms of grid size (1°x1°), years observed, and missing data. This procedure is detailed in section 2.2. Second, both observed and modeled data were deseasonalized by removing the mean monthly seasonal cycle from every month in each dataset. This was done to remove potential errors in trends caused by the seasonal cycle in LWP, specifically due to potential nonuniform sampling of the seasonal cycle in different regions of the globe. The modeled data were regridded, masked, and set to span the same time period as the observations.

3.1.1. Threshold Calculation. Trends were calculated in this study by taking the area weighted average of LWP for each month in a given region, creating a time series from these values and fitting a best fit line using least squares linear regression. However, some months had significantly fewer pixels that contained data compared to other months. If every pixel with data in each month were used in the area weighted LWP calculation, it could potentially create spurious trends. In order to account for this, a method that will henceforth be known as the Threshold Method was used. The first step of the Threshold

Method was to identify all of the pixels in a given region that never had data at any point during the dataset. For the most part, these pixels were landmasses or just offshore of landmasses where the microwave sensors could not retrieve data. Once identified, these pixels were ignored in any further calculations. The next step was to choose a threshold i.e., a percentage of remaining pixels (ones that were not always missing) that needed to be present in order for a given month to be included in the time series which a trend line would be fitted to. For the majority of the regions, this threshold was set at 90% meaning that 90% of remaining pixels needed to have data in order for the month to be included in the time series. For two regions (The Western Pacific Warm Pool and the entire globe), this threshold was set at 85%. This was due to the fact that too many months were eliminated from the time series at higher thresholds for these regions. Pixels in months that had less than their threshold value (90% or 85%) were set to missing and not included in the final time series calculation.

After months below the threshold for a given region were eliminated, the next step in the Threshold Method was to figure out which pixels in the remaining months had data for every month of the dataset. These were the only pixels that were used in the area-weighted average LWP calculation for each month. Pixels that did not contain data in every remaining month were ignored in the area-weighted LWP calculation.

3.2. 27 Year Trends

Figure 3.1 shows the trends in LWP over the past 27 years for both the observations and the CMIP5 model mean. If over 10% of the data for the entire record were missing in a given grid box, the trend was not calculated and the grid box value was set to missing. The first thing that should be noted when comparing the two maps is the difference in magnitude

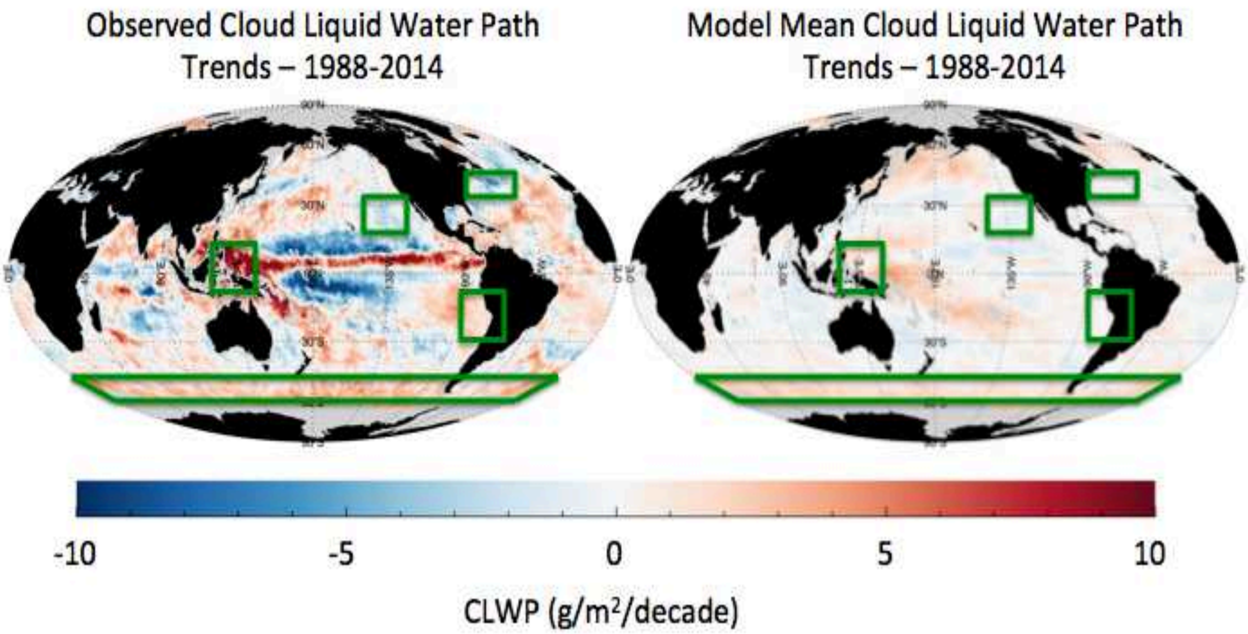

FIGURE 3.1. Global maps of trends in LWP over the past 27 years for (a) passive microwave observations and (b) the CMIP5 model mean. Black shading indicates land while gray shading indicates missing data

between the trends over almost the entire globe. The observed trends tend to be much higher than the ones seen in the CMIP5 model mean, especially in regions such as the equatorial pacific where trends in the observations were found to be almost 4 times greater than the model mean.

Figure 3.2 illustrates potential reasons for the disparity in magnitude of global trends between the model mean and observations. 3.2(a)-(e) each show the 27 year global LWP trends for a different ensemble run of the MIROC miroc5 CMIP5 model. 3.2(f) shows the ensemble mean of (a)-(e). It can be seen that the trends in (a)-(e) are, in general, larger than most of the trends seen in 3.2(f). This is likely due to cancellation effects which help to remove inter-annual variability. These effects can be translated from this individual ensemble/ensemble mean comparison (as is shown in figure 3.2) to an individual model/model mean comparison. Since most climate models cannot explicitly resolve specific events such

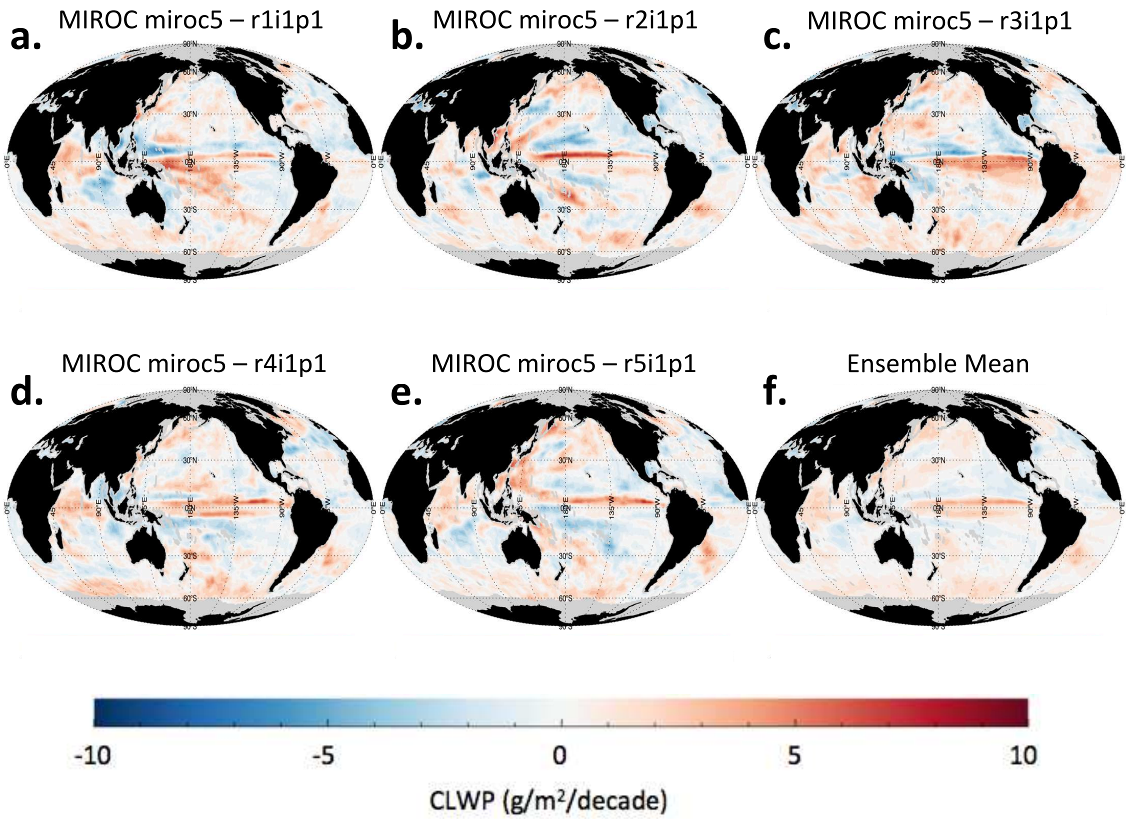

FIGURE 3.2. Maps showing the 27 year global, LWP trends from (a-e) 5 different ensemble runs and (f) the ensemble mean from the MIROC miroc5 model

as those associated with the El-Niño Southern Oscillation, their modeled inter-annual variability is highly dependent on variables such as the way the model is initialized (i.e., initial conditions) and underlying model physics. These differences lead to cancellation effects which remove most of the inter-annual variability between models. This causes remaining trends to mostly arise due to forced variability that is common among models. The observed trends, like the models, arise due to a combination of inter-annual variability and forced variability, however, unlike the model mean trends, the observed trends do not suffer from the cancellation effects that affect models.

With these cancellation effects in mind, figure 3.1 shows that signs of the trends for the observations and the model mean have the tendency to oppose one another in various regions globally. This appears to be due to the model mean shifting certain features relative to the observations. For instance, the model mean appears to put the large positive trend associated with the SPCZ too far north and extends it too far to the east. The model mean also appears to place the negative LWP trends in the North Pacific and North Atlantic storm tracks too far south relative to the observations. Despite these differences, there are still several regions where both the model mean and the observations agree. For instance, both capture the relative positive maxima in the Western Pacific Warm Pool and the robust positive trend in the Southern Ocean.

The similarities and differences between the models and the observations are further illustrated in figure 3.3 which shows the zonally averaged LWP trends in the observations, CMIP5 model mean, and the individual CMIP5 models used in this study. The CMIP5 model mean and the observations both show increasingly positive LWP trends at higher latitudes, except for the high northern latitudes where the observed trends appear to drop off significantly. This is likely due to sea ice effects at these high latitudes. Another feature seen in the observations in figure 3.3 is the large positive trend just north of the equator, roughly the locations of the ITCZ, flanked on either side by negative trends in the observations. This appears to be a manifestation of the ”rich get richer, poor get poorer” concept (e.g., Held and Soden, 2006, Collins et al., 2013) which hypothesizes that, in a warming climate, wet regions (e.g., the ITCZ) will get wetter while dry (e.g., subsidence regions) will get drier. This mechanism appears to be partially responsible for the ’W’ shape of the zonally averaged observed LWP trends. It should be noted that section 4.3 shows that trends in the Western Pacific warm pool are largely driven by inter-annual variability whereas the effects of inter-annual variability appear to have less of an impact on LWP at other latitudes. This indicates that the spike in observed trends around the equator is potentially largely driven

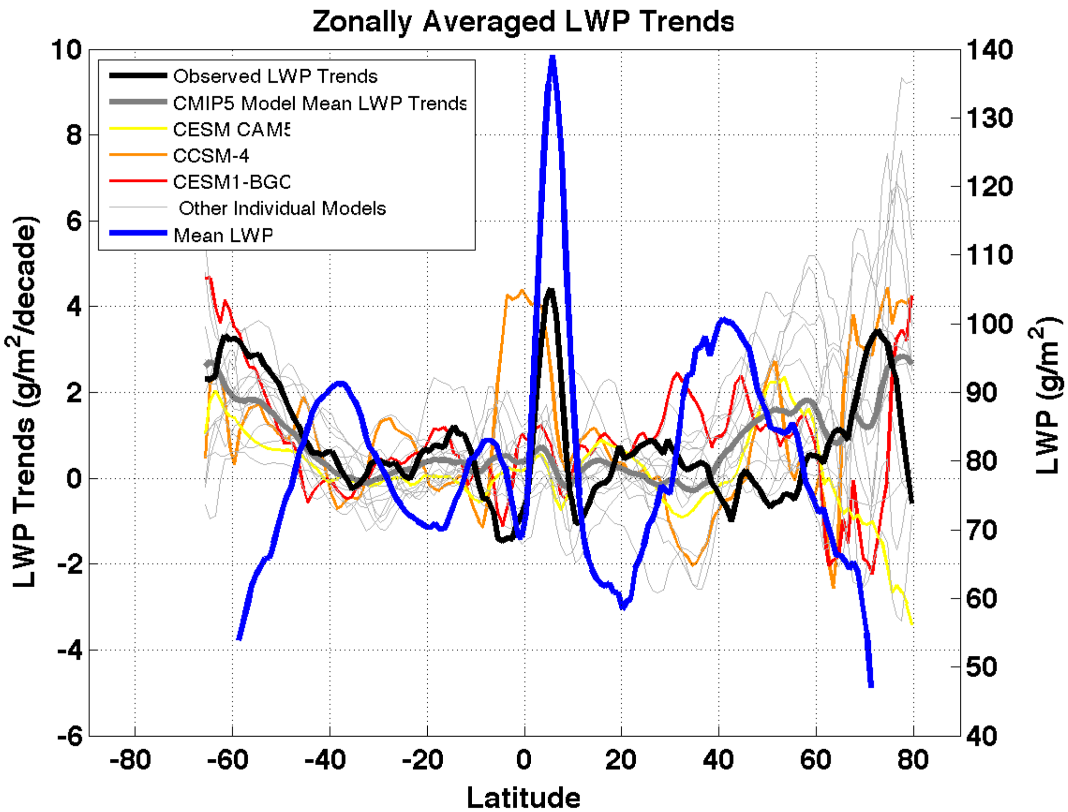

FIGURE 3.3. Curves showing the zonally averaged observed LWP trends, the zonally averaged CMIP5 model mean LWP trends, the zonally averaged LWP trends for the individual models, and the zonally averaged mean state LWP. Several individual models that are discussed in the text are highlighted in color

by inter-annual variability whereas the peaks and dips in the rest of the zonally averaged LWP trends are not.

Interestingly, only one model (CCSM-4) appears to roughly capture the correct magnitude and shape of the observed zonally averaged trends. Lauer and Hamilton (2013) suggest that biases in LWP climatology in CMIP5 models are mainly due to the atmospheric component of the model and showed that models with similar atmospheric components tended to have similar biases in the mean state LWP. This does not appear to be the case in regards to the zonally averaged LWP trends. Although CCSM-4 is the only model that roughly captures the magnitude and shape of the observed zonally averaged LWP trends, it shares a similar atmospheric component to several other models that do not capture the magnitude and shape including CESM1-BGC and CESM CAM5. These qualitative discrepancies and similarities between the models, model mean, and the observations indicate the need to quantitatively examine regional and global trends in LWP which we tackle next.

3.2.1. Regional Trends. Figure 3.4 shows the range of values for trends in the 6 regions described in section 3.1. Light gray bars represent the number of models that fall in a given range of trend values while the dark gray bars represent the number of those which are statistically significant. Trends different from zero at 95% confidence are deemed to be statistically significant. The errors on these trends were calculated using the same method as Santer et al. (2000). This method is described in greater detail in chapter 4. The blue line represents the observed trend with the blue shading indicating the 1σ error associated with the observed trend. Similarly, the orange line indicates the model mean trend for each region. Observations are statistically significant in all but two regions (the North American Stratocumulus Region and the North Atlantic Storm Track). Of these two regions, the North Atlantic Storm Track is very close to being statistically significant.

The regions shown in figure 3.4(a)-(d) show very little statistical significance in their modeled trends. Of these 4 regions, not one has more than 3 modeled trends that are statistically significant. Although this appears to be indicative of poor model performance, it should not be the only metric by which models are judged on their ability to capture trends. Models that are not different from zero at 95% confidence (i.e., are not statistically significant) are not necessarily inconsistent with the observed trends. In order to compute statistical consistency between a model and observations the following equation was used:

$$(T_1 - T_2) \pm \sqrt{{\sigma_1}^2 + {\sigma_2}^2} \tag{3}$$

where T_1 is the modeled trend, T_2 is the observed trend, σ_1 is the error associated with the modeled trend (as calculated from Santer et al., 2000), and σ_2 is the error associated with the observed trend. If the difference in trends divided by the errors that were added in quadrature is less than 2 (i.e., the difference in trends is less than 2 standard deviations away from zero) then the modeled and observed trends are said to agree with one another at 95% confidence (see Chapter 4 for further discussion of statistical error calculations).

Figure 3.5 shows the same data as 3.4 except with the dark gray shading now indicating models whose trends agree with the observed trends at 95% confidence. It can be seen in 3.5(a) and (b) that, despite many models not being statistically significant, almost all of the models agree with the observed trends at 95% confidence. This is likely due to the fact that the errors (due to inter-annual variability) are relatively high on the models and/or the observations as evident by their relative lack of statistical significance. These higher errors (as seen from equation 3) make it more likely that the difference between the modeled and observed trends are less than 2σ away from zero i.e., the modeled and observed trends are statistically consistent at 95% confidence. 3.5(c) and (d) do not have as good of an agreement with the observed trends. Only 5 of the 16 models are statistically consistent in the West Pacific Warm Pool (3.5(c)) and 9 of the 16 models are statistically significant in the South American Stratocumulus Region (3.5(d)). This could potentially be due to the errors relative to the observations in these regions being smaller than the errors relative to the observations seen in 3.5(a) and (b) (evidenced by their statistical significance). These lower errors make it less likely that the observations and models agree with one another at 95% confidence in regions (c) and (d) since the observed error bars are less likely to overlap with those of the models (see equation 3). We can conclude from this that, although the modeled LWP trends in these 4 regions generally agreed with the observations to within

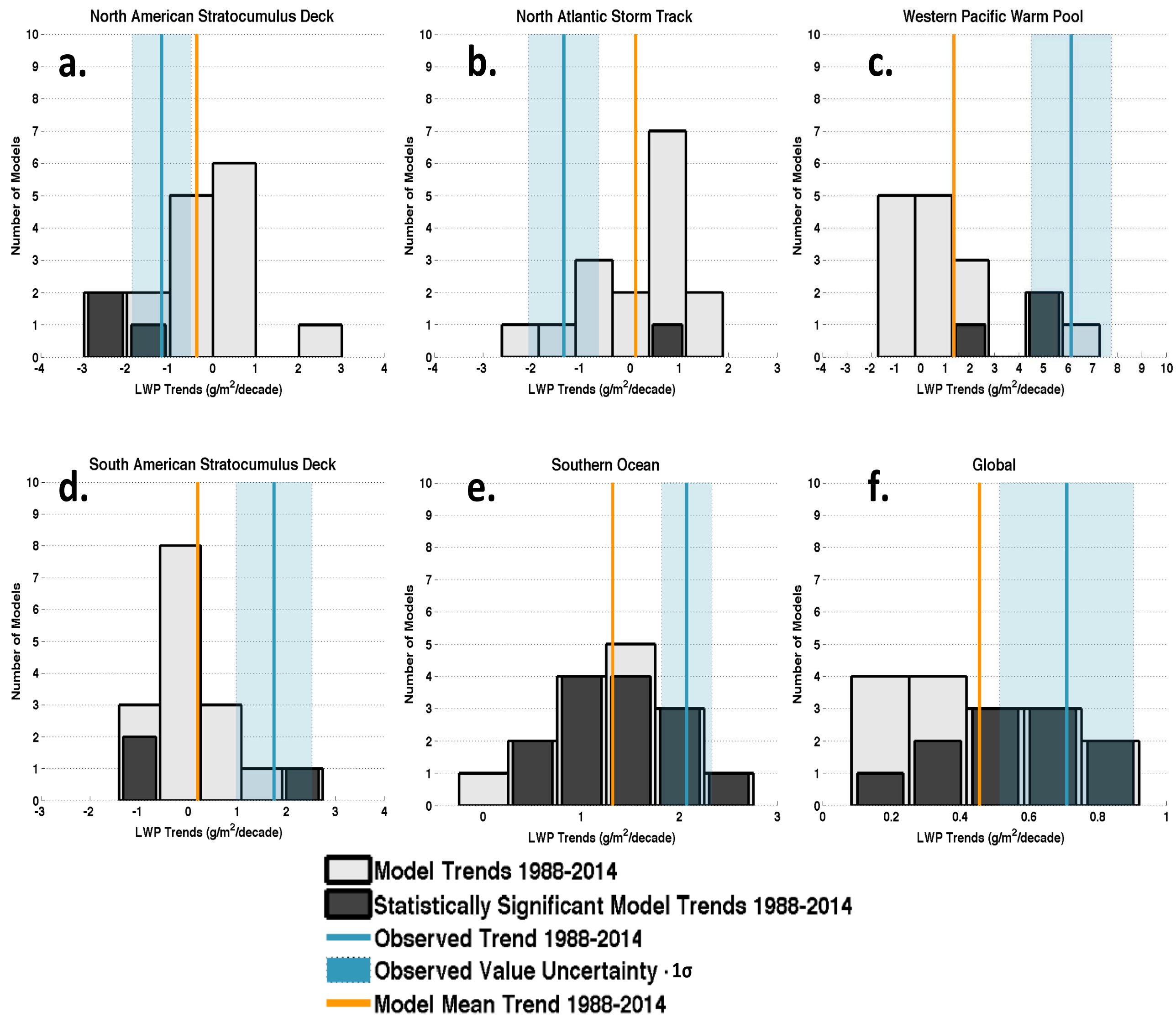

FIGURE 3.4. The LWP trends in the models and the observations in the (a) North American Stratocumulus Deck (b) North Atlantic Storm Track (c) Western Pacific Warm Pool (d) South American Stratocumulus Deck (e) Southern Ocean and (f) Global average for the past 27 years. Light gray bars indicate the number of models that fall in a given range of trend values. Dark gray bars indicate the number of those which are statistically significant. The blue line indicates the observed trend with the light blue shading indicating the uncertainty associated with these observations at 1σ (calculated using the method outlined in Santer et al. (2000)). The orange line indicates the model mean trend value.

the errors, these errors were relatively high (particularly in models) because inter-annual variability still plays a significant role even in a 27-year dataset.

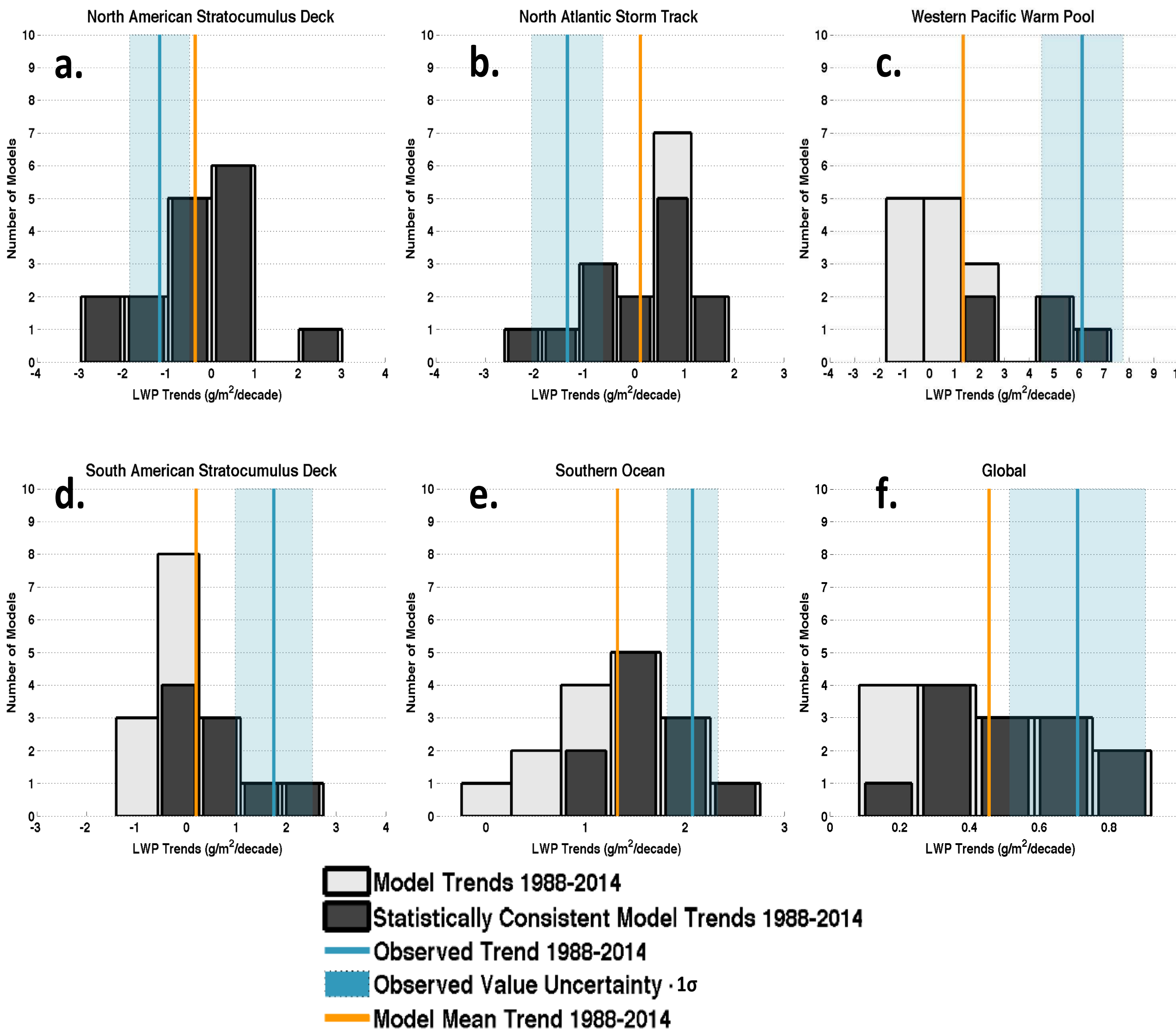

Figure 3.5. Same as figure 3.4 except the dark gray bars indicate models whose trends agree with the observed trends at 95% confidence

The two remaining regions are shown in 3.4 and 3.5(e)-(f). In the Southern Ocean (figure 3.4 (e)), almost every trend is positive and has roughly the same magnitude as the observed trend. It should also be noted that 14 of the 16 models are statistically significant. Figure 3.5(e) further adds further indication of the robustness of these trends, showing 11 of 16 modeled trends agreeing with the observed trend at 95% confidence. This indicates that, not only are most of the modeled and observed errors small relative to their respective trends, the trends themselves are very similar to one another. This is the only region that exhibits this kind of robustness and, from this, we hypothesize that, in this region, inter-annual variability has less of an effect on our modeled and observed trends and/or the trends are merely strong enough to overcome effects of inter-annual variability. Potential explanations for these Southern Ocean positive trends are discussed in section 3.2.2. The mean global LWP trends shown in 3.4(f) are all positive and roughly the same magnitude as the observed trend with 11 of 16 of the models showing statistical significance and 13 of the 16 models agreeing with the observed trend at 95% confidence. Again, this would appear to indicate that not only are most of the modeled and observed errors small relative to their respective trends, the trends themselves are very similar to one another. However, we hypothesize that this is partially due to the inter-annual variability cancellation effects (discussed in section 3.2) since we are averaging over the entire globe and different regions exhibit different inter-annual variabilities. These global trends also appear to suggest that most of the models analyzed in this study are roughly correct in global distribution of positive and negative trends and, when averaged together, cancellations between the two lead to a further reduction in the inter-model spread of globally averaged trends. However, as shown in figures 3.1 and 3.3 the magnitudes of these trends tend to be underestimated in most regions and regions of positive and negative trends are occasionally shifted spatially relative to their observed counterparts.

3.2.2. Southern Ocean Trends. As mentioned in the previous section, almost every model trend in the Southern Ocean is positive and the majority are statistically significant. It is the only region, other than globally, that exhibits this kind of robustness. In other words, almost all of the model trends are positive and are statistically consistent with the observations which implies that the models may have roughly the right trends for the right reason. We now attempt to identify what physical effect may be leading to this increase in cloud liquid water path in the Southern Ocean.

In a warming climate, it has been suggested that optical depth (and thus LWP) will, generally, increase (Paltridge, 1980, Charlock, 1982, Somerville and Remer, 1984). This optical depth feedback (described in section 1) is again outlined here: as the climate warms, the amount of water the air can hold increases, which in turn increases the availability of water vapor that can be condensed into cloud water. From this, the amount of cloud water could be expected to increase, leading to either more or optically thicker clouds. This would tend to increase the albedo of the atmosphere and reflect more incoming solar radiation to space. Thus this can be considered to be a negative feedback (Paltridge, 1980, Charlock, 1982, Somerville and Remer, 1984). Betts (1987) discuss how these optical depth changes with temperature are approximately twice as large in the high latitudes as they are in the tropics. This is due to the fact that, the LWP changes with temperature are closely linked to changes in the slope of the moist adiabat with temperature, which itself is a strong function of temperature (Betts, 1987).

Another possible mechanism that could lead to an LWP increase in a warming climate, especially in mixed phase clouds in the Southern Ocean, is a consistent phase change from ice to liquid over time (e.g., Senior and Mitchell, 1993). As the temperature increases, it can be expected that cloud particles would more often form as water droplets rather than ice crystals due to these warmer temperatures. This would subsequently cause an increase in the LWP of mixed phase clouds, a decrease in the ice water path and roughly no change in the total water path. However, the models do not seem to suggest this as will be shown later in this section.

One final mechanism that could potentially be responsible for the large upward LWP trends in the Southern Ocean is the poleward shift on storm tracks. In a warming climate, the storm tracks are expected to shift poleward (Yin, 2005, Mbengue and Schneider, 2013,

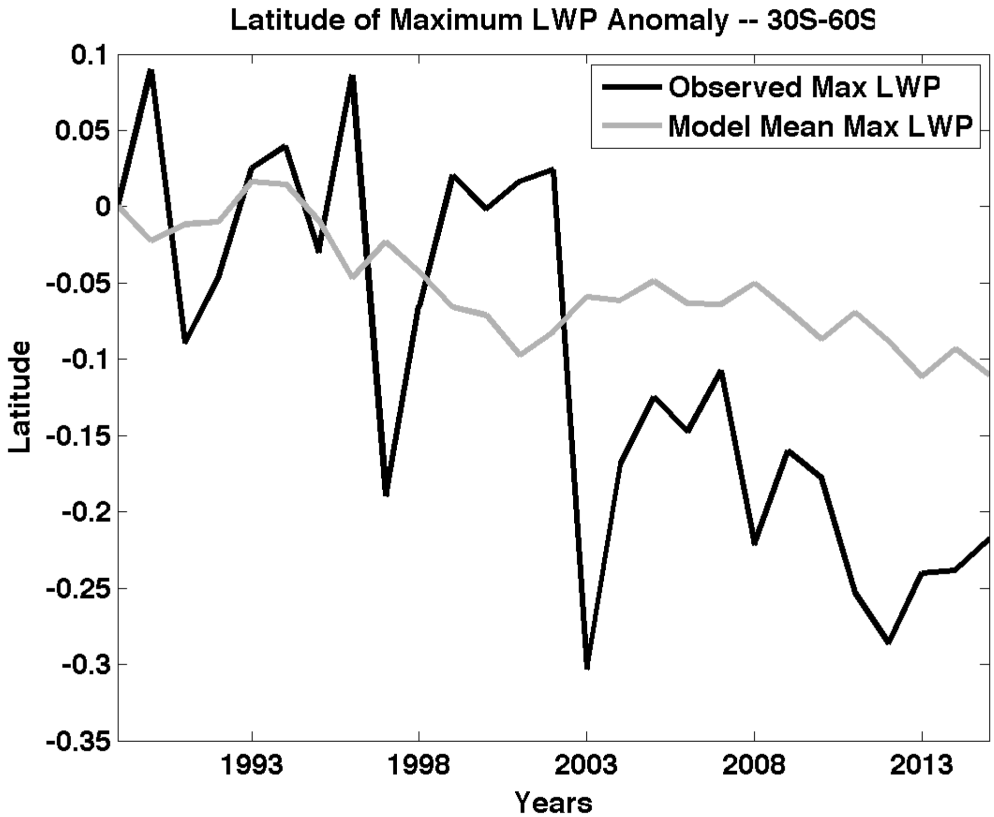

FIGURE 3.6. The anomaly of LWP weighted latitude where the zonally averaged maximum LWP occurs in every year of our observed dataset and in the model mean in the Southern Ocean region defined as 59.5°S-29.5°S, 0.5°E-359.5°E

Barnes and Polvani, 2013). A manifestation of this is suggested by figure 3.1(a). In this figure, there appears to be an increase in LWP across almost all of the Southern Ocean south of approximately 45°S. North of that up to approximately 30°S the trends tend towards being slightly negative. Similarly, looking at the Northern Hemisphere Storm Track Regions i.e., off the East Coast of North America and the East Coast of Northern Asia (from about 35°-50° North), there appear to be significant negative trends. Poleward of 50°N-60°N, the trends seem to switch over from negative to positive. This could potentially be indicative of the storm tracks migrating poleward. Figure 3.6 displays the anomaly in the latitude of the zonally averaged, LWP weighted max LWP in the Southern Ocean region from 59.5°S-29.5°S, 0.5°E-359.5°E for both the observed and model mean LWP. This figure appears to indicate a poleward shift of approximately 0.3 degrees in the location of max LWP (a proxy for storm track location) in the observations over the past 27 years. These observations are roughly consistent with modeling studies that indicate that storm tracks in the Southern Ocean are expected to shift approximately 2° poleward with roughly a doubling of CO_2 by the end of the century (Yin, 2005, Mbengue and Schneider, 2013, Barnes and Polvani, 2013). The model mean appears to show a 0.1 degree poleward shift in the location of maximum LWP over the past 27 years. This number equates to a shift slightly less than the 2° poleward migration predicted with roughly a doubling of CO_2 by the end of the century although this is potentially partially due to the fact that this trend is an average of the trends in 16 different CMIP5 models.

Of these hypotheses, the only one that was explicitly tested in this work was how much of the robust, positive, Southern Ocean LWP trends in the models could be attributed to a phase change. In order to test this, 27 year trends in ice water path (IWP) and total water path (TWP) were calculated from every model in the dataset, which was straightforward as the CMIP5 archive includes ice as well as liquid water path for every model.. If the positive trends in LWP were entirely due to phase changes, it can be expected that the trends in IWP would be equal and opposite to their LWP counterparts. This would mean that the TWP would be close to zero.

Figure 3.7 shows the LWP, IWP, and TWP trends for the Southern Ocean region analyzed in this study. 3.7(b) shows that most IWP trends are roughly zero or slightly negative for the suite of CMIP5 models with the model mean being approximately zero. The TWP, shown in figure 3.7(c), is simply the addition of LWP and IWP for each individual model. Most TWPs have roughly the same magnitude as their LWP counterparts due to the relatively small magnitudes of IWP trends. These results suggest that, in general, a phase change

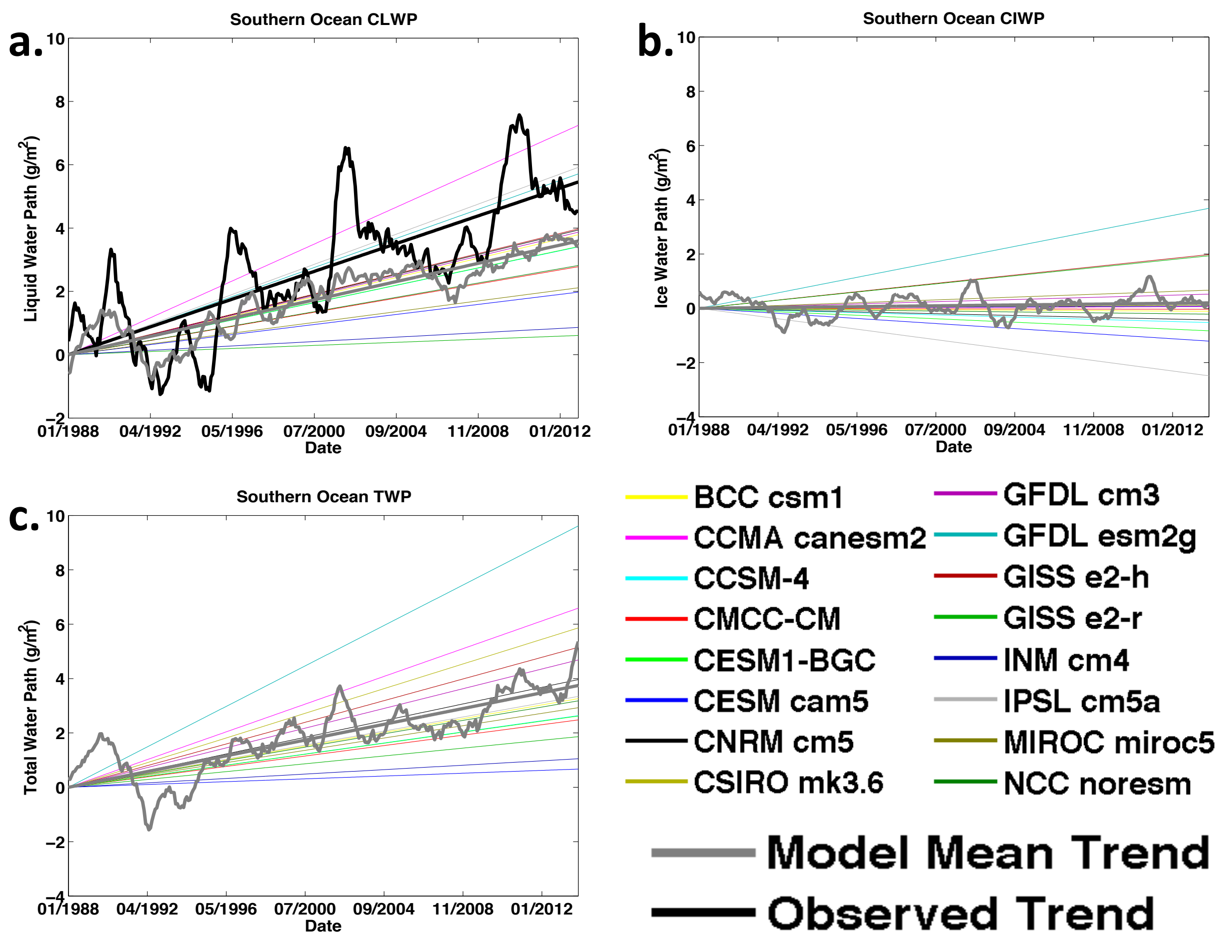

FIGURE 3.7. Observed, model mean, and individual model trends in (a) cloud liquid water path, (b) cloud ice water path, (c) total cloud water path in the Southern Ocean region (59.5°S-44.5°S, 0.5°E-359.5°E) from 1988-2014. It should be noted that the observed cloud liquid water path trend in the Southern Ocean is included in (a)

from ice to liquid in Southern Ocean clouds is generally not occurring in the models at any significant level. This lends more weight to the plausibility of the other hypotheses discussed or other potential mechanisms not discussed in this work.

3.3. AMIP and ERA Trends

The previous sections detail the trends that were calculated in various regions across the globe for the observations and the CMIP5 models. Some of these modeled trends appear to agree quite strongly with observed trends while others showed weaker agreement. Some of this weaker agreement may be caused by incorrect modeling of sea surface temperatures (SSTs), to the extent that clouds trends are related to thermodynamic rather than purely dynamical effects. In order to examine this possibility, trends in LWP were calculated using several other datasets to determine if they were better at capturing the observed trends in LWP. These datasets included the Atmospheric Model Intercomparison Project (AMIP) runs of several CMIP5 models, which use prescribed SSTs but the same atmosphere model as their CMIP5 counterparts, as well as the ERA-interim reanalysis LWP.

3.3.1. AMIP Trends. AMIP experiments are a sub experiment of the CMIP5. In these experiments, modeled SSTs are forced to be the same as the observed SSTs, with the atmospheric model remaining the same as its CMIP5 counterpart. In this way, only the atmosphere is tested; effects from the other modules such as the land, cryosphere, and ocean model will be decoupled from the atmosphere model, which is hence tested in isolation. For this experiment, only 11 of the 16 models we examined performed the AMIP experiment. The models that ran AMIP experiments can be seen in figure 2.4. Different models had various ending years for their corresponding AMIP experiments, with some ending as early as 2008 while others ended as late as 2012. For consistency, and in order to examine as much data as possible, all AMIP trends were computed from 1988-2008.

Figure 3.8 shows the observed, CMIP5 model mean, AMIP model mean time series and the best fit line for the observed time series from 1988-2008 in the 6 regions analyzed in this study. All time series represent the anomaly relative to the starting point in January, 1988. The R-value in each plot represents the correlation coefficient between the de-trended AMIP time series and the de-trended observed time series. This de-trending was done in order for R to be used as a more accurate measure of how well AMIP captures observed inter-annual variability.

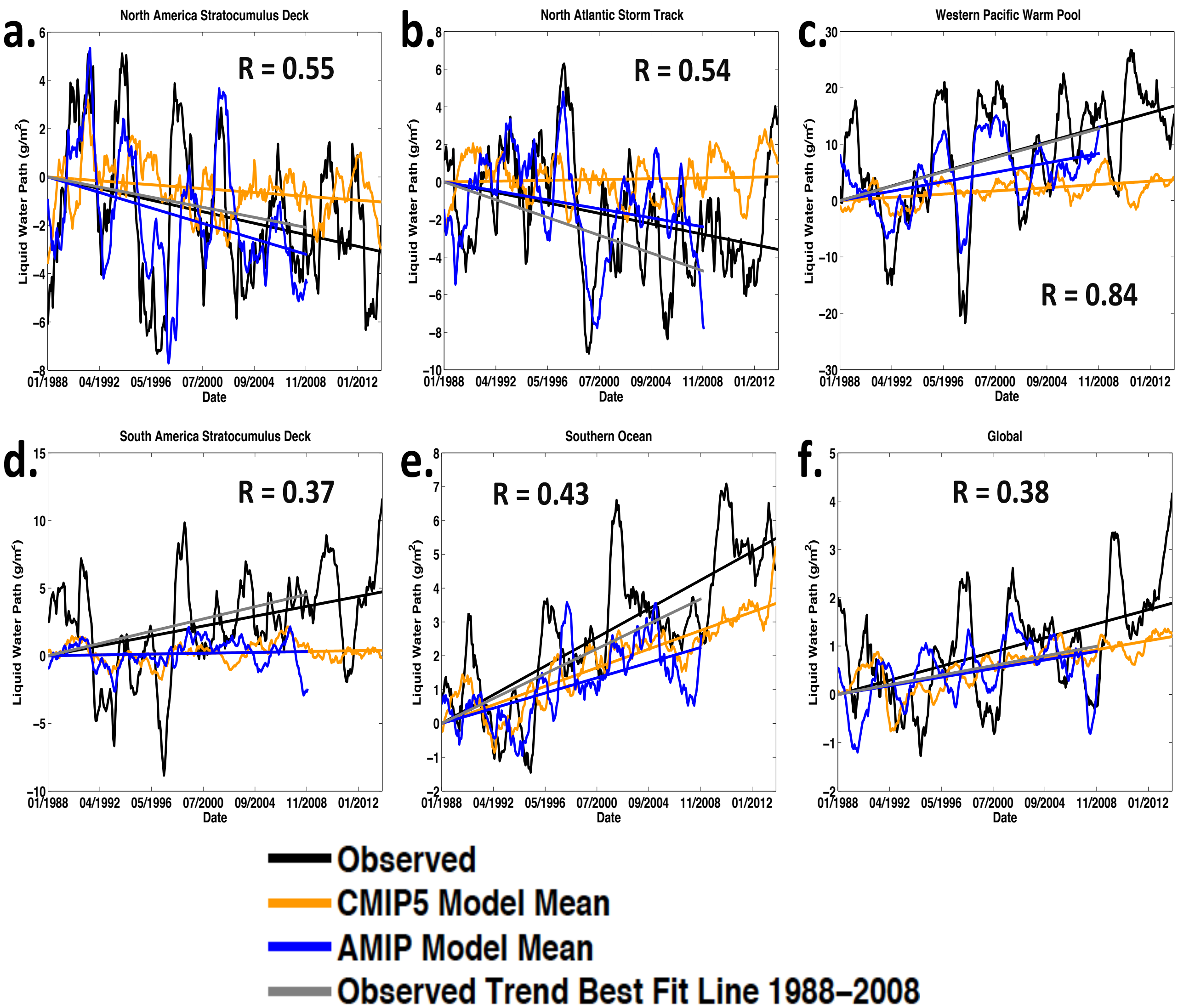

FIGURE 3.8. Observed, model mean, AMIP model mean, and shortened (1988-2008) observed trends for (a) North American Stratocumulus Deck (b) North Atlantic Storm Track (c) Western Pacific Warm Pool (d) South American Stratocumulus Deck (e) Southern Ocean and (f) Global regions. R-values represent the correlation coefficients between the de-trended observed and AMIP time series in each region.

In most every region, the CMIP5 model mean generally does a poor job of capturing both observed trends and inter-annual variability. In contrast, in approximately half of the regions analyzed, the AMIP model means tend to do a better job of capturing the inter-annual variability, with the exceptions being the South American Stratocumulus region, the Southern Ocean, and globally. In the 3 remaining regions, the AMIP models generally replicate major features in the observed time series, implying that the inter-annual variability in LWP in these regions is generally thermodynamically driven.

If modeled AMIP trends tend to capture inter-annual variability more accurately, do they also do a good job of capturing trends more accurately? In several regions (e.g., the North Atlantic Storm Track and the Western Pacific Warm Pool), where the AMIP model mean inter-annual variability more closely tracks that observed, the trends are slightly closer to the observed than the CMIP5 model mean trends. In other regions (e.g., the South American Stratocumulus Deck and the Southern Ocean), where the AMIP model mean inter-annual variability poorly tracks the observed time series, the AMIP trends are roughly the same as the CMIP5 model mean or slightly farther from the observed than the CMIP5 model mean.

3.3.2. ERA Trends. For further comparison with observed and modeled trends, ERA-interim reanalysis LWP data were obtained. The ERA-interim is the 3rd generation atmospheric reanalysis product from the European Centre for Medium-Range Weather Forecasts (ECMWF) that is updated in real time (Dee et al., 2011). Data extends from 1979 to the present day. LWP data that were used for this experiment had the same range as the observations (January, 1988-December, 2014).

Figure 3.9 shows the observed and ERA time series for each regions. Similarly to figure 3.8, all time series are anomalies relative to the mean LWP in January 1988. Again, the R-value in each plot represents the correlation coefficient between the de-trended ERA time series and the de-trended observed time series. Like the AMIP time series, the ERA time series tend to capture the inter-annual variability associated with the observed time series better than the CMIP5 model mean. In fact, the ERA time series capture inter-annual variability better than the AMIP model mean in every region. This can be seen by comparing

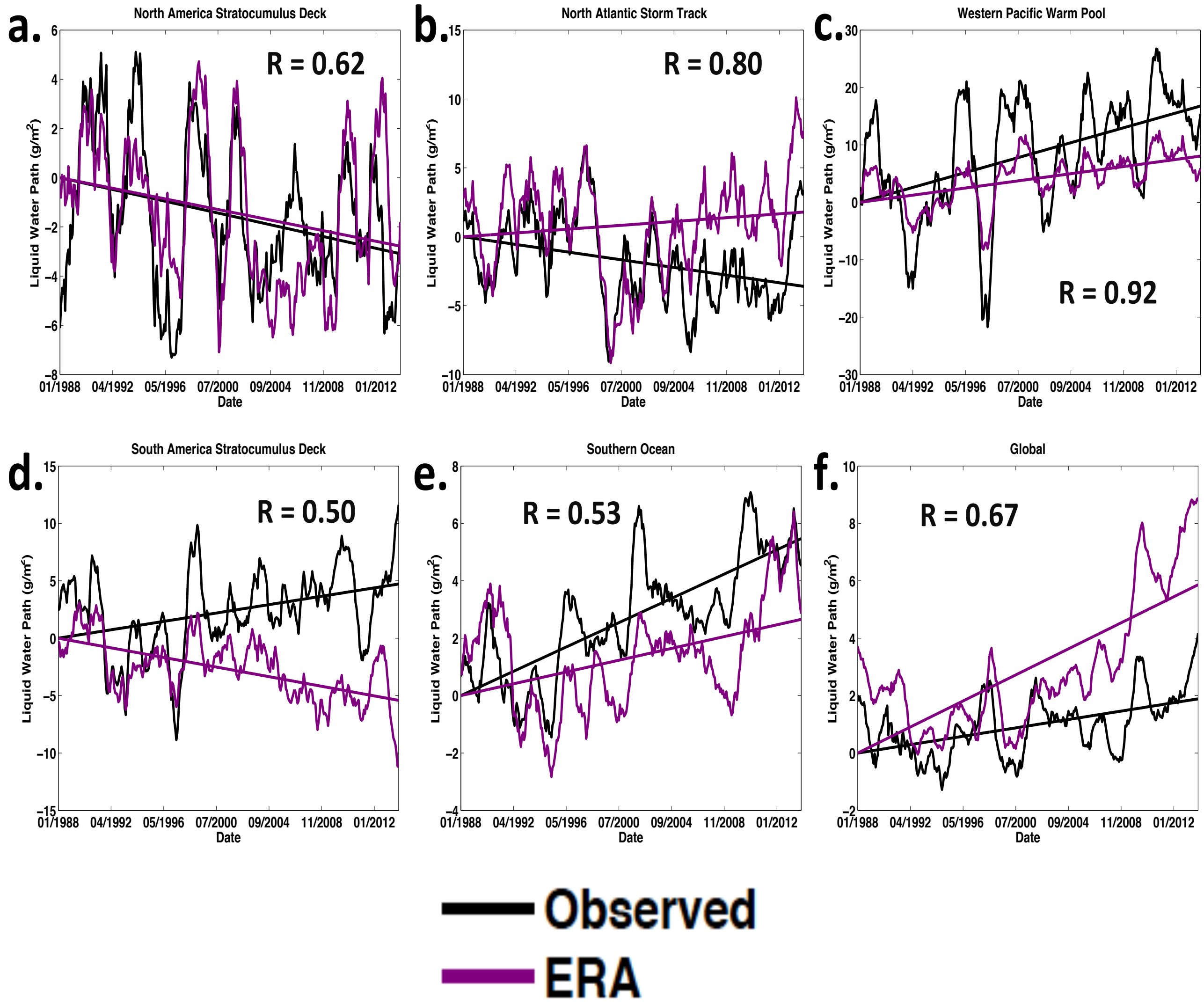

FIGURE 3.9. Observed and ERA LWP trends for (a) North American Stratocumulus Deck (b) North Atlantic Storm Track (c) Western Pacific Warm Pool (d) South American Stratocumulus Deck (e) Southern Ocean and (f) Global regions

the R-values in figures 3.8 and 3.9. In most cases, the ERA time series also appears less dampened than the AMIP model mean, although this is likely due to the fact that the AMIP model mean is the average of 11 different time series, while the ERA time series is not.

In the figure 3.8, we saw that AMIP trends were closer to observed trends when the AMIP time series better captured the inter-annual variability. Surprisingly, this does not appear to be the case in the ERA. In all regions, the ERA better captures the observed inter-annual variability than AMIP. However, it is generally either worse or roughly the same in regards to matching observed trends. This is most apparent in the North Atlantic Storm Track region. The correlation coefficient between the ERA and observed time series is 0.80 while the correlation coefficient between the AMIP model mean and the observed time series is 0.54. Despite this, the AMIP model mean trend is strongly negative and is in good agreement with the observed trend while ERA trend is weakly positive and just barely agrees with the observed trend at 95% confidence. This again could be due to the fact that the AMIP time series is an average of 11 different models, while the ERA time series is not, although, it could also be due to fundamental differences in physics between the AMIP and ERA models. However, both of these are merely speculation and it would require studies beyond the scope of this work to determine the exact cause of this apparent discrepancy.

For the purposes of this study, we choose to focus on the results of the AMIP experiment rather than the ERA, since it is more closely related to the CMIP5 experiments examined in section 3.2. As previously noted, in regions where inter-annual variability is better captured by the AMIP model mean, the trends tend to be closer to that observed than the CMIP5 model mean. This begs the question as to whether or not observed LWP trends in these regions are more due to inter-annual variability as opposed to forced trends, or if they are instead due to thermodynamic physics. If the former is the case, better modeled inter-annual variability will naturally give more accurate trends since that is the main driver. If the latter is the case, correct physics AND correct SSTs in the AMIP (and CMIP5) experiments would lead to more correct inter-annual variability and trends. Such questions represent interesting directions in regards to continuation of this work.

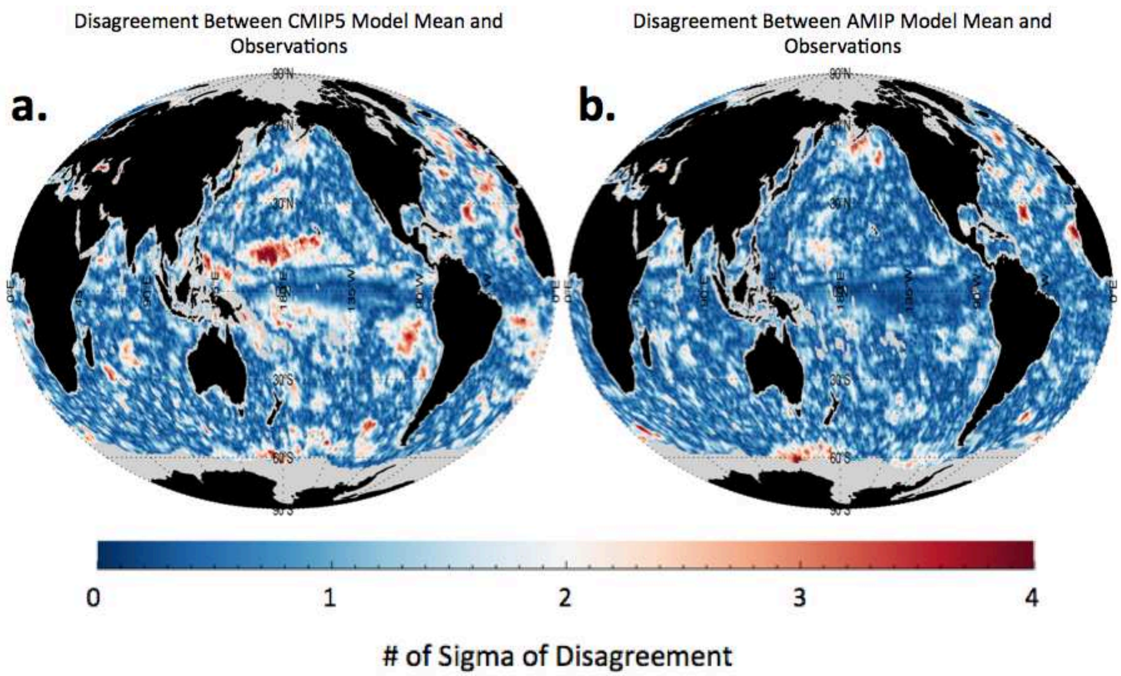

FIGURE 3.10. Disagreement between (a) the CMIP5 model mean and observed trends (b) the AMIP model mean and observed trends at each pixel. Blue indicates areas where the two trends agree (i.e., disagree at less than 95% confidence) while red and white indicate where the trends disagree at 95% confidence or more.

Despite this, there are still some significant discrepancies between AMIP model mean trends with their observed counterparts in certain regions although they show marked improvement over the CMIP5 model mean trends. This can be seen in figure 3.10 which shows the disagreement between the CMIP5 model mean and observed trends (a) and the disagreement between the AMIP model mean and observed trends (b) at each pixel. Blue indicates areas where the trends agree (i.e., disagree at less than 95% confidence) while red and white indicate where the trends disagree at 95% confidence or more. The AMIP model mean shows improvement over the CMIP5 model mean in various areas around the globe, most notably in the Western Pacific Warm Pool and the latitudes just North and South of the equator in the equatorial Pacific. AMIP model mean trends also tend to agree with the observations at 95% confidence or more in regions where the inter-annual variability is better replicated (e.g.

the North American Stratocumulus Deck) and disagree with observations in regions where the inter-annual variability is not as well captured (e.g. the South American Stratocumulus Region). This is consistent with our conclusions that regions that tend to better capture observed inter-annual variability also tend to better capture observed trends.

3.4. Total Water Path

The passive microwave retrieval algorithm used in all the sensors in the MAC-LWP dataset does not actually retrieve LWP, instead it retrieves total water path (TWP). LWP is separated from rainwater path after the retrieval has been made (Wentz and Spencer, 1998, Hilburn and Wentz, 2008). Only scenes with LWP greater than 180 g/m^2 are deemed to be raining in the RSS retrieval (Wentz and Spencer, 1998). For further discussion on the algorithm and cloud-rain partitioning and its potential associated errors, see section 4. Fortunately, the MAC-LWP data set also contains the observed TWP values in exactly the same format as the observed LWP values, so it is possible for us to ask the question: are the inferred LWP trends consistent with the observed TWP trends? If they are not, we may call into question the veracity of some of the observed LWP . Like the LWP variable, the TWP variable is a monthly mean over the oceans gridded at 1°x1° resolution. The only difference is the TWP includes rainwater as well. This portion of the work was done in order to verify that the cloud water-rain water partitioning in the retrieval algorithm appears to be reasonable based on what is known i.e., the fact that only approximately 6% of observed cloudy scenes are raining (Wentz and Spencer, 1998). If this is the case, it can be expected that the trends in total water path should not vary substantially in regards to their LWP counterparts in regions of relatively low annual rainfall. They can be expected to vary slightly more in regions of larger rainfall.

Table 3.1. Observed Regional Trends in Total and Liquid Water Path in g/m^2/decade from the MAC-LWP data set

Region	LWP Trend	TWP Trend
West Pacific Warm Pool	6.102 ± 1.63	12.783 ± 3.63
Southern Ocean	2.071 ± 0.257	2.748 ± 0.299
South American Stratocumulus Deck	1.740 ± 0.777	1.873 ± 0.770
North American Stratocumulus Deck	-1.195 ± 0.687	-3.251 ± 0.971
North Atlantic Storm Track	-1.367 ± 0.720	-2.502 ± 1.20
Global	0.708 ± 0.295	1.007 ± 0.269

Table 3.4 displays the LWP and TWP for each region along with their associated errors. In regions of relatively low precipitation (e.g., the South American Stratocumulus Deck), the trends tend to remain relatively constant between liquid and total water path. Conversely, in regions with relatively frequent, heavy precipitation, such as the West Pacific Warm Pool or the North Atlantic Storm Track, the magnitudes of the TWP trends tend to be greater than their LWP counterparts. Physically, this is because an increase (decrease) in clouds or cloudiness will tend to lead to more (less) rainfall, and does not imply a problem with the observed LWP trends. These observational results indicate that, in less rainy regions, the cloud-rain partitioning will have less of an effect on the resulting LWP trend. In regions of greater precipitation, the cloud-rain partitioning will have a larger effect on the resulting LWP trend. This means that in regions with larger TWP trends, the uncertainty associated with LWP trends will be greater due to the cloud rain-partitioning. However, it is noteworthy that there are not any regions that stand out as "problematic" in this regard, in terms of having an LWP trend than appears inconsistent with the TWP trend.

It has been shown in this chapter that, globally, observed trends tend to be stronger and more robust than modeled trends. Especially in the model mean, where cancellation effects all but remove inter-annual variability. Modeled LWP trends in most regions for most CMIP5 models are not statistically significant, however, in several regions, many modeled trends are statistically consistent with the observed trends at 95% confidence although this is seemingly due to large error bars on the modeled and observed trends in some of these regions due to the still-large role of inter-annual variability in the 27-year time series. It has also been shown that, in regions where inter-annual variability is better captured, AMIP models tend to do a better job of replicating observed trends while the ERA tends to do roughly the same or worse than the AMIP model mean in regards to re-creating observed trends even though the ERA reanalysis better recreates the inter-annual variability. The AMIP model mean results are potentially indicative of a couple scenarios, either: (a) the observed trends are primarily driven by inter-annual variability as opposed to forced trends or (b) they are due to thermodynamic physics. If the former is the case, better modeled inter-annual variability will naturally give more accurate trends since that is the main driver. If the latter is the case, correct physics and correct SSTs in the AMIP (and CMIP5) experiments would lead to more correct inter-annual variability and trends.

CHAPTER 4

Errors and Error Analysis

Thus far in this work, we have been using the MAC-LWP dataset as a tool for diagnosing the robustness of trends in CMIP5. This chapter discusses both the estimation of statistical errors in trends, as well as potential systematic trend errors due to any possible systematic LWP retrieval biases. This is important because we want to assess our level of confidence in our observed trends and their errors. For example, large systematic biases in the trends could render many of our conclusions incorrect. Spurious trends in cloud variables are known to occur due to a number of factors, such as drift in satellite equator crossing time (e.g., Waliser and Zhou, 1997), or multi-satellite series that are not correctly homogenized (Norris and Evan, 2015). The latter of these occurred when large, mult-decadal trends in the Earth's albedo were inferred from the ISCCP dataset (Pallé et al., 2004), but later were discovered to be spurious (Evan et al., 2007) as discussed in Chapter 1. This chapter also addresses potential sources of systematic errors in trends due to choices made in the RSS microwave retrieval algorithm. These choices could lead to systematic errors in our observed LWP trends, but fully testing the magnitude of these errors would require a sensitivity study with the RSS algorithm, which is beyond the scope of this work. Finally, this chapter looks at any apparent trends that could be due to long term climate variability (e.g., the El Niño-Southern Oscillation). Large effects on inter-annual variability due to the El Niño-Southern Oscillation could potentially render our conclusions incorrect. Due to their potential to alter our conclusions based on our observed LWP trends, it is imperative that we address all of these sources of systematic biases and errors.

4.1. Statistical Errors in Trends

In Chapter 3, results of trend calculations were presented along with associated errors due to variability in the time series. Trends different from zero at 95% confidence were deemed to be statistically significant. The following section details the method used for calculating these trend errors. This method of error calculation was adapted from Santer et al. (2000) and was chosen due to the nature of LWP trends which can be affected by both instrument noise and autocorrelation (i.e., inter-annual variability) of monthly or annually-averaged LWP values. In order to illustrate the potential types of manifestations of LWP time series and trends, figure 4.1 shows 4 randomly generated, autocorrelated at lag-1 (in these cases 1 month) time series with an autocorrelation of 0.1 for "low autocorrelation" runs and an autocorrelation of 0.7 for "high autocorrelation" runs, created using an autoregressive model with random noise added. The 'true' trend of these time series with no noise or autocorrelation is equal to 2 g/m^2/decade for these plots. The 4 cases included in this figure are: low noise and low autocorrelation, low noise and high autocorrelation, high noise and low autocorrelation, and finally high noise and high autocorrelation. It can be seen that the trends associated with these various randomly generated time series are never the 'true' value of 2 g/m^2/decade due to effects from both noise and autocorrelation, but tend to be relatively close. The method used by Santer et al. (2000) takes both of these errors into account and provides us with a robust calculation of uncertainty associated with linear trends in noisy data.

The first step in this method was to calculate the residual ($res(t)$) LWP values between the LWP timeseries and the LWP best fit line (calculated from standard least squares linear regression)

$$res(t) = LWP(t) - \widehat{LWP(t)} \tag{4}$$

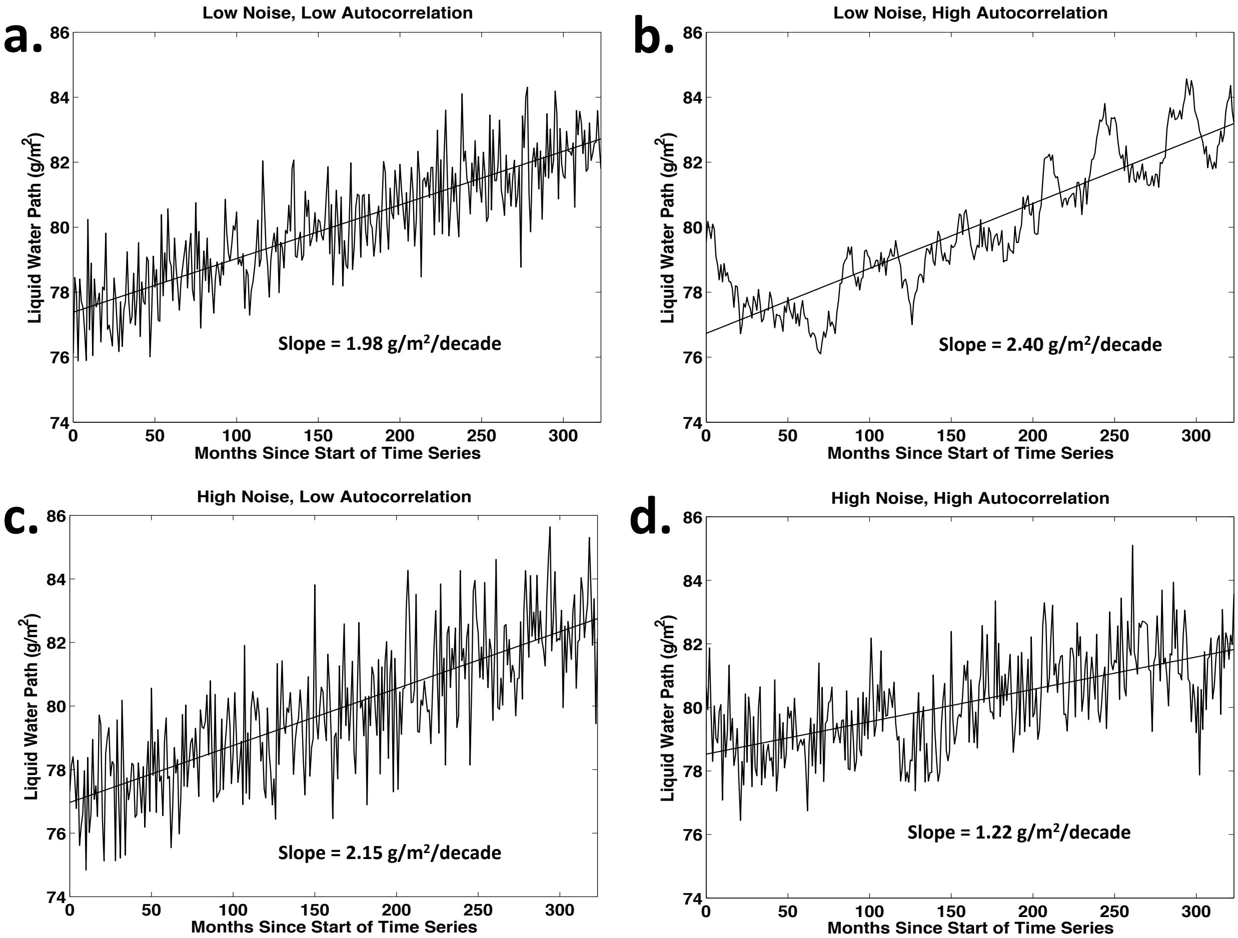

FIGURE 4.1. Shows 4 randomly generated, hypothetical LWP time series for (a) low instrument noise and low autocorrelation, (b) low noise and high autocorrelation, (c) high noise and low autocorrelation, and (d) high noise and high autocorrelation. The slopes of the best fit line for each plot are given. Note that the 'true' value of the slope (i.e. the value to the slope would have with no autocorrelation or noise) is equal to 2 g/m^2/decade

where $LWP(t)$ is the LWP timeseries, $\widehat{LWP(t)}$ is the LWP best fit line, and t is the number of time steps in the data, in this case $t = 1, \ldots, N_t$ where $N_t = 324$ months. If it is assumed that all of the values in $res(t)$ are statistically independent of one another, the error associated with the slope of the best fit trend line can be calculated by

$$\sigma = \frac{\sigma_r}{\sigma_t} \tag{5}$$

where σ_r is the standard deviation of the residuals and is given by

$$\sigma_r = \sqrt{\frac{\sum_{t=1}^{N_t} res(t)^2}{N_t - 2}} \tag{6}$$

note that N_t-2 is the number of degrees of freedom after the 2-parameter linear fit. σ_t is the standard deviation of t which is given by

$$\sigma_t = \sqrt{\sum_{t=1}^{N_t} (t - \bar{t})^2} \tag{7}$$

however, the monthly averaged LWP values in our datasets are not completely statistically independent, so the effective number of degrees of freedom is smaller than N_t-2. There is at least a slight autocorrelation i.e., the monthly averaged LWP value in a given month has at least some dependence on the monthly averaged LWP value in the preceding month. In order to take this autocorrelation into account, N_t is replaced in equation 6 with

$$N_c = N_t \frac{1 - c}{1 + c} \tag{8}$$

where c is the lag-1 autocorrelation of $res(t)$. If there is no autocorrelation at lag-1, N_c simply becomes N_t. Once σ is calculated, statistical significance is determined using the following equation

$$t_s = \frac{s}{\sigma} \tag{9}$$

where s is the slope of the best fit line for a given region in a given model or the observations (i.e., the trend value). As per Santer et al. (2000), t_s is assumed to be distributed as the Student's t from standard statistics. The resulting value of t_s is compared against a chosen threshold value. In this work, this threshold value was chosen to be 2. This value means that trends different from zero at a 95% confidence interval (two standard deviations) are deemed to be statistically significant; i.e., if $t_s \geq 2$ then t_s is different from zero at a 95% confidence interval and is statistically significant. Conversely, if $t_s < 2$, then t_s is not different from zero at 95% confidence and is not statistically significant. This method of error estimation was applied to all trends in this work and was the basis for determining statistical significance of trends.

In order to test this method, a Monte Carlo simulation was developed that randomly generated a specified number of time series (in this case 200) in the same manner that the time series shown in 4.1 were created. Again the 'true value' of the slope was set to 2 g/m^2/decade. For the histogram shown in 4.2(a), The 1 month autocorrelation lag-1 was set to 0.7, the measurement noise on a simulated global average LWP value of 80 g/m^2 was set to 2 g/m^2, and the artificial seasonal cycle amplitude was set to 2 g/m^2 for these particular 324 month (27 year) time series. For the histogram shown in 4.2(b), the 1 month autocorrelation lag-1 was set to 0.9, the measurement noise on a simulated global average LWP value of 80 g/m^2 was set to 5 g/m^2, and the artificial seasonal cycle amplitude was set to 2 g/m^2.

The two histograms in figure 4.2 show how many times trends fell in a given range. A gaussian curve is fitted to these histograms. The mean trend value, μ, its associated 1σ error (σ_{actual} calculated from the fitted Gaussian curve), the mean naive error of the 200 generated trends (σ_{naive} which is calculated sing N_t in equation 6), and the mean Santer method error of the same 200 trends (σ_{Santer} which is calculated sing N_c in equation 6) are given on the plots. Note that the mean trend value is not equal to the true trend value in either case, so an error must be assigned to each.

It can be seen in 4.2(a), using equation (9) setting s equal to μ and having σ equal to σ_{actual}, that the trend is statistically significant. Conversely, if the μ and σ_{actual} from 4.2(b)

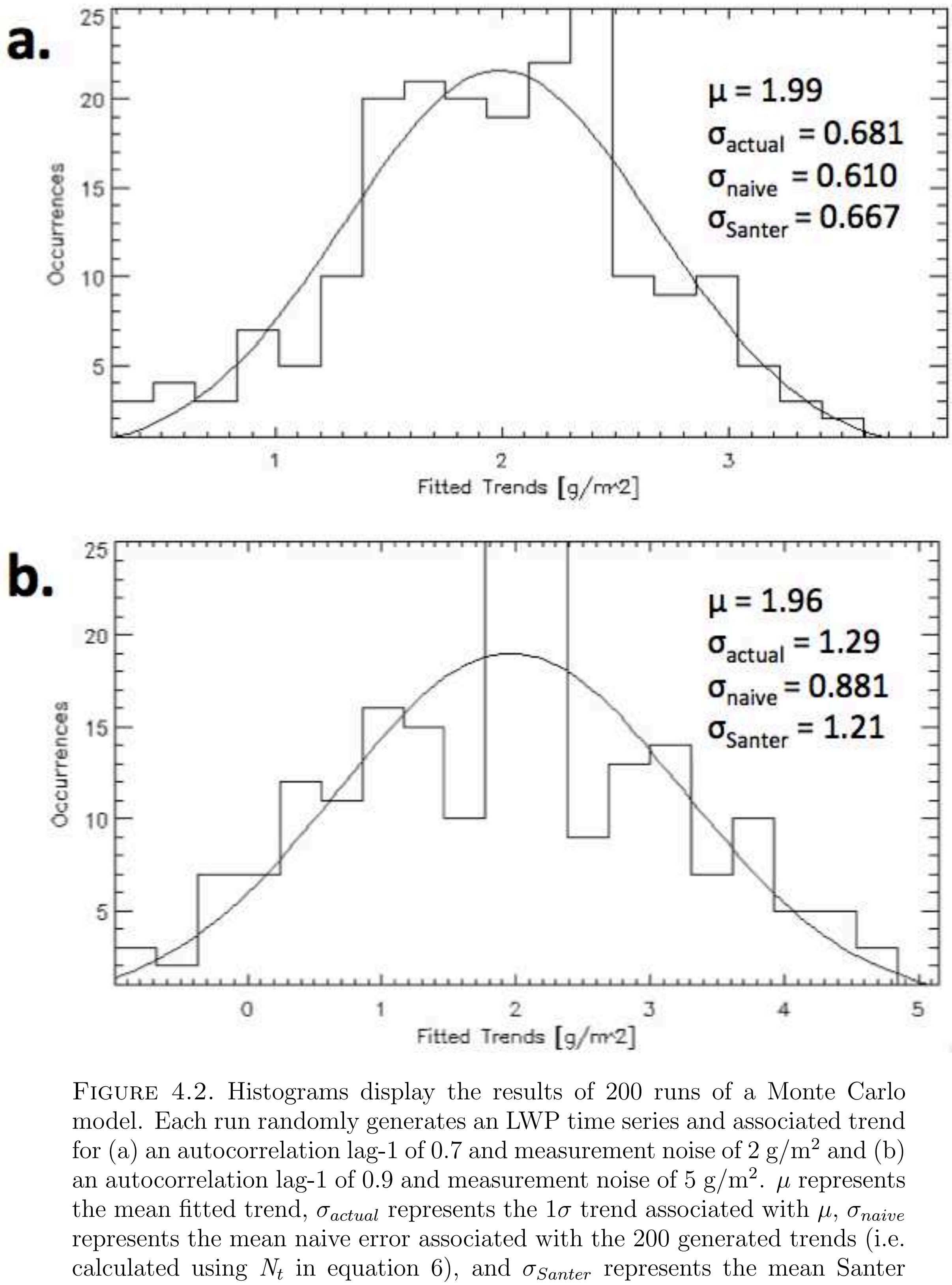

FIGURE 4.2. Histograms display the results of 200 runs of a Monte Carlo model. Each run randomly generates an LWP time series and associated trend for (a) an autocorrelation lag-1 of 0.7 and measurement noise of 2 g/m^2 and (b) an autocorrelation lag-1 of 0.9 and measurement noise of 5 g/m^2. μ represents the mean fitted trend, σ_{actual} represents the 1σ trend associated with μ, σ_{naive} represents the mean naive error associated with the 200 generated trends (i.e. calculated using N_t in equation 6), and σ_{Santer} represents the mean Santer error associated with the same 200 trends (i.e. calculated using N_c in equation 6)

are substituted into equation (9), it is shown that this trend is not statistically significant. This simple exercise using a Monte Carlo simulation shows the benefits of the Santer method in these calculations. For the case with less noise and less autocorrelation (4.2(a)), the mean trend may not be exactly equal to the 'true' value, but the 'true' error associated with the trend (σ_{actual}) encompasses the true value of 2 g/m^2/decade while simultaneously showing that the trend is statistically significant due to relatively low noise and autocorrelation. In this case the Santer error (σ_{Santer}) is shown to be closer to the 'true' value for the error that the naive error (σ_{naive}).

For the case with more noise and autocorrelation (4.2(b)), the mean trend is also not equal to the true value and even though the error encompasses the true value it is not statistically significant due to errors associated with noise and autocorrelation (i.e., inter-annual variability). As with 4.2(a), the Santer error is closer to the true value of σ_{actual} than the naive error. It should be noted, however, that the difference in the Santer and naive errors is much greater in this case. This is due to the relationship between N_t and N_c given in equation (8). As autocorrelation decreases, N_t and N_c converge since the value of N_c is a function of the autocorrelation. It can be seen from these Monte Carlo simulations, that using the Santer method provides a more accurate estimate of the 'true' error, especially in cases of higher autocorrelation while the naive method tends to underestimate the 'true' error.

4.2. Systematic Errors

4.2.1. Retrieved LWP Systematic Errors.

The following section outlines systematic errors in MAC-LWP retrievals, as errors in retrieved LWP could conceivably lead to spurious regional LWP trends. This is merely meant to be a background of mean state LWP systematic errors that precedes a discussion of systematic errors in trends in section 4.2.2. As mentioned in Chapter 2, systematic errors present in the MAC-LWP dataset arising from underlying systematic errors in the "Level-2" retrievals of LWP from the RSS algorithm (Hilburn and Wentz, 2008) can be as large as 30% (O'Dell et al., 2008), depending on a number of factors. These include, but are not limited to: cross-talk errors, effects from ice, cloud top temperature errors, clear-sky biases, and cloud-rain partitioning. O'Dell et al. (2008) details these systematic errors and attempts to quantify each. They are briefly described in this work as they can affect the retrieved monthly values of LWP. Further work on potential systematic errors in the RSS-retrieved LWP was given in Seethala and Horváth (2010).

Cross-talk errors arise from the retrieval of other parameters that are partially used in the calculation of LWP. These include water vapor, surface wind speed, and rainwater path all of which are the actual variables retrieved from the passive microwave sensors used in the MAC-LWP dataset. Another variable used in the calculation of LWP is the sea surface temperature, which is calculated from the Reynolds OI SST database (Reynolds et al., 2002, Hilburn and Wentz, 2008). Errors in these variables can potentially lead to errors in the retrieved LWP. Spurious trends in any of these variables have the potential to create spurious trends in LWP, but at an unknown level.

Effects from cloud ice are generally negligible for most of the microwave spectrum as it is, for all intents and purposes, invisible at most of these wavelengths. However, at wavelengths of approximately 37 GHz, large ice particles can occasionally cause scattering of microwave radiation. This leads to a lowering of the observed brightness temperature which, in turn, can lead to a lower retrieved LWP. Regional trends in cloud ice could therefore cause trends in LWP, but at an unknown level.

Errors in cloud top temperatures affect the retrieved LWP since cloud water absorption is partially a function of temperature in the microwave with colder clouds tending to absorb more radiation than warmer clouds. Cloud top temperature is parameterized as a function of SST and retrieved water vapor in the RSS passive microwave retrieval algorithm (Hilburn and Wentz, 2008). This parameterization is given by equation (17c) in Hilburn and Wentz (2008):

$$T_L = 251.5 + 0.83(T_U - 240) \tag{10}$$

where T_U is a function of water vapor and SST and is given by equations 17a, 17b, 18a, and 18b in Wentz (1997). Since cloud top temperature is a function of these two variables, errors or spurious trends in either can lead to errors in the cloud top temperature and thus errors in the retrieved LWP/LWP trends.

Clear-sky biases are the result of positive LWP values being retrieved from pixels that do not contain any clouds. These lead to spuriously high values of LWP in regions where LWP should theoretically be zero. Several papers have looked into this phenomenon (e.g., Greenwald et al., 2007, Horváth and Davies, 2007, Seethala and Horváth, 2010). Greenwald et al. (2007) found that AMSR-E had an approximately 7g/m^2 clear-sky bias compared to MODIS in the annual global mean while Horváth and Davies (2007) and Seethala and Horváth (2010) found this bias to be approximately 15 g/m^2 and 12 g/m^2 respectively. Figure 4.3 taken from Seethala and Horváth (2010) shows the global mean AMSR-E clear-sky bias from December 2006-November 2007 with values that range from approximately 5 g/m^2 in marine stratocumulus regions to 20 g/m^2 in warm tropical and subtropical regions. Both Seethala and Horváth (2010) and Horváth and Davies (2007) argue that these clear-sky biases are likely due to older surface emissivity and gaseous absorption models used by the RSS retrieval algorithm. However, they acknowledge that this could be due to the MODIS cloud mask incorrectly identifying areas of low trade cumulus clouds as clear scenes (Zhao and Di Girolamo, 2006). Another possible source of this bias is correlations in the RSS retrieval algorithm between retrieved LWP and retrieved wind speed and total precipitable water (Greenwald et al., 2007, Seethala and Horváth, 2010). Ideally the retrieved variables should be uncorrelated, however, this is seemingly not the case. Figure 4.4 was provided by Tom Greenwald (personal communication) and shows the LWP clear-sky bias as a function of retrieved wind speed and total precipitable water. It can be seen that at lower retrieved wind speeds (< 5m/s) and lower retrieved total precipitable water (<10mm), the LWP clear-sky bias is relatively high (approximately 10 g/m^2). The same is true for very high total precipitable water amounts (> 50mm) where LWP clear-sky biases range from approximately 10-15 g/m^2. These correlations have the potential to cause spurious trends in LWP in certain regions. For example, in calm wetter regions (i.e., the lower right in figure 4.4), a true upward trend in water vapor could lead to a spurious trend in LWP due to the fact that the LWP clear-sky bias increases as water vapor increases in these regions.

The final error discussed here is the error in cloud-rain partitioning. At microwave wavelengths, it is difficult to separate the signal of rainwater from that of cloud water. In order to overcome this, the RSS retrieval algorithm sets a total water path threshold of 180 g/m^2 above which, it assumes clouds are precipitating. If the retrieved total water path is below this threshold, it assumed that the cloud is not raining and the LWP is simply equal to the total water path. If the retrieved total water path is above this threshold the LWP is calculated via the following equation given in Wentz and Spencer (1998):

$$LWP = 0.18(1 + \sqrt{HR}) \tag{11}$$

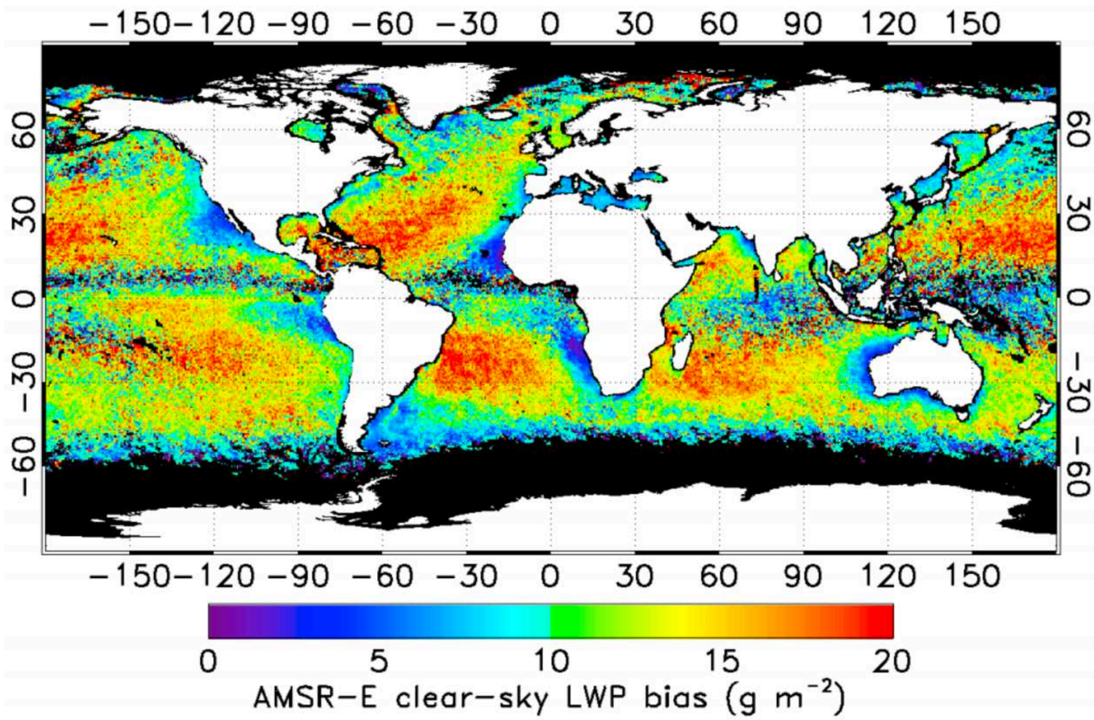

FIGURE 4.3. Taken from Figure 1 in Seethala and Horváth (2010). Displays the AMSR-E global mean clear-sky bias, as determined from comparisons with MODIS clear scenes, from December 2006-November 2007

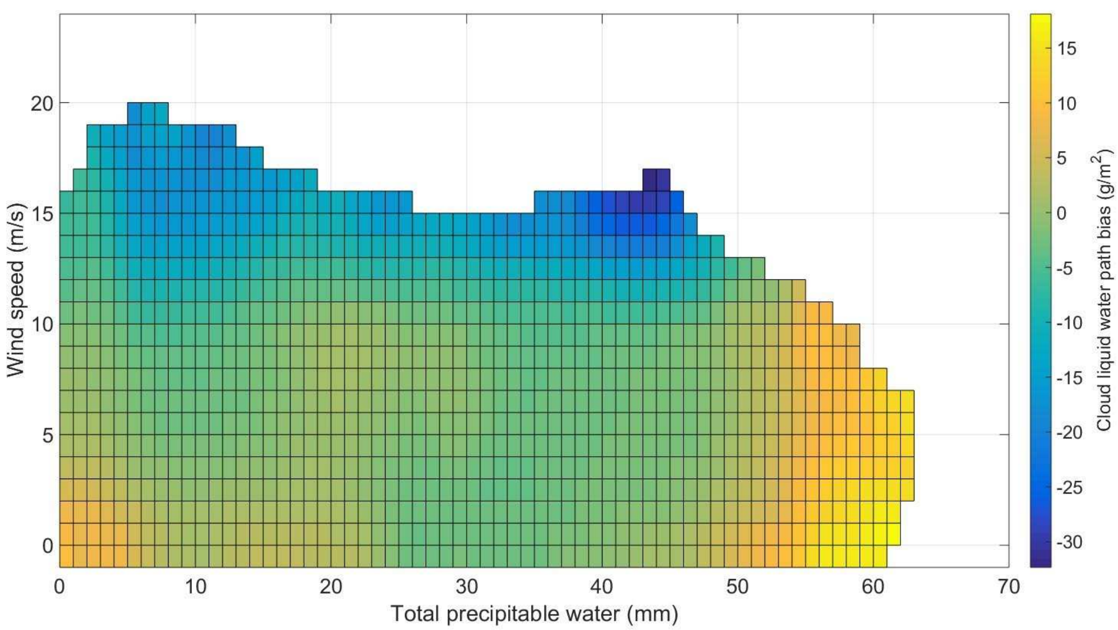

FIGURE 4.4. Figure provided by Tom Greenwald (personal communication) shows the LWP clear-sky bias as a function of retrieved wind speed and total precipitable water

where 0.18 kg/m^2 is the threshold value, H is the height of the rain column (km), parameterized using the Reynolds SST and the freezing level from the National Centers for Environmental Prediction-National Center for Atmospheric Research (NCEP-NCAR) reanalysis (Hilburn and Wentz, 2008), and R is the column averaged rain rate (mm/h). Since the threshold for this calculation is somewhat arbitrary, LWP retrievals have the potential to be over/underestimated depending on whether clouds are precipitating at values below/above this threshold, respectively. Also, since the microwave measures total water path then breaks it apart using the retrieved TWP value and H, the potential exists that incorrect LWP values could be obtained due to an incorrect parameterization of H. Like other systematic errors discussed in this chapter, spurious trends in either of the variables used to parameterize H could lead to spurious trends in LWP, but again, at an unknown level.

Although these systematic errors in the LWP retrievals can lead to errors of approximately 30% (O'Dell et al., 2008) in the retrieved LWP, it is relatively difficult to assign errors caused by these retrievals to errors in LWP trends. For the most part these errors manifest themselves as biases which will have the tendency to cancel in the computation of trends. However, as we have pointed out, spurious trends in non-LWP variables that are used in the LWP retrieval have the potential to cause spurious trends in LWP. In other words, if biases in LWP retrieval errors remain relatively consistent over time, they will have little to no effect on LWP trends. Conversely if the biases change over time, they have the potential to create spurious LWP trends. The extent to which these biases may or may not change and their effects on LWP trends remain unknown at present.

4.2.2. Systematic Errors in Trends Arising from the RSS Algorithm. The previous section detailed systematic errors in the LWP retrieval. The exact effect of these errors on LWP trends is currently unknown. This section details additional systematic errors in the level-2 RSS retrieval beyond those identified in O'Dell et al. (2008) that could also lead to spurious LWP trends. Most of these potential errors arise from the nature of the passive microwave retrieval algorithm used in the MAC-LWP dataset.

For the passive microwave sensors in the MAC-LWP dataset, a complex, semi-empirical retrieval algorithm is used to calculate variables including wind speed, water vapor, and total water path. (Wentz, 1997, Wentz and Spencer, 1998, Wentz and Meissner, 2000, Hilburn and Wentz, 2008). This is known as the RSS algorithm. The RSS algorithm begins with the brightness temperatures observed by the sensor and a set of 3 equations and 3 unknowns (Wentz, 1997). A suite of first guess values for the parameters to be retrieved are input into a brightness temperature model which is part of the aforementioned 3 equations. An iterative process is then used until each modeled brightness temperature is within 0.1K of the observed brightness temperature (Wentz, 1997). The values of water vapor, wind speed, and total water path that were input into the brightness temperature model in order to achieve final agreement are then considered to be the retrieved values.

Figure 4.5 shows how the brightness temperature model/algorithm used for the sensors in the MAC-LWP dataset was developed and tested using a multiple linear regression technique. Wentz (1997) took 42,195 quality controlled radiosonde launches from various island and ship stations across the globe from the time period from 1987-1990. For the radiosonde measurements, the SST, wind speed, and wind direction were all randomly varied to create a suite of scenes (Wentz and Meissner, 2000). From these scenes, T_B's, were computed using the full radiative transfer equation given in Wentz and Meissner (2000) by equations (17), (18), and (19). Noise, distributed in a Gaussian manner, was then added and part of the dataset was withheld for testing the algorithm later. The scenes that were not withheld for testing were used to compute regression coefficients for mathematical relationships used in

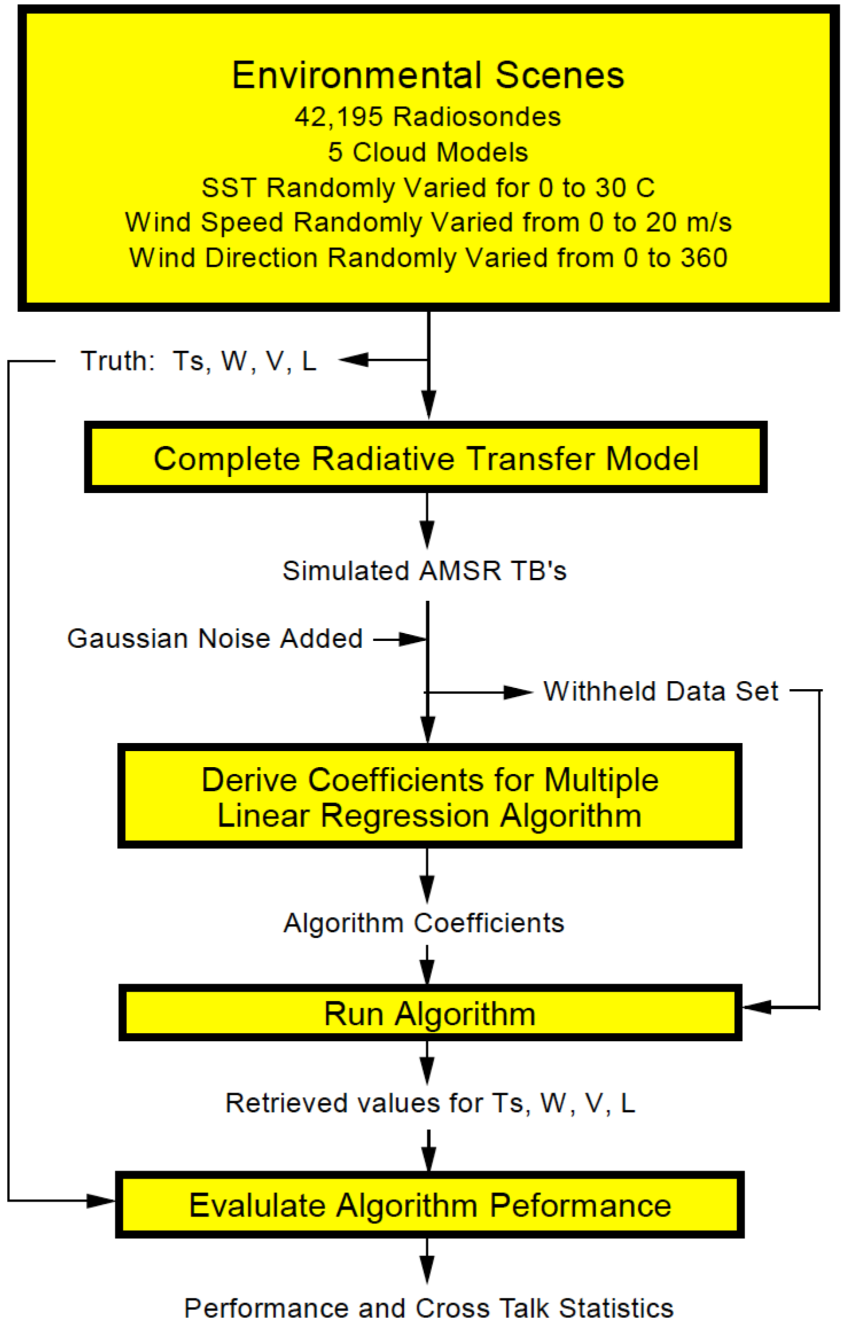

FIGURE 4.5. Flow chart detailing the RSS retrieval algorithm used in the retrieval of water vapor, surface wind speed and total water path. From Wentz and Meissner (2000) (Figure 5)

the RSS algorithm's T_B model. These resulting regression coefficients were then tested by using brightness temperatures from the withheld data into the T_B model and subsequently the algorithm and comparing the resulting values of water vapor, surface wind speed, and total water path to their 'true' values.

The way these regression coefficients were calculated is arguably the biggest potential systematic error in observed LWP trends. The relationships between variables defined by the regression coefficients were calculated using radiosonde measurements from a specific time period (1987-1990) and remained in the algorithm until the present day (Frank Wentz personal communication). If these relationships have changed in the past several decades due to changes in climate, these changes must manifest themselves in other variables in the retrieval algorithm (e.g., LWP) since they cannot manifest themselves in the static relationships defined by regression coefficients. However, it would take fairly large deviations in the atmospheric profile shape of temperature, water vapor, pressure, etc... between the time of the radiosonde measurements and present day for the algorithm to significantly affect trends (Frank Wentz, personal communication).

Another, related, potential source of systematic error is the way ocean salinity is calculated in the retrieval algorithm. The algorithm was initially trained on a constant salinity value of 35 ppt (Wentz, 1997). In recent years this was changed slightly. The brightness temperature is now corrected down from the constant salinity value of 35 ppt using the National Oceanic Data Center's (NDOC) World Ocean Atlas salinity values (Wentz and Meissner, 2007). Much like the trained regression coefficients, effectively training the ocean salinity on a set value can lead to potential systematic errors due to any changes that could occur in salinity with a changing climate. However, like the trained regression coefficients, the salinity would need to deviate significantly from the value of 35 ppt in order for systematic errors to have large effects on the measured LWP trends. Although the potential exists for large systematic errors to create spurious LWP trends, climatic deviations would need to be significant over the course of the past several decades for this to occur in any sort of substantial manner.

4.3. Other Sources of Error

In computing LWP trends, sources of error are not just confined to systematic errors in the retrieval algorithm. Natural variability of the climate and climate system has the potential to create apparent LWP trend values as well. Many studies have been performed that attempt to separate the effects of natural climate variability (e.g., volcanoes and the El-Niño Southern Oscillation) from anthropogenic effects (e.g., greenhouse gases) on the long term surface temperature trends (e.g., Lean and Rind, 2008, Thompson et al., 2009, Foster and Rahmstorf, 2011, Zhou and Tung, 2013). Separating these effects has allowed for a determination of how much recent warming can be attributed to anthropogenic forcing. In this work, we attempt a similar analysis on our observational LWP trends. This would help us determine not only the realism of these trends, but also any potential underlying physical mechanisms that may be closely linked to changes in LWP. This section mainly focuses on one source of natural variability, The El Niño-Southern Oscillation, and its effects on LWP trends. Other sources of natural variability such as environmental variables and other oscillations are discussed as well, but less detail is given in regards to these variables.

4.3.1. El Niño-Southern Oscillation. The El Niño-Southern Oscillation (ENSO) is a natural cycle related to sea surface temperature fluctuations in the Eastern and Central equatorial Pacific (Trenberth, 1997). It consists of two main phases, the warm (El Niño) phase where SSTs in the Eastern and Central equatorial Pacific are anomalously high, and the cool (La Niña) phase where SSTs in the Eastern and Central equatorial Pacific are anomalously low. This oscillation operates on a multi-annual timescale, with El Niño events occurring every few years. Other than SST fluctuations, ENSO is also known to have far reaching effects on various climatic variables e.g., atmospheric circulation and precipitation via teleconnections (e.g., Horel and Wallace, 1981, Trenberth et al., 1998, Dai and Wigley, 2000).

In order to test the effect that ENSO has on our observed LWP trends, the ENSO signal can be regressed out, following similar work on surface temperature (e.g., Lean and Rind, 2008, Foster and Rahmstorf, 2011, Zhou and Tung, 2013). The first step in accomplishing this is to define an ENSO signal. For this, we use the Multivariate ENSO Index (MEI) which combines data from 6 observed variables over the tropical Pacific including: sea-level pressure, zonal wind, meridional wind, sea surface temperature, air temperature, and cloud fraction to create a single value for twelve bi-month windows every year (i.e., December/January, January/February, etc...) that can be used as an indicator of ENSO strength (Wolter and Timlin, 1993). Positive values of MEI indicate an El Niño phase while negative values of MEI indicate a La Niña phase. Once the MEI data were obtained, the ENSO signal could be regressed out of the LWP time series for a given region and the trend could be recomputed.

Figure 4.6 shows global maps of the 27-year LWP trends, the 27-year LWP trends with the MEI ENSO signal regressed out following the method described above, a map that shows the difference in trends between the observed 27-year LWP trends and the ENSO-removed LWP trends, and a map depicting the correlation coefficient between the observed LWP and the MEI. Qualitatively, there does not appear to be too much of a difference between the observed 27-year LWP trends (4.6(a)) and the ENSO-removed 27-year trends (4.6(b)) over most of the globe, with the exception of the central equatorial Pacific where positive trends appear to be more pronounced while negative trends appear more dampened in the

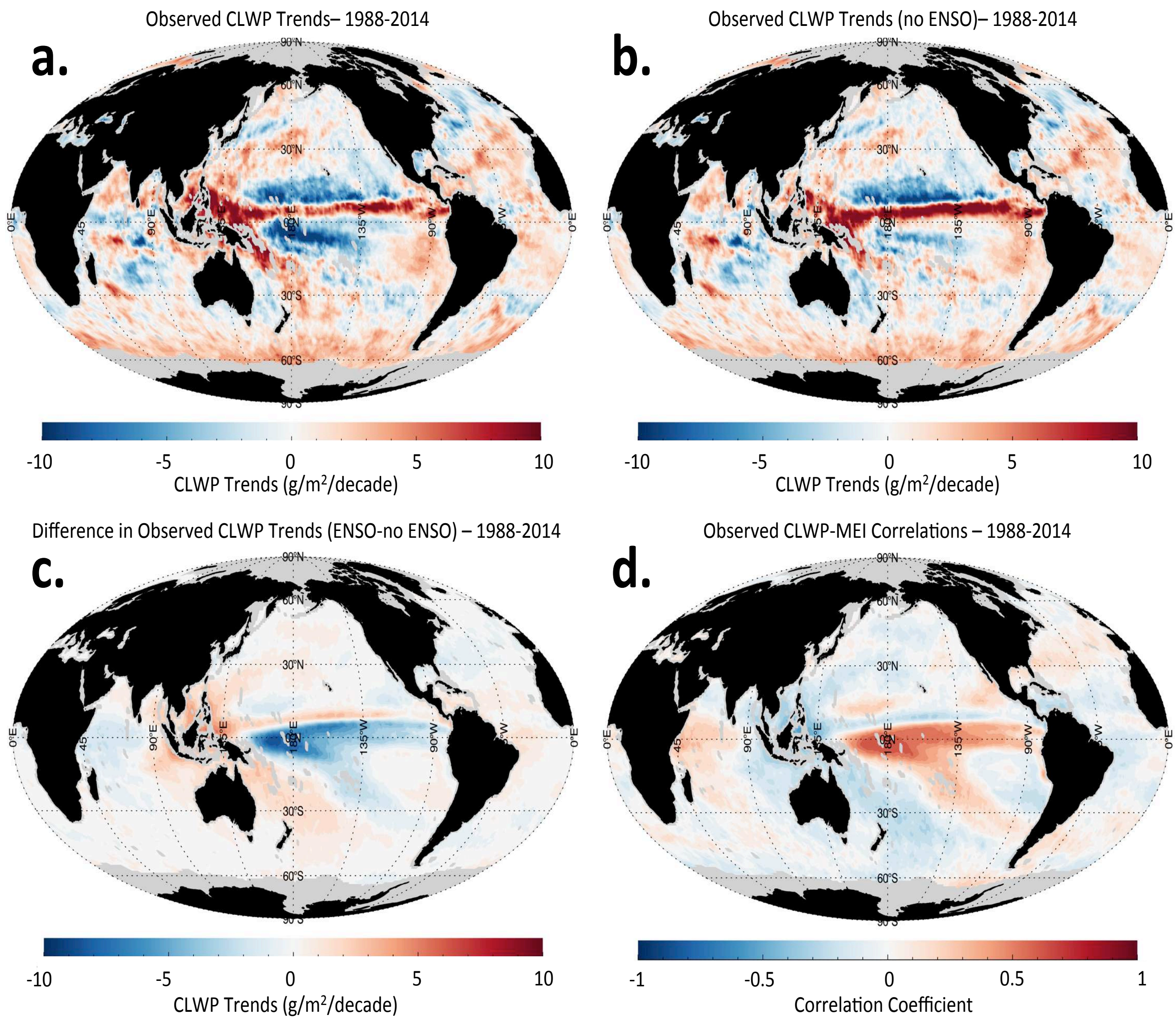

FIGURE 4.6. (a) The 27-year observed LWP trends, (b) the 27-year observed LWP trends with the MEI ENSO signal regressed out, (c) the difference between maps (a) and (b), and (d) the correlation between the MEI and LWP time series in each grid box

trends where ENSO was regressed out. Figure 4.6(c) verifies this qualitative assessment. The largest, most pronounced differences between the observed 27-year LWP trends and the ENSO-removed LWP trends occur in the central equatorial Pacific with the largest differences being approximately -10 g/m^2/decade. The differences between the two maps is minimal at higher latitudes and in tropical regions not in the Pacific. 4.6(d) shows the

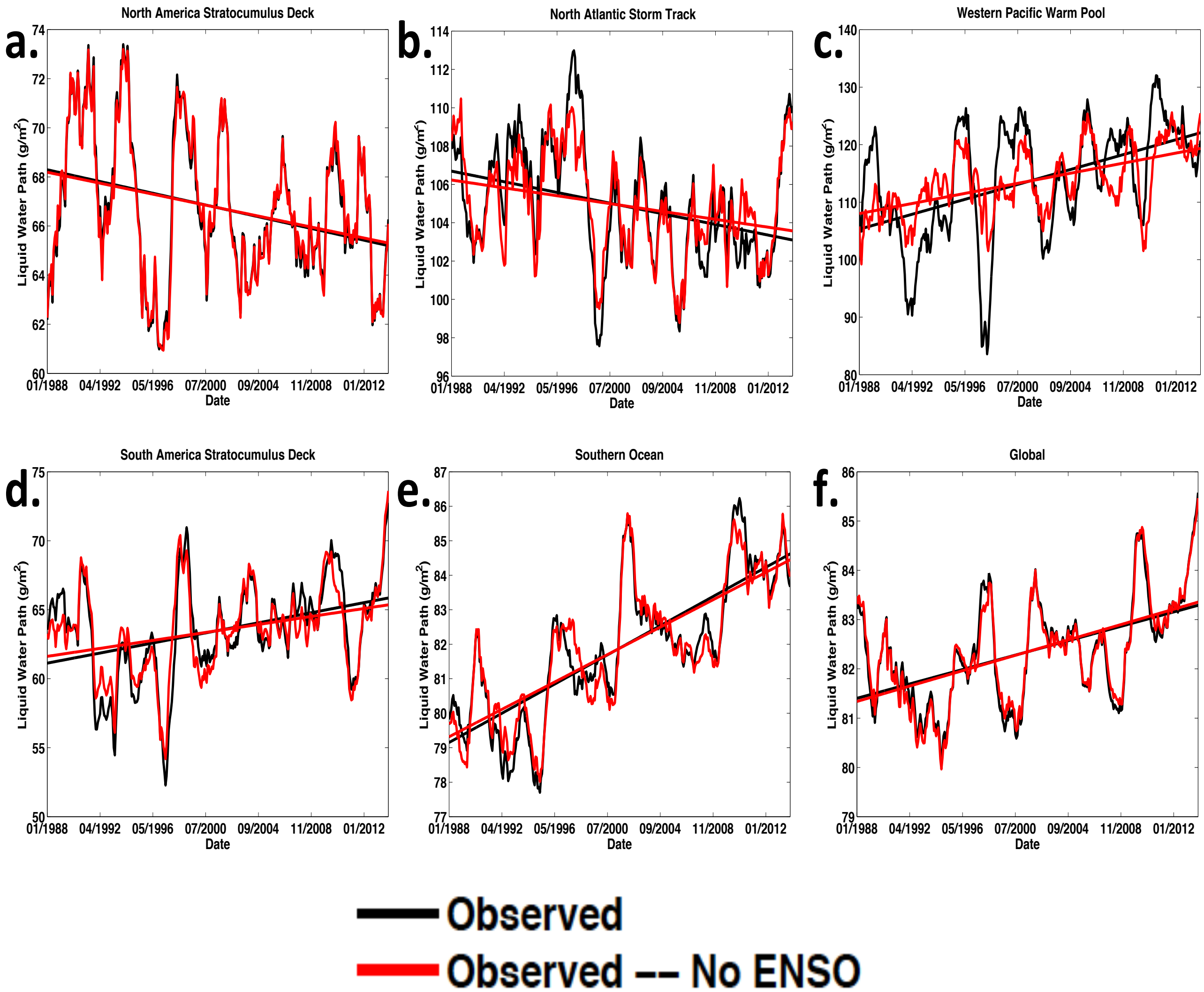

Figure 4.7. Observed 27-year LWP time series and trends and ENSO regressed 27-year time series and trends for the 6 regions analyzed in this study

correlation between the MEI time series and the LWP time series at each grid box. The strongest correlations (both negative and positive) appear to be co-located with the strongest differences between the regular and ENSO-removed trends (4.6(c)). Intuitively, this makes sense since we would expect regions that are more highly correlated with MEI to change more when its signal is regressed out.

Figure 4.7 displays the observed 27-year LWP trends overlaid with the 27-year ENSO-removed trends for the 6 regions analyzed in this study. In most regions, regressing out the

ENSO signal has little effect on either the mean state LWP values or the trends. The one exception being the Western Pacific Warm Pool where the magnitude of the trend decreases by approximately 1/3rd (6.10 $\pm$ 1.63 to 4.02 $\pm$ 1.18). This is to be expected since the Western Pacific Warm Pool is highly affected by changes in circulations and SSTs brought on by ENSO. We conclude from these results that, while ENSO has some effect on observed LWP trends in various parts of the globe, they generally tend to be minimal and are not likely to cause any apparent trends in LWP.

4.3.2. Environmental Variables. Other than ENSO, signals due to other environmental variables have the potential to affect the observed LWP trends. In this work, trends in two variables, local SST and local Total Column Water Vapor, were regressed out of our observed 27-year trends. It should be noted that these variables (ENSO, water vapor, and SST) are being regressed out of LWP trends for different reasons. When regressing out ENSO, we wanted to see if the trends were related to this oscillation which is generally not thought of as climatically forced. If removing ENSO led to a removal of trends, we could postulate that the LWP trends were mostly due to inter-annual variability and may not necessarily be climatically forced. The same is not true for SST and total column water vapor. If the removing SST and water vapor signals led to the removal of LWP trends in a given region, it does not necessarily mean that the LWP trends are incorrect or not climatically forced. Instead, it means cloud-forming mechanisms in said region are closely linked to SST and/or total column water vapor and/or one of these variables has a trend itself which could also potentially be climatically forced. For example, changes in SSTs can be correlated with changes in cloud cover/optical thickness. More evaporation off of a warmer sea surface can lead to larger amounts of convection which would lead to more/thicker clouds which, in turn, would lead to a cooling of SSTs thus creating a negative feedback. Increases (decreases) in

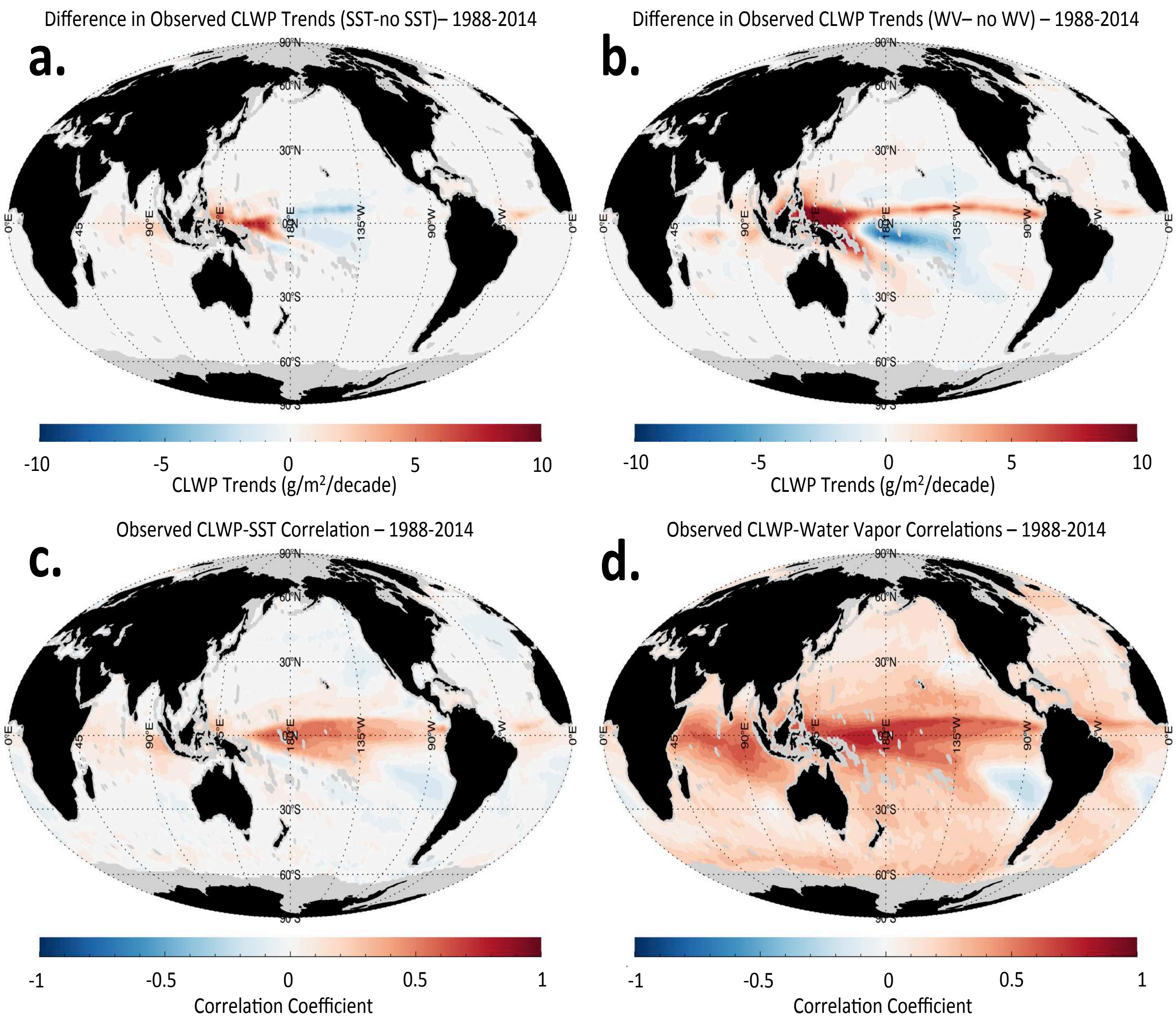

FIGURE 4.8. Difference between the 27-year observed LWP trends and the 27-year LWP trends with (a) the SST and (b) the total column water vapor regressed out. (c) and (d) show the correlation between local SST and local LWP and local total column water vapor and local LWP respectively

total column water vapor can lead to increases in LWP since there is more (less) water available for condensation. Due to these effects and their close relationship to LWP, we felt it would be pertinent to regress signals from these variables out of the observed 27-year LWP trends.

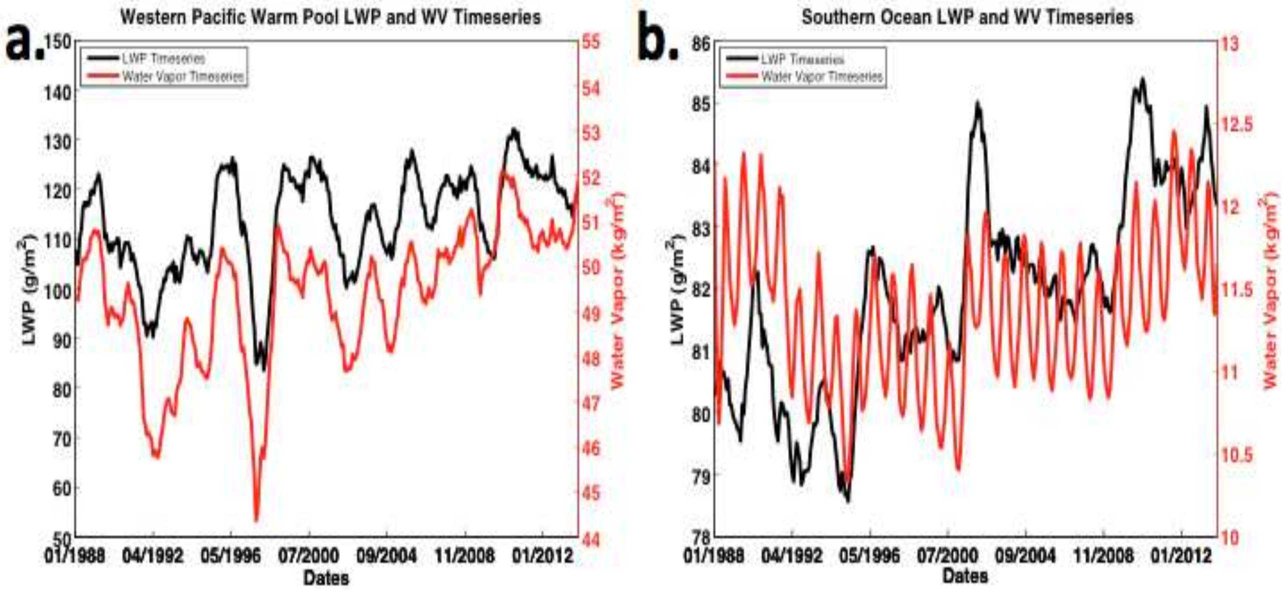

FIGURE 4.9. 27-year LWP and total column water vapor time series for the (a) Western Pacific Warm Pool and (b) Southern Ocean

The Reynolds Optimal Estimation SST dataset was used as our SST dataset (Reynolds et al., 2002). For our total column water vapor dataset, data were taken from the ECMWF reanalysis from the same time period (1988-2014) as our observed data (Dee et al., 2011). The signals from these variables were regressed out in the same manner as the ENSO MEI variable. It should be noted that the signals from these variables were regressed out locally i.e., SSTs and total column water vapor signals in a given grid box were regressed out of LWP trends from the same grid box. This is different from the MEI dataset, where the single MEI index was regressed out of every 1°x1° grid box globally.

Figure 4.8 shows the differences between the observed 27-year LWP trends and the 27-year LWP trends with SST (4.8(a)) and total column water vapor (4.8(b)) regressed out. Similar to ENSO, the strongest differences in both of the variables tend to occur in the equatorial Pacific. However, these differences do not tend to be as strong or widespread as differences in the ENSO regressed maps. Regressing out SST has little to no effect over much of the globe. Regressing out water vapor has slightly more of an effect than regressing out SST. Most of this can be seen in the West Pacific Warm Pool, ITCZ, and SPCZ regions. Upon further investigation, it was found that regressing out the total column water vapor signal has little to no effect on all of the regions analyzed, except for the Western Pacific Warm Pool where it was found that the total column water vapor signal accounts for almost the entire observed LWP trend. Regressing out the total column water vapor signal changes the observed trend from 6.102 ± 1.63 g/m^2/decade to 0.025 ± 1.03 g/m^2/decade. Figures 4.8(c) and 4.8(d) show the correlation coefficient at each grid box between the local SST and local LWP and local total column water vapor and local LWP (respectively). As with the MEI signal (see figures 4.6(c) and 4.6(d)), the regions where the water vapor and SST signals are most strongly correlated with the LWP signal (i.e., the Western Pacific Warm Pool), are the regions where there is the largest difference between the observed LWP trends and the ones with the SST and water vapor signals removed. Again, this intuitively makes sense since we would expect regions that are more highly correlated with SST and water vapor to change more when their signals are regressed out.

The strong relationship between LWP and total column water vapor in the Western Pacific Warm Pool can be seen in figure 4.9(a) which displays the observed 27-year LWP time series in the Western Pacific Warm Pool over-plotted with the ECMWF ERA-interim reanalysis total column water vapor from 1988-2014. The two time series track each other very closely, having a correlation coefficient of 0.89. This close relationship helps to explain why regressing out the water vapor signal leads to such a drastic decrease in the observed LWP trend value in this region. For contrast, 4.9(b) shows the LWP and water vapor time series for the Southern Ocean. These two time series do not track as well as the ones in the Western Pacific Warm Pool, only having a correlation coefficient of 0.37. This helps to explain why there is little to no effect on the Southern Ocean trend when the water vapor is regressed out (2.07 ± 0.257 g/m^2/decade before regression and 2.06 ± 0.257 g/m^2/decade after). These changes in both regions would appear to indicate that LWP trends in the Western Pacific Warm Pool are strongly tied to changes and trends in water vapor (i.e., cloud forming mechanisms), whereas trends in the Southern Ocean are less associated with cloud-forming mechanisms such as water vapor and are potentially due to some other mechanism e.g., the poleward shift of storm tracks (see section 3.2.2)

This work only covered a small portion of natural variability and climatic variables that could potentially affect LWP trends. We picked variables and oscillations that we felt to be the most relevant and would have the biggest potential impact if they were regressed out of the observed 27-year LWP trends. Again it should be noted that removing these variables effects the trends for different reasons. Removing the ENSO signal from LWP trends gives us an indication of how much our observed trends are due to inter-annual variability associated with ENSO. Removing water vapor and SST signals gives us an indication as to how closely LWP trends are tied to cloud-forming mechanisms that may be climatically forced i.e., it provides insight into physical mechanisms for our LWP trends. Given the relatively small impact of regressing these variables out of LWP trends, it seems unlikely that other, less important variables would have a large impact. For example, effects such as those from volcanoes have the potential to alter LWP in various regions, however, they tend to be relatively short-lived (several years) therefore if major volcanic events do not occur near the beginning or ending of an observed LWP time series, it seems unlikely that they would have a substantial effect on trends although regressing out a volcanic index of sorts would be required to verify this hypothesis. Some oscillations with potential far reaching teleconnections act on longer timescales than the data we have available (e.g., the Pacific Decadal Oscillation (Mantua and Hare, 2002)), therefore we cannot test the effects these may have on our observed LWP time series. More years of data are required for such an analysis to be made. Despite this, our work appears to show that the largest potential natural contributors to spurious LWP trends have a minimal effect on observed trends.

CHAPTER 5

Summary and Discussion

5.1. Summary and Conclusions

In this work, trends in observed cloud liquid water path taken from the Multisensor Advanced Climatology of Liquid Water Path (MAC-LWP) dataset were examined and subsequently compared to trends in modeled cloud liquid water path from a suite of 16 models from the Climate Model Intercomparison Project 5 (CMIP5). Mean state values of observed LWP were first compared to those of previous climatologies (e.g., Horvath (2004)) and were found to have relatively good quantitative and qualitative agreements with these previous observations. The MAC-LWP dataset was also found to be consistent with our knowledge of clouds and atmospheric phenomena in regards to regional mean seasonal cycle. Mean state observed LWP variables were then compared both qualitatively and quantitatively to various CMIP5 models. CMIP5 models tended to capture some mean state and mean seasonal cycle LWP features, but the magnitudes exhibited large variations from model to model (figures 2.5 and 2.6). Several metrics were used to compare the observed and modeled mean state LWP and the observed and modeled mean seasonal cycle amplitude in each model (figures 2.7 and 2.8). However, the models' performance in regards to these metrics was found to not be indicative of their abilities to accurately reproduce trends on a regional or global scale. These findings led us to conclude that the MAC-LWP dataset is a potentially useful tool with which to evaluate the realism of anthropogenically-forced trends in climate models. This is evident by its strong agreement with previous LWP studies in regards to mean state LWP and its robust and largely statistically significant trends both regionally and globally.

However, the primary caveat to this is that inter-annual variability in both the observations an models can obscure underlying trends in certain regions, even in a 27-year long record.

Global and regional trends in the observations and the model means were compared. It was found that observational trends were roughly 2-3 times larger in magnitude in most regions globally when compared to the model mean, although this was thought to be at least partly caused by cancellation effects due to differing inter-annual variabilities and physics between models (illustrated in figure 3.2). Several regions had consistent signs in trends between the observations and the model mean, while others did not due to spatial inconsistencies in certain trend features between the model mean and the observations. Trends were examined in individual regions. Statistical errors were calculated for each trend, under the assumption that there was at least a slight autocorrelation (i.e., the observations in one month at least partially depended on the observations from the previous month) and noise in each time series. In four of the six regions analyzed, the observational trends were statistically significant within 2σ. In the two regions which were not statistically significant (the North American Stratocumulus Deck and the North Atlantic Storm Track) the North Atlantic Storm Track region was almost statistically significant. In most regions, very few models had trends that were statistically different from zero at 95% confidence (i.e., were statistically significant). However, in certain regions, the majority of modeled trends were statistically consistent with the observed trends (i.e., they agreed with the observations at 95% confidence) although this was typically due to large estimated errors in the observations and/or models, most likely caused by large inter-annual variability. I.e., without longer time series or smaller inter-annual variability, it was difficult to rule out regional model trends from single ensemble runs at high confidence. From this, we conclude that while the CMIP5 LWP trends in the majority of regions analyzed generally agreed with the observations to within the errors, these errors were rather large because inter-annual variability still plays a significant role (particularly in models), even in a 27-year dataset.

In two regions examined (the Southern Ocean and globally), trends showed the strongest similarities to the observed trends. Like the observations, almost all Southern Ocean trends were robustly positive and statistically significant (14 of the 16 models were statistically significant at 2σ and 11 of 16 models agreed with the observed trend at 95% confidence). From this, we hypothesize that, in this region, inter-annual variability has less of an effect on our modeled and observed trends and/or the trends are merely strong enough to overcome effects of inter-annual variability. Similar to the Southern Ocean, the observed and modeled global trends were all positive with 11 of the 16 models showing statistical significance and 13 of the 16 models agreeing with the observed trend at 95% confidence. We conclude that global trends likely show strong agreement mainly due to cancellation effects which cause a reduction in both inter-annual variability effects and the spread in magnitudes of trends. Possible reasons for the large positive Southern Ocean trends in most models and the observations were discussed. The only one that was explicitly tested was whether or not the robust positive trends could be attributed to phase changes from ice to liquid as the climate warms. This was deemed to not be a large factor in modeled LWP trends and thus lent more credibility to other possible explanations (e.g., storm track shift and optical depth feedbacks).

CMIP5 model mean and observational trends were compared regionally to AMIP model mean and ERA trends. It was found that AMIP model mean and ERA LWPs were better than the CMIP5 model mean at capturing the inter-annual variability in the observed time series in most regions, leading to trends that were more similar to the observed in some regions, such as the West Pacific Warm Pool. It was found that the AMIP model mean better replicated the observed trends when the inter-annual variability was better captured. The ERA reanalysis tended to replicate the inter-annual variability better than the AMIP model mean in almost every region, but, surprisingly, was either worse or roughly the same as the AMIP model mean in regards to matching observed trends. Since AMIP is more closely coupled to the CMIP5 models we decided to mainly focus on those results. The fact that the regions where the AMIP model mean better captures inter-annual variability are the same regions where the observed trends are better captured is potentially indicative of a couple scenarios, either: (a) the observed trends are primarily driven by inter-annual variability as opposed to forced trends or (b) they are due to thermodynamic physics. If the former is the case, better modeled inter-annual variability will naturally give more accurate trends since that is the main driver. If the latter is the case, correct physics and correct SSTs in the AMIP (and CMIP5) experiments would lead to more correct inter-annual variability and trends. Despite this, there are still some significant discrepancies between AMIP model mean trends with their observed counterparts in certain regions (see figure 3.10) although it shows marked improvement over the CMIP5 model mean

Potential errors in the observed dataset and how these might lead to systematic errors in the observed trends were discussed. Systematic errors in the mean state such as errors due to cloud top temperature, ice effects, cross-talk, clear-sky biases, and cloud-rain partitioning were briefly described. It was determined that these errors generally manifest themselves as biases in LWP. If these biases in the LWP retrieval remain relatively consistent over time, they will have little to no effect on LWP trends. Conversely, if the biases change over time, they have the potential to create spurious LWP trends. The extent to which these biases may or may not change and their effects on LWP trends remains unknown at present. Further work is needed to quantify how the effects of these errors translate over to LWP trends.

Potential systematic errors due to the RSS retrieval algorithm (Wentz, 1997) are discussed. These primarily include the use of an older dataset to calculate regression coefficients in the algorithm (i.e., the algorithm is "trained" on these data) and the use of a climatological value of sea surface salinity. It was determined (based on personal communication with Frank Wentz) that, unless present day values deviated significantly from these older datasets, it was unlikely that these would lead to significant spurious trends in LWP. Several signals were regressed out of the LWP time series in order to determine their potential to create apparent trends. These included the ENSO, water vapor, and sea surface temperature (SST) signals. Regressing these signals out was found to have a minimal effect on trends in most areas of the globe (figures 4.6 and 4.8) except for the equatorial Pacific where the ENSO and water vapor signals were highly correlated with LWP. This was confirmed when analyzing individual regional trends (figure 4.7 and 4.9). The fact that the removal of natural variability brought about by ENSO caused minimal changes in most regional LWP trends, gave us further confidence in the potential for the MAC-LWP dataset to be a useful tool when evaluating the realism of anthropogenically-forced trends in climate models.

5.2. Future Work

Several avenues of future work can be followed from this research. Firstly, as more data become available and the MAC-LWP dataset becomes longer, observed trends will become more robust and the errors will be reduced, thereby making this dataset an even better diagnostic tool. As the time series gets longer, the effects that any oscillations that act on multidecadal timescales may have on LWP trends will become more apparent. It is also important that we make further attempts to characterize inter-annual variability in the MAC-LWP observations so we can remove it, thus any obscuring effect it may have on long-term

LWP trends. Secondly, as mentioned previously, LWP contains information on both cloud fraction and cloud optical depth, however, the relative contributions of these two to changes in LWP seen in the MAC-LWP dataset cannot be discerned at present. It could potentially be enlightening to attempt to divide changes in LWP into changes from cloud fraction and cloud optical depth, perhaps through the use of other cloud fraction and cloud optical depth datasets. Thirdly, it is important to quantify the effects of systematic retrieval errors have on observed LWP trends. This would require the use of either the RSS algorithm itself or a toy version that contains similar biases. Such a toy model would allow one to characterize biases due to a number of potential sources, such as cross-talk between different variables, trends in salinity, the presence of unaccounted-for ice, etc... Finally, it may be possible to approximately quantify the relationship between LWP and CRF, which would allow us to relate the observed LWP changes to changes in radiative forcing and hence cloud feedbacks.. This would show how relevant changes in LWP are to cloud feedbacks compared to changes in other climate variables. It seems highly likely that changes in LWP are relevant to cloud feedbacks based on this work and works such as Zelinka et al. (2012a,b), such that even an approximate quantification would be invaluable for reducing the spread in modeled cloud feedbacks. However, this work has shown that LWP trends, particularly those in models, have relatively large errors associated with them because inter-annual variability still plays a significant role, even in a 27-year dataset. These errors related to inter-annual variability must be reduced in both models and observations in order for the observed LWP trends to be more accurately related to modeled LWP trends and thus cloud feedbacks and subsequently equilibrium climate sensitivity.

References

Arora, V., Scinocca, J., Boer, G., Christian, J., Denman, K., Flato, G., Kharin, V., Lee, W., and Merryfield, W.: Carbon emission limits required to satisfy future representative concentration pathways of greenhouse gases, Geophysical Research Letters, 38, 2011.

Barnes, E. A. and Polvani, L.: Response of the midlatitude jets, and of their variability, to increased greenhouse gases in the CMIP5 models, Journal of Climate, 26, 7117–7135, 2013.

Bellomo, K., Clement, A. C., Norris, J. R., and Soden, B. J.: Observational and model estimates of cloud amount feedback over the Indian and Pacific Oceans, Journal of Climate, 27, 925–940, 2014.

Betts, A. K.: Thermodynamic Constraint on the Cloud Liquid Water Feedback, Journal of Geophysical Research, 92, 8483–8485, 1987.

Bony, S. and Dufresne, J.-L.: Marine boundary layer clouds at the heart of tropical cloud feedback uncertainties in climate models, Geophysical Research Letters, 32, 2005.

Borg, L. A. and Bennartz, R.: Vertical structure of stratiform marine boundary layer clouds and its impact on cloud albedo, Geophysical research letters, 34, 2007.

Boucher, O., Randall, D., Artaxo, P., Bretherton, C., Feingold, G., Forster, P., Kerminen, V.-M., Kondo, Y., Liao, H., Lohmann, U., et al.: Clouds and aerosols, in: Climate change 2013: the physical science basis. Contribution of Working Group I to the Fifth Assessment Report of the Intergovernmental Panel on Climate Change, pp. 571–657, Cambridge University Press, 2013.

Campbell, G. G.: View angle dependence of cloudiness and the trend in ISCCP cloudiness, in: Thirteenth Conference on Satellite Meteorology and Oceanography, American Meteorological Society, Boston P, vol. 6, 2004.

Cess, R., Zhang, M., Ingram, W., Potter, G., Alekseev, V., Barker, H., Cohen-Solal, E., Colman, R., Dazlich, D., Del Genio, A., et al.: Cloud feedback in atmospheric general circulation models: An update, Journal of Geophysical Research: Atmospheres (1984–2012), 101, 12 791–12 794, 1996.

Cess, R. D. and Udelhofen, P. M.: Climate change during 1985–1999: Cloud interactions determined from satellite measurements, Geophysical research letters, 30, 19–1, 2003.

Cess, R. D., Potter, G., Blanchet, J., Boer, G., Del Genio, A., Deque, M., Dymnikov, V., Galin, V., Gates, W., Ghan, S., et al.: Intercomparison and interpretation of climate feedback processes in 19 atmospheric general circulation models, Journal of Geophysical Research, 95, 601 216, 1990.

Charlock, T. P.: Cloud optical feedback and climate stability in a radiative-convective model, Tellus, 34, 245–254, 1982.

Clement, A. C., Burgman, R., and Norris, J. R.: Observational and model evidence for positive low-level cloud feedback, Science, 325, 460–464, 2009.

Collins, M., Knutti, R., Arblaster, J., Dufresne, J.-L., Fichefet, T., Friedlingstein, P., Gao, X., Gutowski, W., Johns, T., Krinner, G., et al.: Long-term climate change: projections, commitments and irreversibility, 2013.

Conley, A. J., Garcia, R., Kinnison, D., Lamarque, J.-F., Marsh, D., Mills, M., Smith, A. K., Tilmes, S., Vitt, F., Morrison, H., et al.: Description of the NCAR Community Atmosphere Model (CAM 5.0), 2012.

Dai, A. and Wigley, T.: Global patterns of ENSO-induced precipitation, Geophysical Research Letters, 27, 1283–1286, 2000.

Dee, D., Uppala, S., Simmons, A., Berrisford, P., Poli, P., Kobayashi, S., Andrae, U., Balmaseda, M., Balsamo, G., Bauer, P., et al.: The ERA-Interim reanalysis: Configuration and performance of the data assimilation system, Quarterly Journal of the Royal Meteorological Society, 137, 553–597, 2011.

Dessler, A. and Loeb, N.: Impact of dataset choice on calculations of the short-term cloud feedback, Journal of Geophysical Research: Atmospheres, 118, 2821–2826, 2013.

Dessler, A. E.: A determination of the cloud feedback from climate variations over the past decade, Science, 330, 1523–1527, 2010.

Donner, L. J., Wyman, B. L., Hemler, R. S., Horowitz, L. W., Ming, Y., Zhao, M., Golaz, J.-C., Ginoux, P., Lin, S.-J., Schwarzkopf, M. D., et al.: The dynamical core, physical parameterizations, and basic simulation characteristics of the atmospheric component AM3 of the GFDL global coupled model CM3, Journal of Climate, 24, 3484–3519, 2011.

Dufresne, J.-L. and Bony, S.: An assessment of the primary sources of spread of global warming estimates from coupled atmosphere-ocean models, Journal of Climate, 21, 5135–5144, 2008.

Dufresne, J.-L., Foujols, M.-A., Denvil, S., Caubel, A., Marti, O., Aumont, O., Balkanski, Y., Bekki, S., Bellenger, H., Benshila, R., et al.: Climate change projections using the IPSL-CM5 Earth System Model: from CMIP3 to CMIP5, Climate Dynamics, 40, 2123–2165, 2013.

Dunne, J. P., John, J. G., Adcroft, A. J., Griffies, S. M., Hallberg, R. W., Shevliakova, E., Stouffer, R. J., Cooke, W., Dunne, K. A., Harrison, M. J., et al.: GFDL's ESM2 global coupled climate-carbon Earth System Models. Part I: Physical formulation and baseline simulation characteristics, Journal of Climate, 25, 6646–6665, 2012.

Elsaesser, G., O'Dell, C., and Teixeira, J.: Algorithm Theoretical Basis Document (ATBD) Version 1, Multi-Sensor Advanced Climatology of Liquid Water Path (MAC-LWP), 2015.

Evan, A. T., Heidinger, A. K., and Vimont, D. J.: Arguments against a physical long-term trend in global ISCCP cloud amounts, Geophysical Research Letters, 34, 2007.

Flato, G., Marotzke, J., Abiodun, B., Braconnot, P., Chou, S. C., Collins, W., Cox, P., Driouech, F., Emori, S., Eyring, V., et al.: Evaluation of climate models, in: Climate Change 2013: The Physical Science Basis. Contribution of Working Group I to the Fifth Assessment Report of the Intergovernmental Panel on Climate Change, pp. 741–866, Cambridge University Press, 2013.

Foster, G. and Rahmstorf, S.: Global temperature evolution 1979–2010, Environmental Research Letters, 6, 044 022, 2011.

Gent, P. R., Danabasoglu, G., Donner, L. J., Holland, M. M., Hunke, E. C., Jayne, S. R., Lawrence, D. M., Neale, R. B., Rasch, P. J., Vertenstein, M., et al.: The community climate system model version 4, Journal of Climate, 24, 4973–4991, 2011.

Greenwald, T. J., Stephens, G. L., Vonder Haar, T. H., and Jackson, D. L.: A physical retrieval of cloud liquid water over the global oceans using Special Sensor Microwave/Imager (SSM/I) observations, Journal of Geophysical Research: Atmospheres (1984–2012), 98, 18 471–18 488, 1993.

Greenwald, T. J., Stephens, G. L., Christopher, S. A., and Vonder Haar, T. H.: Observations of the global characteristics and regional radiative effects of marine cloud liquid water, Journal of climate, 8, 2928–2946, 1995.

Greenwald, T. J., Christopher, S. A., and Chou, J.: Cloud liquid water path comparisons from passive microwave and solar reflectance satellite measurements: Assessment of sub-field-of-view cloud effects in microwave retrievals, Journal of Geophysical Research: Atmospheres (1984–2012), 102, 19 585–19 596, 1997.

Greenwald, T. J., L'Ecuyer, T. S., and Christopher, S. A.: Evaluating specific error characteristics of microwave-derived cloud liquid water products, Geophysical Research Letters, 34, 2007.

Held, I. M. and Soden, B. J.: Robust responses of the hydrological cycle to global warming, Journal of Climate, 19, 5686–5699, 2006.

Hilburn, K. and Wentz, F.: Intercalibrated passive microwave rain products from the unified microwave ocean retrieval algorithm (UMORA), Journal of Applied Meteorology and Climatology, 47, 778–794, 2008.

Horel, J. D. and Wallace, J. M.: Planetary-scale atmospheric phenomena associated with the Southern Oscillation, Monthly Weather Review, 109, 813–829, 1981.

Horvath, A.: Differences between satellite measurements and theoretical estimates of global cloud liquid water amounts, 2004.

Horváth, Á. and Davies, R.: Comparison of microwave and optical cloud water path estimates from TMI, MODIS, and MISR, Journal of Geophysical Research: Atmospheres (1984–2012), 112, 2007.

Jiang, J. H., Su, H., Zhai, C., Perun, V. S., Del Genio, A., Nazarenko, L. S., Donner, L. J., Horowitz, L., Seman, C., Cole, J., et al.: Evaluation of cloud and water vapor simulations in CMIP5 climate models using NASA A-Train satellite observations, Journal of Geophysical Research: Atmospheres (1984–2012), 117, 2012.

Joyce, R., Janowiak, J., and Huffman, G.: Latitudinally and seasonally dependent zenith-angle corrections for geostationary satellite IR brightness temperatures, Journal of Applied Meteorology, 40, 689–703, 2001.

Kirkevåg, A., Iversen, T., Seland, Ø., Hoose, C., Kristjánsson, J., Struthers, H., Ekman, A. M., Ghan, S., Griesfeller, J., Nilsson, E. D., et al.: Aerosol–climate interactions in the Norwegian Earth System Model–NorESM1-M, Geoscientific Model Development, 6, 207–244, 2013.

Lauer, A. and Hamilton, K.: Simulating clouds with global climate models: A comparison of CMIP5 results with CMIP3 and satellite data, Journal of Climate, 26, 3823–3845, 2013.

Lean, J. L. and Rind, D. H.: How natural and anthropogenic influences alter global and regional surface temperatures: 1889 to 2006, Geophysical Research Letters, 35, 2008.

Lin, B. and Rossow, W. B.: Observations of cloud liquid water path over oceans: Optical and microwave remote sensing methods, Journal of Geophysical Research: Atmospheres (1984–2012), 99, 20 907–20 927, 1994.

Lindsay, K., Bonan, G. B., Doney, S. C., Hoffman, F. M., Lawrence, D. M., Long, M. C., Mahowald, N. M., Keith Moore, J., Randerson, J. T., and Thornton, P. E.: Preindustrial-control and twentieth-century carbon cycle experiments with the Earth System Model CESM1 (BGC), Journal of Climate, 27, 8981–9005, 2014.

Liu, G. and Curry, J. A.: Determination of characteristic features of cloud liquid water from satellite microwave measurements, Journal of Geophysical Research: Atmospheres (1984–2012), 98, 5069–5092, 1993.

Loeb, N. G., Wielicki, B. A., Doelling, D. R., Smith, G. L., Keyes, D. F., Kato, S., Manalo-Smith, N., and Wong, T.: Toward optimal closure of the Earth's top-of-atmosphere radiation budget, Journal of Climate, 22, 748–766, 2009.

Mantua, N. J. and Hare, S. R.: The Pacific decadal oscillation, Journal of oceanography, 58, 35–44, 2002.

Mbengue, C. and Schneider, T.: Storm track shifts under climate change: What can be learned from large-scale dry dynamics, Journal of Climate, 26, 9923–9930, 2013.

Nakajima, T. and King, M. D.: Determination of the optical thickness and effective particle radius of clouds from reflected solar radiation measurements. Part I: Theory, Journal of the atmospheric sciences, 47, 1878–1893, 1990.

Norris, J. R.: What can cloud observations tell us about climate variability?, Space Science Reviews, 94, 375–380, 2000.

Norris, J. R. and Evan, A. T.: Empirical removal of artifacts from the ISCCP and PATMOS-x satellite cloud records, Journal of Atmospheric and Oceanic Technology, 32, 691–702, 2015.

O'Dell, C. W., Wentz, F. J., and Bennartz, R.: Cloud liquid water path from satellite-based passive microwave observations: A new climatology over the global oceans, Journal of Climate, 21, 1721–1739, 2008.

Pallé, E., Goode, P., Montañés-Rodríguez, P., and Koonin, S.: Changes in Earth's reflectance over the past two decades, Science, 304, 1299–1301, 2004.

Paltridge, G.: Cloud-radiation feedback to climate, Quarterly Journal of the Royal Meteorological Society, 106, 895–899, 1980.

Petty, G. W.: On the response of the Special Sensor Microwave/Imager to the marine environment-Implications for atmospheric parameter retrievals, Ph.D. thesis, NASA, 1990.

Randall, D. A., Wood, R. A., Bony, S., Colman, R., Fichefet, T., Fyfe, J., Kattsov, V., Pitman, A., Shukla, J., Srinivasan, J., et al.: Climate models and their evaluation, in: Climate Change 2007: The physical science basis. Contribution of Working Group I to the

Fourth Assessment Report of the IPCC (FAR), pp. 589–662, Cambridge University Press, 2007.

Reynolds, R. W., Rayner, N. A., Smith, T. M., Stokes, D. C., and Wang, W.: An improved in situ and satellite SST analysis for climate, Journal of climate, 15, 1609–1625, 2002.

Roeckner, E., Schlese, U., Biercamp, J., and Loewe, P.: Cloud optical depth feedbacks and climate modelling, Nature, 329, 138–140, 1987.

Rossow, W. B. and Schiffer, R. A.: Advances in understanding clouds from ISCCP, Bulletin of the American Meteorological Society, 80, 2261–2287, 1999.

Rotstayn, L. D., Collier, M. A., Dix, M. R., Feng, Y., Gordon, H. B., O'Farrell, S. P., Smith, I. N., and Syktus, J.: Improved simulation of Australian climate and ENSO-related rainfall variability in a global climate model with an interactive aerosol treatment, International Journal of Climatology, 30, 1067–1088, 2010.

Santer, B. D., Boyle, J., Hnilo, J., Taylor, K., Wigley, T., Nychka, D., Gaffen, D., and Parker, D.: Statistical significance of trends and trend differences in layer-average atmospheric temperature time series, Journal of Geophysical Research, 105, 7337–7356, 2000.

Schlesinger, M. E.: Negative or positive cloud optical depth feedback?, Nature, 335, 303–304, 1988.

Schmidt, G. A., Kelley, M., Nazarenko, L., Ruedy, R., Russell, G. L., Aleinov, I., Bauer, M., Bauer, S. E., Bhat, M. K., Bleck, R., et al.: Configuration and assessment of the GISS ModelE2 contributions to the CMIP5 archive, Journal of Advances in Modeling Earth Systems, 6, 141–184, 2014.

Schneider, S. H.: Cloudiness as a global climatic feedback mechanism: The effects on the radiation balance and surface temperature of variations in cloudiness, Journal of the Atmospheric Sciences, 29, 1413–1422, 1972.

Scoccimarro, E., Gualdi, S., Bellucci, A., Sanna, A., Giuseppe Fogli, P., Manzini, E., Vichi, M., Oddo, P., and Navarra, A.: Effects of tropical cyclones on ocean heat transport in a high-resolution coupled general circulation model, Journal of Climate, 24, 4368–4384, 2011.

Seethala, C. and Horváth, Á.: Global assessment of AMSR-E and MODIS cloud liquid water path retrievals in warm oceanic clouds, Journal of Geophysical Research: Atmospheres (1984–2012), 115, 2010.

Senior, C. and Mitchell, J.: Carbon dioxide and climate. The impact of cloud parameterization, Journal of Climate, 6, 393–418, 1993.

Shell, K. M., Kiehl, J. T., and Shields, C. A.: Using the radiative kernel technique to calculate climate feedbacks in NCAR's Community Atmospheric Model, Journal of Climate, 21, 2269–2282, 2008.

Soden, B. J. and Held, I. M.: An assessment of climate feedbacks in coupled ocean-atmosphere models, Journal of Climate, 19, 3354–3360, 2006.

Soden, B. J., Broccoli, A. J., and Hemler, R. S.: On the use of cloud forcing to estimate cloud feedback, Journal of climate, 17, 3661–3665, 2004.

Soden, B. J., Held, I. M., Colman, R., Shell, K. M., Kiehl, J. T., and Shields, C. A.: Quantifying climate feedbacks using radiative kernels, Journal of Climate, 21, 3504–3520, 2008.

Somerville, R. C. and Remer, L. A.: Cloud optical thickness feedbacks in the CO2 climate problem, Journal of Geophysical Research: Atmospheres (1984–2012), 89, 9668–9672, 1984.

Stephens, G.: Radiation profiles in extended water clouds. II: Parameterization schemes, Journal of the Atmospheric Sciences, 35, 2123–2132, 1978.

Stephens, G. L.: Cloud feedbacks in the climate system: A critical review, Journal of climate, 18, 237–273, 2005.

Taylor, K. E., Stouffer, R. J., and Meehl, G. A.: An overview of CMIP5 and the experiment design, Bulletin of the American Meteorological Society, 93, 485–498, 2012.

Thompson, D. W., Wallace, J. M., Jones, P. D., and Kennedy, J. J.: Identifying signatures of natural climate variability in time series of global-mean surface temperature: Methodology and insights, Journal of Climate, 22, 6120–6141, 2009.

Trenberth, K., Branstator, G., Karoly, D., Kumar, A., Lau, N., and Ropelewski, C.: Progress during TOGA in understanding and modeling global teleconnections associated with tropical, Journal of Geophysical Research, 103, 14–291, 1998.

Trenberth, K. E.: The definition of el nino, Bulletin of the American Meteorological Society, 78, 2771–2777, 1997.

Turner, D., Vogelmann, A., Austin, R., Barnard, J., Cady-Pereira, K., Chiu, J. C., Clough, S., Flynn, C., Khaiyer, M., Liljegren, J., et al.: Thin liquid water clouds: Their importance and our challenge, Bulletin of the American Meteorological Society, 88, 177–190, 2007.

Voldoire, A., Sanchez-Gomez, E., y Mélia, D. S., Decharme, B., Cassou, C., Sénési, S., Valcke, S., Beau, I., Alias, A., Chevallier, M., et al.: The CNRM-CM5. 1 global climate model: description and basic evaluation, Climate Dynamics, 40, 2091–2121, 2013.

Volodin, E., Dianskii, N., and Gusev, A.: Simulating present-day climate with the INMCM4. 0 coupled model of the atmospheric and oceanic general circulations, Izvestiya, Atmospheric and Oceanic Physics, 46, 414–431, 2010.

Waliser, D. E. and Zhou, W.: Removing satellite equatorial crossing time biases from the OLR and HRC datasets, Journal of Climate, 10, 2125–2146, 1997.

Watanabe, M., Suzuki, T., O'ishi, R., Komuro, Y., Watanabe, S., Emori, S., Takemura, T., Chikira, M., Ogura, T., Sekiguchi, M., et al.: Improved climate simulation by MIROC5: mean states, variability, and climate sensitivity, Journal of Climate, 23, 6312–6335, 2010.

Weng, F., Grody, N. C., Ferraro, R., Basist, A., and Forsyth, D.: Cloud liquid water climatology from the Special Sensor Microwave/Imager, Journal of climate, 10, 1086–1098, 1997.

Wentz, F. and Meissner, T.: Algorithm theoretical basis document, 2000.

Wentz, F. J.: A well-calibrated ocean algorithm for special sensor microwave/imager, Journal of Geophysical Research: Oceans (1978–2012), 102, 8703–8718, 1997.

Wentz, F. J.: SSM/I version-7 calibration report, Remote Sensing Systems Rep, 11012, 46, 2013.

Wentz, F. J. and Meissner, T.: Supplement 1 algorithm theoretical basis document for AMSR-E ocean algorithms, NASA: Santa Rosa, CA, USA, 2007.

Wentz, F. J. and Spencer, R. W.: SSM/I rain retrievals within a unified all-weather ocean algorithm, Journal of the Atmospheric Sciences, 55, 1613–1627, 1998.

Wolter, K. and Timlin, M. S.: Monitoring ENSO in COADS with a seasonally adjusted principal component index, in: Proc. of the 17th Climate Diagnostics Workshop, pp. 52–7, 1993.

Wu, T., Yu, R., Zhang, F., Wang, Z., Dong, M., Wang, L., Jin, X., Chen, D., and Li, L.: The Beijing Climate Center atmospheric general circulation model: description and its performance for the present-day climate, Climate dynamics, 34, 123–147, 2010.

Wu, T. et al.: The 20th century global carbon cycle from the Beijing Climate Center Climate System Model (BCC CSM), J Clim, 2012.

Yin, J. H.: A consistent poleward shift of the storm tracks in simulations of 21st century climate, Geophysical Research Letters, 32, 2005.

Zelinka, M. D., Klein, S. A., and Hartmann, D. L.: Computing and partitioning cloud feedbacks using cloud property histograms. Part I: Cloud radiative kernels, Journal of Climate, 25, 3715–3735, 2012a.

Zelinka, M. D., Klein, S. A., and Hartmann, D. L.: Computing and partitioning cloud feedbacks using cloud property histograms. Part II: Attribution to changes in cloud amount, altitude, and optical depth, Journal of Climate, 25, 3736–3754, 2012b.

Zhao, G. and Di Girolamo, L.: Cloud fraction errors for trade wind cumuli from EOS-Terra instruments, Geophysical research letters, 33, 2006.

Zhou, C., Zelinka, M. D., Dessler, A. E., and Yang, P.: An analysis of the short-term cloud feedback using MODIS data, Journal of Climate, 26, 4803–4815, 2013.

Zhou, J. and Tung, K.-K.: Deducing multidecadal anthropogenic global warming trends using multiple regression analysis, Journal of the Atmospheric Sciences, 70, 3–8, 2013.

, , , , , , , , , , , , , ,